SYNTHESIS AND STUDY OF CARBOHYDRATE BASED HYDROGELS AND SELF ASSEMBLED GLYCOACRYLAMIDES FOR BIOMEDICAL APPLICATIONS

By

JUBY K. AJISH

CHEM 01201104016

Bhabha Atomic Research Centre, Mumbai

A thesis submitted to the board of studies in Chemical Sciences

In partial fulfillment of requirements for the degree of

DOCTOR OF PHILOSOPHY

Of

HOMI BHABHA NATIONAL INSTITUTE

May 2016

Homi Bhabha National Institute

Recommendations of the Viva-Voce Board

As members of the Viva-Voce Board, we certify that we have read the dissertation prepared by **Mrs. Juby K. Ajish** entitled "***Synthesis and study of carbohydrate based hydrogels and self assembled glycoacrylamides for biomedical applications***" and recommend that it may be accepted as fulfilling the dissertation requirement for the Degree of Doctor of Philosophy.

S K Sarkar

---------- Date: 15/12/16

Chairman: Dr. S. K. Sarkar

Manmohan Kumar

---------- Date: 15/12/2016

Guide/Convener: Dr. Manmohan Kumar

C.P. Rao

----------Date: 15/12/2016

External Examiner: Prof. C.P.Rao

---------- Date: 15/12/2016

Member 1: Dr. Lalit Varshney

Lalit Varshney

---------- Date: 15/12/2016

Member 2: Dr. A. K. Pandey

Pandey

---------- Date: 15/12/2016

Member 3: Dr. B. S. Patro

Final approval and acceptance of this dissertation is contingent upon the candidate's submission of the final copies of the dissertation to HBNI.

I hereby certify that I have read this dissertation prepared under my direction and recommend that it may be accepted as fulfilling the dissertation requirement.

Date: 15/12/2016

Place: BARC, Mumbai

Manmohan Kumar

STATEMENT BY AUTHOR

This dissertation has been submitted in partial fulfillment of requirements for an advanced degree at Homi Bhabha National Institute (HBNI) and is deposited in the library to be made available to borrowers under ruled of the HBNI.

Brief quotations from this dissertation are allowable without special permission, provided that accurate acknowledgement of source is made. Requests for permission for extended quotation from or reproduction of this manuscript in whole or in part may be granted by the Competent Authority of HBNI when in his or her judgment the proposed use of the material is in the interests of scholarship. In all other instances, however, permission must be obtained from the author.

Juby K. Ajish

DECLARATION

I, hereby declare that the investigation presented in the thesis has been carried out by me. The work is original and has not been submitted earlier as a whole or in part for a degree/diploma at this or any other Institution/University.

Juby

Juby K. Ajish

List of publications arising from the thesis

1. Glycopolymeric gel stabilized *N*-succinyl chitosan beads for controlled doxorubicin delivery.

   Juby K. Ajish, K. S. Ajish Kumar, S. Chattopadhyay, Manmohan Kumar, *Carbohydrate Polymers* **2016**, *144*, 98-105.

2. D-glucose based bisacrylamide crosslinker: Synthesis and study of homogeneous biocompatible glycopolymeric hydrogels.

   Juby K. Ajish, K. S. Ajish Kumar, Mahesh Subramanian, Manmohan Kumar, *RSC Advances*, **2014**, *4*, 59370-59378.

3. Silver nanoparticle loaded PVA/gum acacia hydrogel: Synthesis, characterization and antibacterial study.

   K. A. Juby, Charu Dwivedi, Manmohan Kumar, Swathi Kota, H. S. Misra, P. N. Bajaj, *Carbohydrate Polymers,* **2012**, *89,* 906-913.

4. Fluorescence turn-on sensing of lectins and cell imaging based on aggregation-induced emission of glycoacrylamides.

   Juby K. Ajish, K. S. Ajish Kumar, Mahesh Subramanian, S. Chattopadhyay, Manmohan Kumar, *RSC Advances,* **2016** (Communicated).

List of publications: associated with research work

1. Copper hexacyanoferrate–polymer composite beads for cesium ion removal: Synthesis, characterization, sorption, and kinetic studies. Charu Dwivedi, Amar Kumar, Krishan Kant Singh, **Ajish K. Juby**, Manmohan Kumar, P. K. Wattal, P. N. Bajaj, *Journal of Applied Polymer Science*, **2013**, 152-160.
2. PC-88A - Impregnated polymeric beads: Preparation, characterization and application for extraction of Pu (IV) from nitric acid medium. S. K. Pathak, Subhash C. Tripathi, K. K. Singh, A. K. Mahtele, Charu Dwivedi, **K. A. Juby**, Manmohan Kumar, P. M. Gandhi, P. N. Bajaj, *Radiochimica Acta*, **2013**, *101*,761-771.
3. Resorcinol-formaldehyde coated XAD resin beads for removal of cesium ions from radioactive waste: synthesis, sorption and kinetic studies. Charu Dwivedi, Amar Kumar, **Juby K. Ajish**, Krishan Kant Singh, Manmohan Kumar, P. K. Wattal, P. N. Bajaj, *RSC Advances*, **2012**, *2*, 5557-5564.
4. Preparation and evaluation of alginate-assisted spherical resorcinol–formaldehyde resin beads for removal of cesium from alkaline waste. Charu Dwivedi, Amar Kumar, **Kuttan Ajish Juby**, Manmohan Kumar, P. K. Wattal, P. N. Bajaj, *Chemical Engineering Journal*, **2012**, *200-202*, 491-498.

Poster presentations in international conferences

1. "*N*-succinyl chitosan/PVA hydrogel: Synthesis, characterization and antibacterial study".

   Juby K. Ajish, Manmohan Kumar, Swathi Kota, H. S. Misra and P. N. Bajaj, *4th Interdisciplinary Symposium on Materials Chemistry* **2012**, BARC Mumbai, India

2. "Synthesis and characterization of glycopolymer /N-succinyl chitosan beads for anticancer drug delivery".

   Juby K. Ajish, K. S. Ajish Kumar and Manmohan Kumar, *Interdisciplinary Symposium on Materials Chemistry,* **2014**, BARC Mumbai, India.

3. "Fluorescent self assembly of glycoacrylamides resembling natural proteins".

   Juby K. Ajish, K. S. Ajish Kumar, Mahesh Subramanian and Manmohan Kumar. *Trombay Symposium on Radiation & Photochemistry / Asia Pacific Symposium on Radiation Chemistry* **2016**, BARC Mumbai, India.

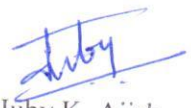

Juby K. Ajish

DEDICATIONS

Dedicated to my Husband and Parents

ACKNOWLEDGEMENTS

At this stage of writing the acknowledgements part of my Ph.D thesis, I look back through the last five years of Ph.D life, when I really feel the importance of each and every person involved in my doctoral work. This thesis does not only represent my work at the keyboard. Now at this final stage, I would like to express my heartfelt gratitude to all those who made this happen.

First and foremost I want to thank my supervisor ***Dr. Manmohan Kumar*** for his continuous support till the final stage of Ph.D work. I appreciate all his contributions of time, effort, ideas and encouragements throughout the tenure of my research. His guidance in every stage of the project has helped me in gaining a better knowledge about the subject. Dr. Manmohan Kumar was relentless in providing timely advice, direction and hope when things were not going right. Thanks a lot sir, for being such a good human being.

I convey my warm gratitude to ***Dr. B. N. Jagatap***, Director, Chemistry group and ***Dr. D. K. Palit***, Head, Radiation and Photochemistry division (RPCD) of BARC, Mumbai for providing me all the facilities in BARC to carry out my PhD work.

I am immensely thankful to all the doctoral committee members ***Dr. S. K. Sarkar***, ***Dr. Lalit Varshney***, ***Dr. Ashok Pandey*** and ***Dr. B. S. Patro*** for their valuable guidance, timely cooperation and guidance. I am equally obliged to ***Dr. S. Chattopadhyay***, Head, Bio-sciences Group, for the scientific discussions during the course of my research work, which helped me a lot. I take this

opportunity to thank ***Dr. P. N. Bajaj*** for his valuable time and suggestions during article correction.

Words would not be enough to express my gratitude towards my husband and main collaborator in the Ph.D work, ***Dr. Ajish Kumar K. S***, without whom it would have been difficult to carry out the work. My research work was benefitted immensely with the molecules synthesized with your help. The molecules were just tailor made for my work and helped improving the quality of the work.

I am grateful to my lab mates ***Mr. Krishankant Singh***, ***Mr. Anant Kanagare*** and ***Ms. Aakansha Ruhela*** for their assistance in experimental work. Working with them is always a pleasure. I am equally grateful to ***Dr. Chetan P. Shah*** and ***Dr. Charu Dwivedi***, who were there with me during the initial stages of my Ph.D work.

My sincere thanks to all my fellow lab mates ***Mrs. Ridhima Chadha***, ***Mr. Abhishek Das***, ***Dr. Nandita Maiti***, ***Mr. Akshay Dhayagude***, ***Mr. Sugosh R. Prabhu***, ***Mr. Tushar Debnath***, ***Mr. Aruna Kumar Mora*** and ***Mrs. Laboni Das***, all of you call for a special mention. Thank you all for being such good friends which made my daily work enjoyable and fun. Avery special thanks to my dear and dearest friend ***Dr. Neha Thakur*** for her glorious presence in my life. Thank you for being such a gem of a friend who gave a soothing hand during the most difficult times. I also extend my sincere thanks to all my friends and colleagues of Radiation and Photochemistry Division for their love and support.

My parents and in-laws deserve special mention for their support in all my pursuits and their persistent confidence in me. I owe my every achievement to them. I would also like to mention the sweetest person in my life my son, ***Abhiram***, who made me laugh at the end of the day and made me forget all the frustrations and worries of Ph.D work. I also thank my brother ***Mr. Biju Kuttan*** for his love and support all the time. I am privileged to have such a supportive family.

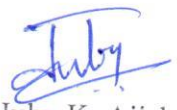

Juby K. Ajish

B. A. R. C.
Mumbai
May, 2016

CONTENTS

SYNOPSIS

Polymers in various forms like hydrogels, polymeric beads, thin films, nanoparticles so on and so forth; have become a part of our day to day life. These materials have become inevitable especially with advancement of technology. Hence development of new materials and investigating the properties with better applicability has become a major area of research these days. This dissertation is therefore aimed at the synthesis and study of bulk hydrogels as well as gel beads for antibacterial and drug delivery applications. Apart from this, the last part of the thesis also focuses on the aggregation induced emission studies of new glycoacrylamides, for cell imaging and biosensing applications.

Chapter 1: Introduction

This chapter deals with a general introduction about the polymeric hydrogels, methods of synthesis and their applications in various biomedical fields. It begins with a brief note on the existing methods of hydrogel synthesis and the advantages of radiation-induced polymerization method. A detailed literature survey on the nanoparticles loaded hydrogels, their properties, applications, etc., have been discussed. In the next part a background about the synthetic glycopolymers, their biorecognition ability and use in targeted drug delivery is given. Later part of the chapter portrays the self assembly behaviour of small molecules, aggregation-induced emission and its importance in cell imaging as

well as biosensing applications. The chapter ends with the scope of the work and future possibilities in the fields presented in the dissertation.

Chapter 2: Experimental Techniques

This chapter gives a brief description about the experimental techniques utilized for the work mentioned in the thesis. Basic working principles of the instruments used like Rheometer, Thermogravimeter (TG), Differential scanning calorimeter (DSC), Infrared spectrometer (IR), Elemental analyzer, Dynamic light scattering (DLS), UV-vis and Fluorescence spectrophotometry, is presented briefly in this chapter. The working principle and experimental arrangement of microscopic techniques, like Scanning electron microscopy (SEM), Tunneling electron microscopy (TEM), and Confocal microscopy (CM) is also given. The chapter also contains a brief description about the Nuclear magnetic resonance spectroscopy (NMR) which was utilized for characterization of the synthesized glycoacrylamides and chitosan derivatives.

Chapter 3: Silver nanoparticle loaded antibacterial PVA/gum acacia hydrogel

This chapter deals with a simple one-pot method for in-situ synthesis of silver nanoparticles (AgNPs), within polyvinyl alcohol-gum acacia (PVA–GA) hydrogel matrix, by γ-radiation induced cross-linking. While considering the synthesis of hydrogels, its biocompatibility is an important parameter for biomedical applications. Synthesis of biocompatible hydrogel matrix from a nontoxic,

economical, and easily available materials, such as polysaccharides, is more advantageous than that from synthetic polymers[1]. However, polysaccharides like GA cannot be cross-linked by γ-irradiation, whereas PVA can and results in formation of hydrogels, induced by gamma, as well as electron irradiation. The highly biocompatible, economical and environmental friendly nature of both gum acacia and PVA make this obvious choice for the synthesis of a composite hydrogel matrix. Recent studies have shown that, silver, in the form of nanoparticles, is very effective as antimicrobial agent, both in-vivo and in-vitro, as compared to bulk silver, or silver ions, due to their enhanced permeation and retention (EPR) effects[2]. Thus, a combination of water soluble biopolymer GA and synthetic polymer PVA with silver nanoparticles (AgNPs) can produce new hydrogel matrix, with antimicrobial property.

The AgNPs were generated in-situ in the hydrogel matrix by γ-irradiation. This chapter gives a brief description about the reactions taking place in aqueous solutions during γ-radiolysis, which leads to crosslinking and reduction of silver ions[3]. The synthesized gels were tested for thermal stability, equilibrium swelling, AgNPs release kinetics, size of AgNPs leached out and its dependence on the antibacterial activity against E.*coli* bacteria. Major objective of this study was to determine how the size and rate of leaching out of AgNPs affect the antibacterial activity. It was observed that higher the crosslinking density, smaller is the size of AgNPs and better is the antibacterial activity, even though the rate of leaching is slow.

In addition, gel point of the synthesized hydrogel was determined rheologically by Chambon-Winter (CW) criterion[4]. A radiation dose of 25.34 kGy was calculated to be the gel point which is close to the sterilization dose for biomedical applications.

Chapter 4: Synthesis and study of biocompatible glycopolymeric hydrogels

This chapter contains the synthesis of D-glucose derived glycoacrylamides and glycopolymeric hydrogels. The objective of synthesizing a glycopolymeric gel was to generate a material which can be targeted to specific cellular site. The ability of sugar pendants in glycopolymers to mimic that on the cell surface makes them a unique class of materials for targeted drug delivery applications[5]. Generally, sugar based hydrogels are synthesized from low molecular weight gelators (LMWG) like alkyl gluconamides, phenyl β-D-glucopyranoside etc. However, it has been reported that hydrogels derived from LMWG possess several disadvantages that include aggregation, crystallization or precipitation with time[6]. One of the ways to overcome this is to synthesize hydrogel from low molecular weight carbohydrate derivative by radiation polymerization. This technique has the potential to overcome most of the limitations that arise from LMWG, as the radiation crosslinked hydrogels possess more lifetime stability due to covalent crosslinking. An added advantage of radiation-induced synthesis is that, by applying appropriate radiation dose, a sterilized hydrogel can be achieved in a one pot process.

Citing the significance of glycopolymeric hydrogels, D-glucose based bisacrylamide substituted at C-3 and C-6 carbon of sugar (Glc-bis) and monoacrylamide substituted at C-6 position (Glc-acryl) was synthesized and their gelation was studied using radiation polymerization. The synthesized Glc-bis and Glc-acryl were characterized by ^{1}H and ^{13}C-NMR. The molecular structure, water content, viscoelasticity, thermal stability, cytotoxicity and lectin recognition of the synthesized hydrogels (Glc-gel) were studied using the techniques, like FT-IR spectroscopy, Oscillatory rheology, Thermogravimetric-Differential Scanning Calorimetric (TG-DSC) analysis, MTT assay and UV-vis spectroscopy, all of which have been discussed in detail in this chapter.

Chapter 5: Glycopolymer gel stabilized *N*-succinyl chitosan beads for controlled doxorubicin delivery

This chapter involves the synthesis and study of *N*-succinyl chitosan (NSC) based hydrogel beads, stabilized with glycopolymeric network (NSC/Glc-gel), for application in delivery of anticancer drug, doxorubicin (DOX). We hypothesized that the Glc-gel would provide the required stability for the NSC beads against dissolution upon drug loading, and could control the drug release. The biocompatible Glc-gel used for stabilization of the beads was made from bisacrylamide (Glc-bis) and monoacrylamide (Glc-acryl) derived from D-glucose. The bio-recognition of lectins by the NSC/Glc-gel beads was also studied by UV-vis spectrophotometry.

The extent of DOX loading was proportional to the degree of succinylation and the swelling kinetics of the beads exhibited pH dependency. The beads exhibited sustained release of DOX over a period of more than 15 days in an acidic environment, mimicking the microenvironment of tumor cells. While the rate of DOX release at physiological pH was found to be much slower[7]. Release exponent 'n' derived from Korsmeyer-Peppas model implied that the NSC88/Glc-gel beads with 88% succinylation of chitosan followed fickian diffusion controlled release mechanism, whereas the NSC75/Glc-gel beads with 75% succinylation of chitosan followed zero order release profile[8]. The synthesized beads also showed specificity to lectin Concanavalin A. This stabilized polysaccharide based glycopolymeric gel bead could be a suitable base for pharmaceutical applications.

Chapter 6: Self assembled fluorescent glycoacrylamides

The design and synthesis of fluorescent self assembled nanostructures are of great interest due to their applicability in drug delivery, molecular actuators, functional biomaterials and analytical biosensors. Multiple weak non covalent interactions play a major role in formation of interesting structures with a particular arrangement, which imparts some amazing properties that make them stimuli responsive. These non-covalent interactions in self assembled systems make them fluorescent and this property can be utilized in bio-sensing, cell imaging, etc.

Syntheses of amphiphilic molecules containing carbohydrate moieties, which can self assemble to well defined nanostructures, can be promising scaffolds for interacting with biological receptors. The glucose based C-6 acrylamide (Glc- acryl) and C-3, C-6 bisacrylamide (Glc-bis) exhibit pH dependent self assembly with fluorescent emission. The building blocks contain hydrophobic acrylamide units which act as the fluorescent probe by virtue of its stacking through weak π-π interaction and the hydrophilic glucose units serve as the lectin binding moiety. Significant fluorescence enhancement upon interaction with Con A arises due to enhanced Aggregation Induced Emission (AIE) effect[9]. The biocompatibility and cell uptake behaviours of Glc-acryl and Glc-bis were also studied using human intestinal cell lines (INT407), as it contain receptors which can specifically identify D-glucose moieties[10].

Chapter 7: Conclusions and Future Perspectives

This chapter gives a brief summary and highlights of the present investigation with future perspectives that can be explored utilizing the present knowledge on synthesis of hydrogels and self assembled nanoparticles. The main findings are as follows:

- AgNPs loaded hydrogels utilizing naturally occurring polysaccharide can be made by gamma radiation induced method.
- The size of AgNPs as well as its rate of leaching plays an important role in antibacterial applications.

- A purely glycopolymer based hydrogel utilizing the synthesized glycoacrylamides as the constituents were synthesized by γ- radiation induced polymerization and crosslinking.
- The glycopolymeric hydrogel showed specificity to lectins and can be utilized for drug delivery applications.
- Glycopolymer stabilized *N*-succinyl chitosan beads were synthesized for anticancer drug, doxorubicin (DOX) delivery.
- The NSC/Glc-gel beads exhibited a slow and sustained pH dependent delivery of the drug over a period of about 18 days.
- The synthesized glycoacrylamides were found to self assemble in water which results in pH dependent fluorescent emission.
- A comparative study of emission, cellular uptake, and lectin biosensing was carried out for both the synthesized glycoacrylamides Glc-acryl and Glc-bis.

References

1. Francis, S.; Varshney, L. and Kumar, M. *Radiat. Phys. and Chem.* 2004, ***69***, 481-486.
2. Kora, A. J.; Sashidhar, R. B. and Arunachalam, J. *Carbohydr. Polym.* 2010, ***82***, 670-679.
3. Rao, Y. N.; Banerjee, D.; Datta, A.; Das, S. K.; Guin, R and Saha, A. *Radiat. Phys. and Chem.* 2010, ***79***, 1240-1246.

4. Chambon, F.; Petrovic, Z. S.; MacKnight, W. J. and Winter, H. H. *Macromolecules*, 1986, ***19***, 2146-2149.
5. Kopecek, J.; Kopeckova, P.; Brondsted, H.; Rathi, R.; Rihova, B.; Yeh, P. Y. and Ikesue, K. *J. Control. Release*, 1992, ***19***, 121-130.
6. Raeburn, J.; Cardoso, A. Z. and Adams, D. J. *Chem. Soc. Rev.* 2013, ***42***, 5143-5156.
7. Duan, C.; Gao, J.; Zhang, D.; Jia, L.; Liu, Y.; Zheng, D.; Liu, G.; Tian, X.; Wang, F. and Zhang, Q. *Biomacromolecules*, 2011, ***12***, 4335-4343.
8. Korsemeyer, R. W.; Gurny, R.; Doelker, E.; Buri, P. and Peppas, N. A. *Intl. J. Pharm.*1983, ***15***, 25-35.
9. Sanji,T.; Shiraishi, K.; Nakamura, M. and Tanaka, M. *Chem. Asian J.* 2010, ***5***, 817-824.
10. Lu, Z.; Mei, L.; Zhang, X.; Wang, Y.; Zhao,Y. and Li, C. *Polym. Chem.* 2013, ***4***, 5743-5750.

LIST OF FIGURES

List of Schemes

List of Tables

CHAPTER 1

INTRODUCTION

Introduction

Polymers and macromolecules in general have become a major part of our day to day lives that it has become a necessity. As per the requirement or application they are used in various forms, like hydrogels, nanoparticles, thin films, spherical beads so on and so forth. For example, hydrogels have gained attention for various biomedical applications, due to their biocompatibility imparted by high water content in the three dimensional network.[1,2] Hydrogels contain polymeric units with hydrophilic domains which are hydrated in an aqueous environment, creating the hydrogel structure. Hydrogels or gels in general can be synthesized by chemical or physical crosslinks. Chemical crosslinks involves the construction of covalent linkages between the polymer chains leading to the formation of 'permanent' or irreversible' gels whereas, physical crosslinks comprise interactions like interpenetrating networks (IPNs) or secondary forces like ionic interaction, H-bonding or hydrophobic forces. Unlike chemicals crosslinks, the gels formed through physical crosslinks are 'physical' or 'reversible' gels.[3] The hydrogels prepared by these crosslinks can exist in different physical forms including solid molded forms, powdered matrices, microparticles, coatings, membranes or sheets, etc.

Hydrogels can be made from natural or synthetic polymers. Natural polymers, inspite of their various advantages like biodegradability, derivatization at suitable reactive sites, etc., have disadvantages like enzymatic cleavage of glycosidic bonds, batch wise variation and low mechanical strength.[4] Synthetic

polymers are advantageous in various aspects of hydrogel formation like, they can be made responsive to external stimuli and their physical properties can be varied by modifying the synthetic conditions. But they have several drawbacks like low biodegradability and interference of various toxic side products arising during synthesis which limits their usage in biomedical field. Considering all pros and cons of synthetic and natural polymers, combinations of these polymers have attracted much interest for manufacturing hydrogels.[5]

1.1. Radiation induced formation of hydrogels

Radiolysis of an aqueous solution by γ- radiation mainly produces hydroxyl radical ($HO^{\bullet}$), hydrogen radicals ($H^{\bullet}$) and hydrated electrons (e^{-}_{aq}) species along with some molecular products due to radiolysis of solvent (equation 1.1).

$$H_2O \xrightarrow{\gamma\text{-radiation}} e^{-}_{aq}, H_3O^{+}, H_2, H^{\bullet}, HO^{\bullet}, H_2O_2 \qquad (1.1)$$

Among the transient species $HO^{\bullet}$ is oxidizing while, $H^{\bullet}$ and e^{-}_{aq} are reducing in nature. Hydrated electrons exhibit low reactivity towards simple, hydrophilic gel forming polymers, due to the absence of efficient scavengers. The main species which are responsible for the formation of reactive polymer radicals are mainly the hydroxyl radicals formed during water radiolysis. The macroradicals formed during the interaction of $HO^{\bullet}$ with the polymer chains undergoes intermolecular crosslinks i.e, recombination of two polymeric radicals to form gel. Other reactions which compete with the intermolecular crosslinking include

intramolecular crosslinks, inter and intramolecular disproportionation, processes involving reactions like hydrogen transfer or chain scission, which do not lead to the formation of macroscopic gels. Hence the concentration of the reactive species should be optimized to form strong crosslinked networks. The hydrogels formed by radiation induced method leads to formation of sterilized and permanent three dimensional networks concurrently, at appropriate dose.[7]

1.2. Hydrogel based antibacterial wound dressings

Even though hydrogels are increasingly used in various biomedical fields, its use in wound dressing applications is highly pronounced. The hydrogel wound dressings produced by radiation based technology has following advantages:

1. It forms an efficient barrier for bacteria and prevents excessive loss of body fluids.
2. Hydrogels allow diffusion of oxygen into the wound.
3. Hydrogels are soft and elastic but possess sufficient mechanical strength.
4. It has good non-sticky adhesive properties to the wound and healthy skin, enabling painless removal/exchange of the dressing without disturbing the healing process.
5. The transparency of the hydrogel dressing helps in easy monitoring of wound healing process.
6. Controlled release of a drug to the wound can be done with the hydrogel dressing.
7. Hydrogel maintains constant humidity on the wound environment.

8. Hydrogels can also be utilized as sprays, emulsions, ointments and creams.

The ability of hydrogels to absorb and retain water not only gives hydrogels a strong superficial resemblance to living tissues, but also makes them permeable to small molecules such as oxygen, nutrients and metabolites. The soft and flexible nature of swollen hydrogels minimizes frictional irritation felt by the surrounding cells and tissues.[8]

1.3. States of water in hydrogels

Water in hydrogels maintains a moist environment in the region of application thereby facilitating processes like wound healing. In, addition, it also helps in transport of various active agents through the network. A completely dried hydrogel matrix can swell even 1000 times their initial weight. The amount of absorbed water is usually expressed as the equilibrium water content (EWC, equation 1.2).

$$EWC = \frac{W_w}{W_t} X\ 100 \qquad (1.2)$$

W_w = weight of water in hydrogel

W_t = total weight of the hydrated gel

EWC is the water holding capacity of a hydrogel and is one of the most important parameter which determines the potential efficiency of the hydrogel in biomedical field.

The swelling process in hydrogels is a complicated process consisting of three main steps. In the first step, the most polar and hydrophilic groups are hydrated resulting in the formation of *primary bound water*. In the second step, the interaction of water molecules with the exposed hydrophobic groups leads to formation of hydrophobically bound water or *secondary bound water*. Primary and secondary bound water together form *total bound water*. The third step involves the water uptake due to resistance of osmotic driving force of the network towards infinite dilution by covalent or physical cross-links. The water absorbed up to the equilibrium swelling level is called *bulk water or free water*; which fills the space or voids between the networks.[9] Major techniques used to characterize water in the hydrogels are use of small molecular probes, Differential Scanning Calorimetry (DSC), and Nuclear Magnetic Resonance (NMR) spectroscopy.

1.4. Metal nanoparticle embedded hydrogels

Metal nanoparticles embedded hydrogels are those in which nanoparticles are stabilized by the three dimensional polymeric network of the hydrogels. This combination of metal nanoparticles with hydrogels provides superior functionality to these materials, which can find applications in electronics, drug delivery, biosensing, catalysis, nano-medicine and environmental remediation.[10] The nanoparticle embedded hydrogels have got synergistic enhancement in properties of each component, like mechanical strength of the hydrogel and concomitantly, decreased aggregation of the embedded nanoparticles. For example, silica

nanoparticle loaded hydrogels made of modified polyethylene glycol exhibit remarkable enhancement in tissue adhesion and mechanical strength than the unloaded ones.[10] Similarly poly *N*-isopropyl amide hydrogels with gold nanoparticles showed significant changes in mechanical properties and thermal response.[11] The result of such a combination of nanoparticles and hydrogels is that it leads to the development of advanced materials with unique properties better than that of individual constituents.[12]

However properties such as mechanical toughness, swelling ratio, stimuli responsiveness, and biocompatibility/biodegradability of such composites need to be investigated and optimized for effective applications. Silver nanoparticles (Ag-NPs) have been incorporated into polyacrylamide (PAAm),[13] polyacrylic acid (PAA),[14] poly *N*-isopropyl acrylamide (PNIPAAm),[15] polymethyl methacrylate (PMMA),[16] and polyvinyl alcohol (PVA) based hydrogels.[17] Efforts in recent years have been shifted to utilizing naturally occurring polymers such as chitosan,[18] gum acacia, dextran[19] and gelatin[20] to produce bio-compatible/degradable composite materials that have potential applications as implantable dressings. The controlled-release of AgNPs from the dressing provides consistent protection for a good period of time, without frequent removal of the dressings.

Different approaches used for synthesis of a hydrogel network with uniform distribution of nanoparticles are:

1. Hydrogel formation in nanoparticle suspension.

2. Gelation of hydrogel matrix followed by physical embedding of nanoparticles.
3. Reactive nanoparticle formation within a preformed gel.
4. Nanoparticle assisted hydrogel formation.

1.4.1. *Hydrogel formation in nanoparticle suspension*

This is the simplest approach for making a nanoparticle-hydrogel composite. It involves gelation of a hydrogel forming monomer solution with preformed nanoparticles. A major drawback of this method is that the nanoparticles may leach out of the hydrogel matrix if the crosslinking density is low.

1.4.2. *Gelation of hydrogel matrix followed by physical embedding of nanoparticles*

Incorporation of nanoparticles physically into the gel is a kind of 'breathing in' mechanism which is repeated several times to obtain sufficient nanoparticle density. The gel initially is made to 'breathe out' by expulsion of water by placing in acetone. The shrunken gel is then equilibrated with a solution containing preformed nanoparticles. This cause the gel to swell (breathing in) leading to uptake of suspended nanoparticles as well. Finally, the gel is washed thoroughly with water to remove any weakly adsorbed nanoparticles on the surface. In the next breathing out cycle, the nanoparticles are bound to the gel matrix through some physical entanglement or H-bonding interactions between the polymer chains and capping on the nanoparticles. The increase in nanoparticles density inside the hydrogel can be monitored after every cycle using techniques like X-

ray Photoelectron Spectroscopy (XPS), and Atomic Absorption Spectroscopy (AAS).

1.4.3. *Reactive nanoparticle formation aided by hydrogel network*

This approach was developed by Langer's group, where nanoparticle precursors are loaded into the gel rather than preformed nanoparticles.[21] For example free-radical crosslinking polymerization of acrylamide monomer in an aqueous solution containing Ag^+ ions yields Ag^+ ions functionalized polyacrylamide hydrogel matrix, which is reduced to yield AgNPs within the hydrogel network. The resulting hydrogel contained un-aggregated nanoparticles throughout the matrix. Ionizing radiations like gamma or electron beam induced formation of nanoparticles in the hydrogel network also belongs to this category where in the aqueous solution containing nanoparticle precursor and the crosslinking polymer is irradiated. As mentioned before, radiolysis of water generates $HO^{\bullet}$ and $H^{\bullet}$ radicals that are mainly responsible for crosslinking/degradation of polymeric solutes. The reducing radicals like $H^{\bullet}$ and e_{aq}^- reduce the metal ions to corresponding nanoparticles.

1.4.4. *Nanoparticle assisted hydrogel formation*

In this method, nanoparticles or groups present on the surface of nanoparticles assist the crosslinking process to form hydrogels. For example, the semiconductor nanoparticles-based hydrogels, where CdSe and CdTe function as inorganic

initiators to form stable gels with *N*,*N*-dimethylacrylamide (DMAA) on irradiation using visible light.[22]

1.5. Antibacterial activity of silver nanoparticles (AgNPs) loaded hydrogels

Among the inorganic antibacterial agents, silver has been employed most extensively, since ancient times, to fight infections and control spoilage.[23] The antibacterial and antiviral actions of silver, silver ion, and silver compounds have been thoroughly investigated.[24-26] At very low concentrations, silver is nontoxic to human cells. The epidemological history of silver has established its nontoxicity in normal use. Catalytic oxidation by metallic silver and reaction with dissolved monovalent silver ion probably contribute to its bactericidal effect.[27] Microbes are unlikely to develop resistance against silver, as they do against conventional and narrow-target antibiotics, because the metal attacks a broad range of targets in the organisms. Therefore, microbes have to develop a host of mutations simultaneously to protect themselves. Hence, silver ions have been used as an antibacterial ingredient in dental resin composites[28], in synthetic zeolites[29], and in coatings of medical devices.[30] A number of encouraging results about the bactericidal activity of silver nanoparticles of either a simple or composite nature have been reported.[31, 32] Elechiguerra and coworkers[33] found that silver nanoparticles undergo a size-dependent interaction with human immunodeficiency virus type 1, preferably *via* binding to gp120 glycoprotein knobs. The same group also investigted the size-dependent interaction of AgNPs with gram-negative bacteria.[34] AgNPs loaded hydrogels gain importance when it

comes to the necessity of sustained antimicrobial efficacy. AgNP-hydrogel composites also provide functional coatings for various applications as shown in the figure 1.1.

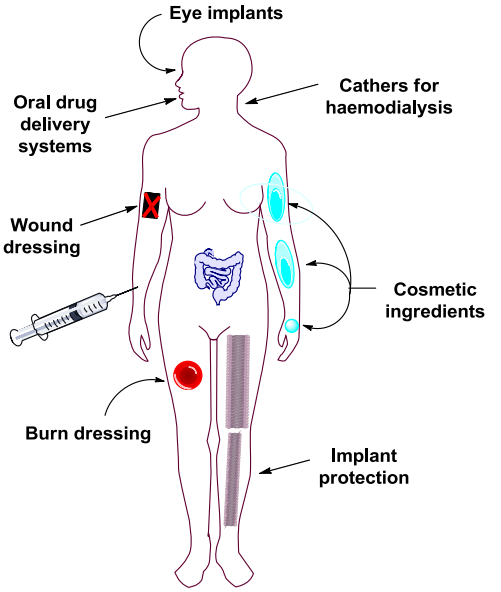

Figure 1.1: An overview of potential bio-medical applications of AgNP-hydrogel composites.

1.6. Next generation of nanocomposite hydrogels

Even though nanocomposite hydrogels are being increasingly evaluated for various biomedical applications, most of the existing nanocomposite approaches lack control over some essential features such as stimuli responsiveness and biodegradation. To address these challenges, alternate strategies have been developed to design nanocomposite hydrogels with multiple functionalities. Recent trends in designing advanced biomaterials aimed at designing stimuli-responsive nanocomposites. These biomaterials show significant change in their physical, chemical/biological properties with environmental stimuli. For example,

(PNIPAAm) based nanoparticles/hydrogels were used to design therapeutics device for tissue engineering and drug delivery applications. PNIPAAm exhibits a negative swelling transition at 34 ^{o}C, which makes it an attractive system for applications in drug delivery. Such polymeric systems were further decorated with appropriate nanoparticles to develop stimuli responsive matrices. The type of nanoparticles embedded within the hydrogel networks determines the type of stimuli to which they respond. A range of stimuli responsive elements such as mechanically adaptive, pH/enzyme/ion responsive, electrically stimulating, thermo- and magnetic responsive can be incorporated within nano-composite hydrogels. These types of responsive nano-composite hydrogels will direct the development of next generation of nanocomposite hydrogels. In a recent effort, Au nanoparticles were entrapped within interpenetrating polymer network of thermally responsive polyacrylamide (PAAm)-poly(acrylic acid) (PAA) to design therapeutic hydrogels.[35] Au nanoparticles have the ability to absorb visible-to-near infrared (530–1,200 nm) light and thus can be used to generate heat locally. The local heating by the nanoparticles was used to trigger swelling/deswelling of the polymeric network and can result in the release of entrapped macromolecules. The covalently crosslinked PAAm-PAA interpenetrating polymer network can be used to deliver therapeutics using external trigger for a range of biomedical and drug delivery applications.

In future, it is expected that hybrid materials will merge with other types of technologies such as micro-fabrication approaches to understand cell-

nanomaterial interactions. Microscale technologies are emerging as one of the powerful technologies to address some of the challenges in tissue engineering. Additionally, future studies of nanocomposite hydrogels will also focus on understanding the interactions between polymeric chains and nanoparticles at different length scale. This will tailor the properties of the nanocomposite hydrogels for required applications.[36]

1.7. Hydrogels for controlled drug delivery applications

The limitations associated with the conventional therapeutics have led to the need of targeted controlled drug delivery (TCDD) vehicles with improved biocompatibility and biodegradability. In recent years, the pharmaceutical industry is involved in developing hydrogel based systems in various forms by tuning the structure, shape and surface modifications of the biopolymers. Hydrogels can be formulated in a variety of physical forms, including slabs, microparticles, beads, nanoparticles, coatings, and films. Hence they find application in various biomedical fields including tissue engineering, regenerative medicine,[37] diagnostics,[38] cellular immobilization,[39] separation of biomolecules or cells,[40] and barrier materials to regulate biological adhesions.[41]

The unique physical properties of hydrogels, like their highly porous nature, can be easily tuned by controlling the crosslinking density of the matrix. This expands its application in the region of interest. Also the high water content and the physiochemical similarity of hydrogels with human tissues have sparked interest in their use in drug delivery applications. The porosity permits loading of drugs

into the gel matrix and subsequent drug release at a rate which is dependent on the diffusion coefficient of the small molecules or the macromolecules through the gel network. The pharmacokinetics of drug release from the hydrogel matrix facilitates slow and sustained elution, maintaining a high local concentration of drug in the surrounding tissues over an extended period, although they can also be used for systemic delivery. Biocompatibility is promoted by the high water content of hydrogels and the physiochemical similarity of hydrogels to the native extracellular matrix, both compositionally (particularly in the case of carbohydrate-based hydrogels) and mechanically. Hydrogels can be made biodegradable *via* enzymatic, hydrolytic or environmental pathways. The muco- or bioadhesive properties of some hydrogels are advantageous in immobilizing them at particular sites even on surfaces which are not horizontal.[42]

Hydrogels, based on their response to external stimuli, can be classified as pH sensitive, temperature sensitive; enzyme sensitive, electrical sensitive etc. pH sensitive hydrogels can be neutral or ionic in nature. The anionic hydrogels contain negatively charged moieties, cationic networks contain positively charged moieties, and neutral networks either do not contain ionic moieties or contain both positively and negatively charged moieties. In neutral hydrogels, the driving force for swelling arises from the water-polymer thermodynamic mixing contributions, and elastic-polymer contributions. In ionic hydrogels, the swelling is due to the previous two contributions, as well as ionic interactions between charged polymer and free ions. The presence of ionizable functional groups like carboxylic acid,

sulfonic acid or amine groups, renders the polymer more hydrophilic, and results in high water uptake.

In the case of anionic polymeric network containing carboxylic or sulphonic acid groups, ionization takes place as the pH of the external swelling medium rises above the pKa of the ionizable moiety. The dynamic swelling change of the anionic hydrogels can be used in the design of intelligent controlled release devices for site-specific drug delivery. The change in the pH of the external environment will act as a stimulus, and the response to the stimulus is the change in swelling properties of the hydrogels, causing the release of the drug.

The cationic hydrogels show swelling at pH values below pKa of the cationic group. The amine groups are protonated at pH lower than pKa, and become hydrophilic and absorb water. At pH greater than pKa, the polymeric hydrogel is hydrophobic, and excludes water.[43]

1.7.1. *Methods of hydrogel synthesis*

Several techniques are known for the synthesis of hydrogels, out of which the commonly used are:

1.7.1.1. *Bulk polymerization*

Bulk polymerization involves only monomer and monomer soluble initiators. Because of high concentration of monomer, high rate of polymerization and degree of polymerization occurs. The bulk polymerization of monomers to form homogeneous hydrogels produces hard, glassy and transparent polymer matrix. It becomes soft and flexible when immersed in water. Heat generated during bulk

polymerization has to be avoided by controlling the reaction at low conversions. The best example is preparation of poly(2-hydroxyethyl methacrylate)[44] hydrogels from hydroxyethyl methacrylate, using ethylene glycol dimethacrylate as crosslinking agent.

1.7.1.2. *Suspension polymerization or inverse–suspension polymerization*

In this method of dispersion polymerization, the products are obtained as powder or microspheres. When water in oil (W/O) process is chosen instead of the more common oil in water (O/W), the polymerization is referred as "inverse suspension". This technique involves dispersion of monomers and initiators as a homogeneous mixture in the hydrocarbon phase. The viscosity of the monomer solution, agitation speed, rotor design and the dispersant type governs the resin particle size and shape. The dispersion is thermodynamically unstable and requires both continuous agitation and hydrophilic-lipophilic balance (HLB) suspending agent. Hydrogel microparticles of poly (vinyl alcohol) and poly (hydroxyethyl methacrylate) have been prepared using this method.[45]

1.7.1.3. *Solution polymerization*

Here the ionic or neutral monomers are mixed with the multifunctional crosslinking agent. The polymerization is initiated by UV-irradiation or by a redox initiator system. In solution polymerization, solvent acts as a heat sink. The prepared hydrogels has to be washed with distilled water to remove any unreacted monomers, oligomers, crosslinking agents, the initiator and other impurities. After formation of the heterogeneous hydrogel, phase separation occurs when the

amount of water during polymerization is more than the water content corresponding to the equilibrium swelling. Commonly used solvents are water, ethanol, water-ethanol mixtures and benzyl alcohol. The solvent is finally removed by swelling the hydrogels in water.

1.7.1.4. *Polymerization by irradiation*

Irradiation of aqueous polymer solution by high energy radiation like gamma and electron beam, have been used to prepare the hydrogels the details of which is given in section 1.1.[46] Even sterile hydrogels can be produced by tuning the required radiation dose for the crosslinking. Examples of polymers crosslinked by radiation method include poly (vinyl alcohol),[47] poly (ethylene glycol),[48,49] poly (acrylic acid).[50] The major advantage of radiation induced technique over chemical initiation is the production of relatively pure, residue-free hydrogels.

1.7.2. ***Classification of hydrogels***

1.7.2.1. *Chemically crosslinked hydrogels*

Polymers containing functional groups like -OH, -COOH, $-NH_2$ can be used to prepare hydrogels by forming covalent linkages between the polymer chains and functional group pairs such as amine-carboxylic acid, isocyanate- OH/NH_2 or by Schiff base formation. Glutaraldehyde can be used as a crosslinking agent to prepare hydrogels of polymers containing -OH groups like poly (vinyl alcohol) and polymers containing amine groups (albumin, gelatin, polysaccharides). However crosslinking agents like glutaraldehyde is highly toxic, and hence

unreacted agents have to be extracted before using material for biomedical applications.

1.7.2.2. *Physically crosslinked hydrogels*

In physical gels, as mentioned before, the nature of crosslinking process is physical. This is achieved through various physical processes such as hydrophobic association, chain aggregation, crystallization and hydrogen bonding. Poly vinyl alcohol (PVA) is a water soluble polymer, the aqueous solution of which is stored at room temperature to form gel of low mechanical strength. But once the aqueous solution of this polymer undergoes freeze-thawing process, a strong and highly elastic gel is formed. This is due to formation of PVA crystallites that act as physical crosslinking sites in the network. Crosslinking between poly (methacrylic acid) and poly (ethylene glycol) through hydrogen bond formation also leads to hydrogel formation. The hydrogen bond formation takes place between the oxygen of poly (ethylene glycol) and carboxylic acid group of poly (methacrylic acid).

1.7.2.3. *Ionically crosslinked hydrogels*

Most of the covalent crosslinking agents are known to be toxic, even in small traces. Reversible ionic crosslinking can avoid the purification step post- hydrogel synthesis. Chitosan, a polycationic polymer can react with negatively charged components, either ions or molecules, forming a network through ionic bridges between the polymeric chains. Among anionic molecules, phosphate bearing groups, particularly sodium tripolyphosphate has been widely studied. Ionic

crosslinking is a simple method compared to covalent crosslinking as no auxiliary molecules are required. Chitosan is also known to form polyelectrolyte complex with poly (acrylic acid) which undergoes slow erosion, thus making them more biodegradable material than covalently crosslinked hydrogels.

1.7.3. *Drug release mechanisms from hydrogel devices*

Hydrogels can imbibe large quantities of water because of which, the release mechanism is very much different from hydrophobic polymers. Based on the rate limiting step for controlled release of an active agent from hydrogel matrix, the models of drug release are classified as follows:

1.7.3.1. *Diffusion controlled delivery systems*

In case of macroporous hydrogels, with pore size much larger than the molecular dimensions of the drug, the diffusion coefficient can be related to the porosity and the tortuosity of the hydrogels.[51] However, for non-porous hydrogels and for porous gels with pore sizes comparable to the drug molecular size, the steric hindrance provided by polymer chains within the crosslinked networks decrease the drug diffusion coefficients.[51, 52, 53] Due to the usually high permeabilities of hydrogel networks and the advantages of *in situ* fabrication, most research efforts are focused on understanding diffusion-controlled release of encapsulated drugs from three-dimensional hydrogel matrices. Diffusion-controlled hydrogel delivery systems can be either reservoir or matrix systems.[54]

(i) Reservoir system:

In reservoir drug delivery system, a uniform polymeric membrane of hydrogel with a drug-enriched core (often termed as reservoir) is present and the membrane allows the diffusion of drug through it (Figure 1.2).[46, 47] As the system comes in contact with water, water diffuses into the system and dissolves the drug and provides a concentration equivalent to the saturation solubility of the drug (Cs). The drug diffuses through the membrane to the external environment and the concentration falls below Cs. The solid drug present in the core dissolves and restores the concentration back to Cs. This maintains a constant rate of release of drug from the core and follows zero order kinetics as long as the solid drug is present in the core. Once the solid drug is exhausted, the release becomes concentration dependent following first order kinetics. These kinds of drug delivery systems are mainly used to deliver the active agents by oral, ocular, uterine, or transdermal routes.

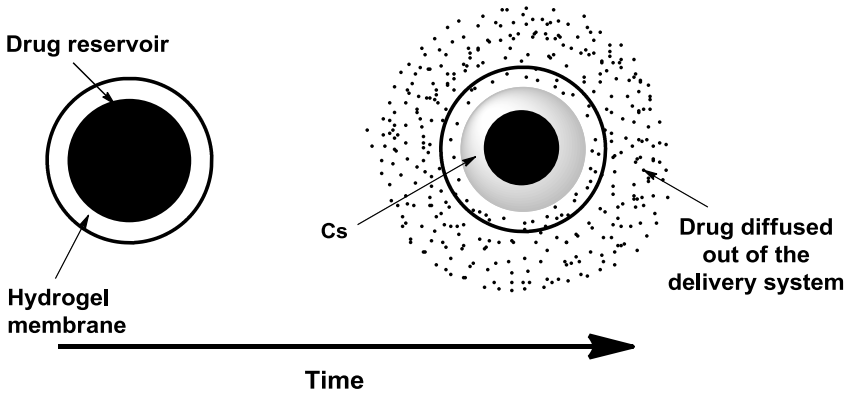

Figure 1.2: Drug delivery from a typical reservoir device

(ii) Matrix system:

Here the hydrogel acts as the matrix in which the active agent is homogeneously dispersed (Figure 1.3) and the properties of the matrix determines the release of

the drug. When the matrix is in contact with an aqueous medium, the system gets hydrated initially as water starts diffusing into the matrix. This hydration process starts at the surface and continues towards the center of the core. The release of drug is dependent on the diffusion of water into the matrix followed by the dissolution of the drug and finally the diffusion of the dissolved drug from the matrix. Initially inert polymer matrices were used to prepare such delivery systems but of late, bio-degradable polymers have also been used to design such delivery systems.

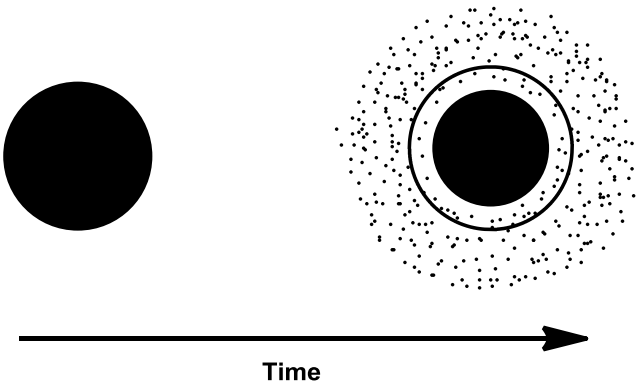

Figure 1.3: Drug delivery from a typical matrix drug delivery system

For a reservoir system where the drug depot is surrounded by a polymeric hydrogel membrane, Fick's first law of diffusion can be used to describe drug release through the membrane (equation 1.3):

$$J_A = -D\left[\frac{dC_A}{dx}\right] \tag{1.3}$$

Here, J_A is the flux of the drug, D is the drug diffusion coefficient, and C_A is drug concentration.

For a matrix system where the drug is uniformly dispersed throughout the matrix, unsteady-state drug diffusion in a one-dimensional slab-shaped matrix can be described using Fick's second law of diffusion (equation 1.4):

$$\frac{dC_A}{dt} = D\left[\frac{d^2C_A}{dx^2}\right] \quad (1.4)$$

Here, the drug diffusion coefficient is again assumed as a constant.

When diffusivity is concentration dependent the equation 1.5 is used:

$$\frac{dC_A}{dt} = \frac{d}{dx}\left[D(C_A)\frac{dC_A}{dx}\right] \quad (1.5)$$

Another empirical equation developed by Peppas *et al*. assumes a time-dependent power law function (equation 1.6).[57,58]

$$\frac{M_t}{M_\alpha} = Kt^n \quad (1.6)$$

Here, K is a structural/geometric constant for a particular system and n is designated as release exponent representing the release mechanism. Table 1.1 lists the n values for delivery matrices with different geometries and release mechanisms.[58] It is noteworthy that in a purely swelling-controlled slab-based delivery system, the fractional drug release (M_t/M_∞) appears to be zero-order as the release exponent equals unity. The power law is easy to use and can be applied to most diffusion-controlled release systems. In diffusion-controlled systems where n = 0.5, the power law is only valid for the first 60% of the release profile.

Matrix geometry	Diffusion-controlled delivery system (Case I)	Swelling controlled delivery system (Case II)
Slab	n = 0.50	n = 1.00
Cylinder	n = 0.45	n = 0.89
Sphere	n = 0.43	n = 0.85

Table 1.1: Release exponent values (n) in the empirical power law model

These empirical models can only predict the release profile after certain release experiments are conducted and have limited capability to predict how the release profiles will change as the chemical or network properties of the system are varied.

1.7.3.2. *Swelling controlled delivery systems*

Swelling controlled drug delivery devices, in a broader sense, are those in which swelling is the most important release rate controlling step but other mass transport processes also play a major role (eg: drug dissolution, drug diffusion and polymer dissolution). Swelling controlled delivery systems consists of hydrophilic polymeric networks. Hydrogels may undergo a swelling-driven phase transition from a glassy state where entrapped molecules remain immobile to a rubbery state where molecules rapidly diffuse. In these systems, the rate of molecular release depends on the rate of gel swelling. One example of swelling-controlled drug delivery systems is hydroxypropyl methylcellulose (HPMC).

After oral administration, HPMC polymer absorbs liquid and a rapid glassy-to-rubbery phase transition occurs once the glass transition temperature (Tg) is reached, causing the systematic release of loaded drugs. The drug release rates are

modulated by the rate of water transport and the thickness of the gel layer. Drug diffusion time and polymer chain relaxation time are the two key parameters that determine drug delivery from polymeric matrices. In swelling-controlled delivery systems the time-scale for polymer relaxation (λ) is the rate-limiting step. The Deborah number (De) is used to compare these two time-scales (equation 1.7)

$$De = \frac{\lambda}{t} = \frac{\lambda D}{\delta t^2} \quad (1.7)$$

In diffusion-controlled delivery systems ($De \ll 1$), Fickian diffusion dominates the drug release process and diffusion equations described in the previous section can be used to predict molecule release. In swelling-controlled delivery systems ($De \gg 1$), the rate of molecule release depends on the swelling rate of polymer networks.

1.7.3.3. *Chemically controlled delivery systems*

Chemically controlled release systems can be classified into two (i) purely kinetic-controlled release systems where polymer degradation (bond-cleavage) is the rate-determining step and diffusion term is assumed to be negligible; and (ii) reaction-diffusion-controlled release in which both reaction (e.g. polymer degradation, protein–drug interaction) and diffusion terms must be included in the model to accurately predict drug release.

(i) *Kinetic-controlled release*

There are two types of kinetic-controlled-release systems: (a) pendant chain (prodrugs) and (b) surface-eroding systems.

(a) Pendant chain (prodrugs)

Pendant chain systems are those in which the drugs are covalently linked to the hydrogel network and the rate of cleavage of spacer controls the rate of drug release. So drug diffusion is not the rate determining factor in such systems. Prodrugs or polymer-drug conjugates enhance the therapeutic efficacy of the drug and are useful for delivering substrates which are susceptible to proteolytic degradation like growth factors, peptide based drugs, etc. Generally, the release of covalently tethered prodrugs is determined by the degradation rate of the polymer–drug linkage. These systems are designed in such a way that the degradation of covalently linked prodrugs follows simple first order kinetics.

(b) Surface-eroding systems

Surface erosion is a phenomenon which occurs when the rate of water transport into the polymer is much slower than the rate of bond hydrolysis. But due to the high water content of hydrogels, this is not observed. Surface erosion is only seen in enzymatic-degrading systems where the transport of enzyme into the gel is slower than the rate of enzymatic degradation. Surface erosion of enzymatically degradable poly(ethylene glycol)-polycaprolactone block copolymer (PCL-b-PEG-b-PCL) hydrogels has been observed *in vitro* by Rice *et al*. when exposed to relatively high concentrations of lipase.[62]

Most of the models focusing on surface-eroding polymers are based on hydrolytic-degrading polymers. These relationships, however, can also be applied to enzymatically degradable, surface-eroding hydrogel systems. Surface-eroding matrices are advantageous for drug delivery applications as the structural integrity

of the carrier device is maintained during delivery and zero-order release of the encapsulated molecules can be readily obtained by appropriate choice of device geometry.

(ii) *Reaction-diffusion-controlled release* (*bulk degrading systems*)

With the development of more complicated drug delivery systems, mechanisms like diffusion, swelling or degradation alone was not sufficient enough to explain the drug release. For instance coupling of reaction and diffusion phenomena can be seen in bulk degrading networks where drug release profiles are governed by both network degradation and molecule diffusion.

1.8. Design and synthesis of glycopolymers: Multivalent recognition with lectins

Carbohydrates are involved in a myriad of biological events including cellular recognition, inflammation, signal transmission so on and so forth.[61-66] Even though there exist naturally occurring polysaccharides (figure 1.4), there is lot of interest in synthesizing and studying synthetic sugar containing polymers. Homo- or co-polymerisation of unsaturated carbohydrate derivatives yields synthetic polysaccharides with a chemically and biologically stable C-C backbone and pendent hydrophilic carbohydrate residues so-called 'glycopolymers'. This definition includes macromolecules presenting diverse architectures, comb polymers, dendrimers and cross-linking hydrogels. The first glycopolymer was synthesized in 1978 *via* free radical polymerization of acrylamide and allyl

glycosides of various sugars **7** (Figure 1.5) in water, using ammonium persulfate as initiator and tetramethylethylenediamine (TMEDA) as catalyst.

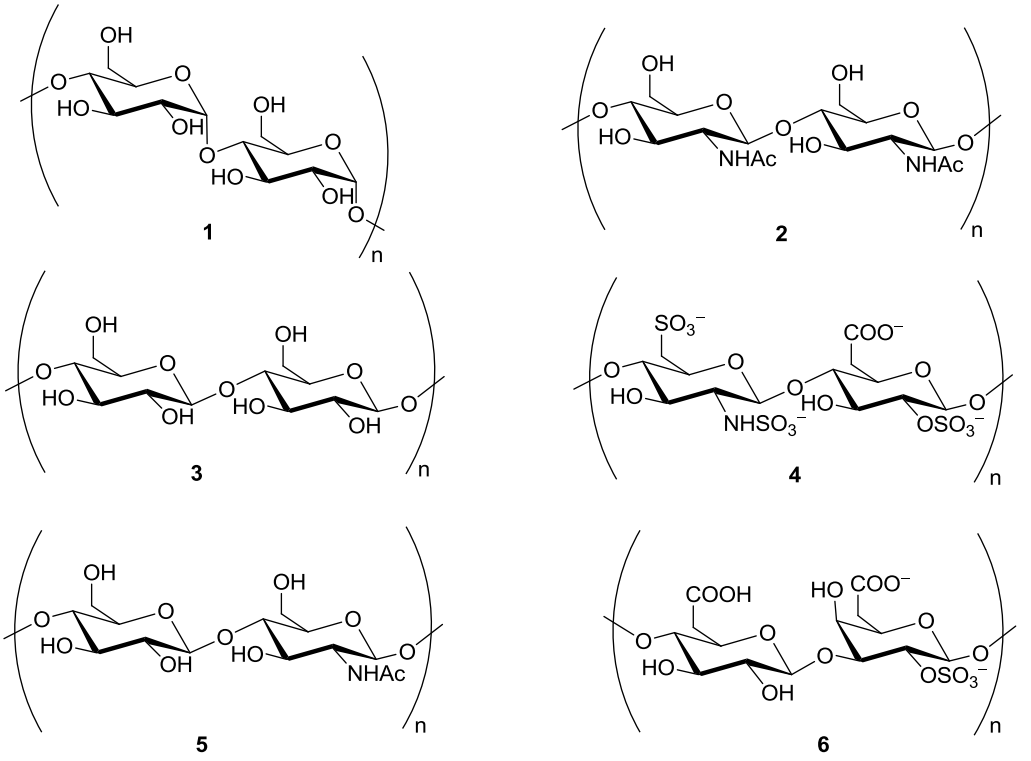

Figure 1.4: Structures of natural polysaccharides. (**1**) starch; (**2**) chitin; (**3**) cellulose; (**4**) heparin; (**5**) hyaluronan; (**6**) chondroitin sulfate.

Advances in synthetic chemistry have accelerated the preparation of well defined and multi-functional glycopolymers in a relatively facile manner.[67]

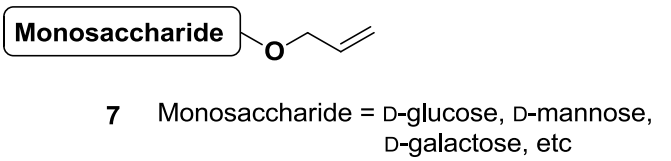

Figure 1.5: Allyl glucosides derived from various monosaccharides (**7**).

It is important to control the chain length, composition and topology of the glycopolymer since these factors determine the location/distance between the carbohydrates on the polymer chain.[68,69] Importantly, precise recognition properties can be achieved by an absolute control over the microstructure of the glycopolymer. The area of synthetic glycopolymers became popular in 1990s with the increasing interest in biomimics, and most of the attempts were based on the polymerization of monomers containing carbohydrate moieties.[70-74] In 1990, Kitazawa *et al*. reported an elegant method to obtain novel acrylic monomers containing a pendent monosaccharide 8–11 (Figure 1.6), by glycosidation of methyl glycosides with 2-hydroxyethyl acrylate or methacrylate in the presence of a heteropolyacid catalyst.

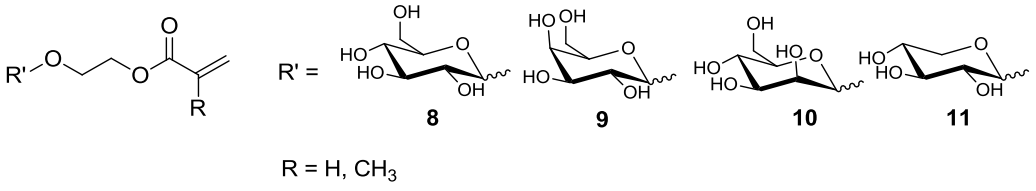

Figure 1.6: Methacrylate and Ethyl acrylate of glucopyranosyloxy (**8**), galactopyranosyloxy (**9**), mannopyranosyloxy (**10**), xylopyranosyloxy (**11**)

In 1992, Roy and coworkers reported a new method for synthesizing acrylamide monomers containing sugar residues. The glycosyl bromide and *p*-nitrophenol were reacted under phase transfer catalysis conditions, which gave 4-nitrophenyl-*β*-glycoside with total anomeric stereocontrol. This nitrophenyl derivative was then easily transformed into acrylamide-based monomer by reaction with

appropriate amine. Using this method, 4-acrylamidophenyl β-lactoside **12** was successfully synthesized (Figure 1.7).[75]

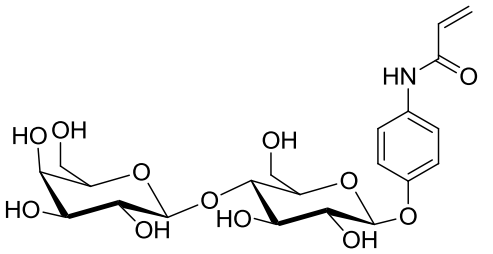

12

Figure 1.7: 4-acrylamidophenyl *β*-lactoside (**12**)

Polymerisation and co-polymerisation with various comonomers were easily carried out under free radical polymerisation conditions. Different techniques like free radical, controlled radical, anionic, cationic, ring opening and ring opening metathesis polymerization were utilized for polymerizing these glycomonomers (sugar carrying monomers).[72,76,77] Until last decade, very limited attempts were carried out to react a functional polymeric backbone with a carbohydrate moiety to obtain a glycopolymer. This was because of the difficulty in introducing sufficiently reactive pendant groups onto the polymer backbone to react with carbohydrates. Modification of poly (vinylalcohol) with 4-nitrophenyl carbonate groups was the first successful attempt to form synthetic glycopolymers (Figure 1.8).[78] The reactive nitrophenyl carbonate groups were transformed with D-glucosamine to form glycopolymers, which were subsequently investigated for their interaction with a commonly used lectin, Concanavalin A (Con A).[79]

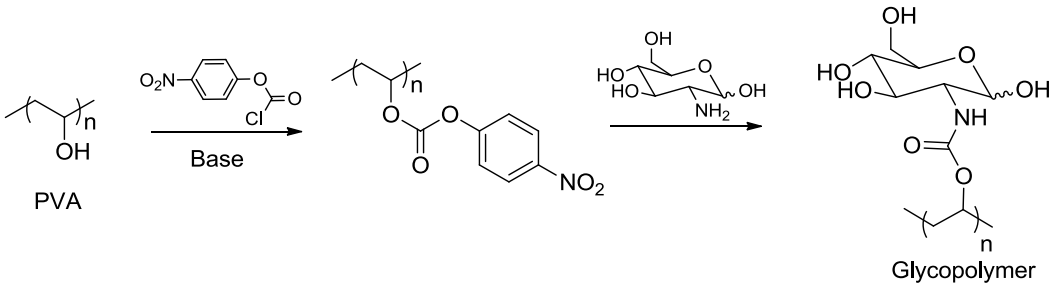

Figure 1.8: Coupling of D-glucosamine to polyvinyl alcohol functionalized with 4-nitrophenyl carbonate groups.

Carbohydrates can form a glycocode which can convey bulk of information. In peptides and oligonucleotides, the number of amino acids present and their sequences decide the information carried by them, whereas in carbohydrates, information is also encoded in the position and configuration (α or β) of the glycosidic units and in the occurrence of branch points. Therefore, it is calculated that four different monosaccharides can form 35,560 tetrasaccharides whereas four amino acids or nucleotides can form only 24 tetramers! Carbohydrates also become more diverse by functionalization of the hydroxyl groups. Thus, in theory, an enormous number of oligosaccharides can be derived from a relatively small number of monosaccharides. Concurrently due to their potential for coding biological information, carbohydrates were found on the surface of nearly every cell in the form of polysaccharides, glycoproteins, glycolipids or other glycoconjugates.[78]

As mentioned before, carbohydrates play a major role in many recognition events. Recognition is important for initializing variety of biological processes and the

first step in numerous phenomena based on cell–cell interactions, such as fertilization, embryogenesis, cell migration, organ formation, immune defense, microbial and viral infection, inflammation, and cancer metastasis.[80,81] These recognition processes are thought to proceed by specific carbohydrate–protein interactions. The proteins involved in such processes are most frequently found on cell surfaces and are generically named lectins. They have the ability to bind specifically and non-covalently to carbohydrates.[82] The mechanism involved in the carbohydrate–lectin interaction and the structures of the glycopolymers leading to these recognition processes is still largely unknown. Consequently, synthetic complex carbohydrates and carbohydrate-based polymers, which are "glycomimics", are emerging as an important tool for investigating glycopolymer–protein interactions.[83,84]

1.9. Lectin–carbohydrate interaction, "the cluster glycoside effect"

Lectins (latin: *legere* (to select)) are sugar-binding proteins that bind with carbohydrates reversibly but with high specificity. This class of proteins can be found in all biological systems and they play a pivotal role in many biological events such as cell adhesion. The reaction between lectins and carbohydrates form the basis of cell agglutination such as hemagglutination.[85,86] Cell recognition follows the concept of lock-and-key type of mechanism, as first mentioned by Emil Fisher in1897. More recently, Ambrosi *et al*. have described lectins as tools for the molecular understanding of the glycocode.

Hundreds of lectins have now been identified and isolated from plants, animals and microorganisms. All these lectins have certain biological properties in common such as the binding to carbohydrates, their diversity in terms of structure and size. Many of them can be grouped into families depending on their function or certain functional parameters. Lectins can be classified as follows based on their origin:

1.9.1. *Plant lectins*

1.9.1.1. *Legumes*[87]

The largest family among the simple lectins is the legume family with more than 70 lectins being isolated and many of them have been structurally characterized.[88] Main source of these lectins have been from seeds of plants belonging to the Fabaceae family. Molecular weights of legumes are usually below 40 kD and their interactions with carbohydrates often require the presence of Ca^{2+} and Mn^{2+} ions. They usually consist of 2 or 4 subunits with typically one binding site per subunit. The main representatives of the legume family are:

(a) Concanavalin A (Con A), lectin extracted from jack beans, is the most widely abundant lectin within the legume family. The abundance is due to the ease of isolation and their interactions with wide range of saccharides has led to many in-depth studies of this member of the legume family.[86,89] Con A has a strong affinity to mannose, but binds to glucose as well.

(b) Peanut agglutinin (PNA, Arachis hypogaea), legume which binds specifically to galactose, preferably to galactosyl (β-1,3) *N*-

acetylgalactosamine. PNA does not require any divalent cations for binding, but binding is enhanced in the presence of Ca^{2+} ions.

1.9.1.2. *Cereal lectins*

Cereal lectins consist of two subunits with usually 2 binding sites per subunit. The presence of ions such as Ca^{2+} is not required. Cereal lectins are known to be rich in disulfide bonds. Wheat germ agglutinin (WGA) consists of two identical subunits whilst being rich in cysteine.[90]

Even though function of plant lectins is unknown, but it has been suggested that they act as defense system for the plant.

1.9.2. ***Animal lectins***

Animal lectins were originally divided into C-type lectins (need Ca^{2+}-ions) and S-type lectins (sulfydryl-dependent). Later more and more groups were identified and the list now includes: C-type, S-type (galectins), I-type (siglecs and others), P-type (phosphomannosyl receptors) etc. and some single lectins that cannot yet be assigned to any of these groups.[91] Only C-Type and S-Type (Galectins) are discussed here:

1.9.2.1. *C-Type*

C-Type lectins are dependent on Ca^{2+} ions for their reactions with carbohydrates. They can have complex structures consisting of a carbohydrate recognition domain (CRD) of around 120 amino acids. C-Type lectins therefore, can have a variable number of subunits with 1–8 binding sites per subunit.

A C-type lectin is the endocytic lectin, which is more frequently described as the hepatic asialoglycoprotein (hepatic lectin), a lectin specific for galactose/*N*-acetylgalactosamine.[85,92] In depth studies have been carried out using copolymers with galactose moieties for the interactions with hepatic lectins and results suggested that high sugar concentrations facilitated binding.[93,94]

1.9.2.2. *S-Type (Galectins)*

S-type lectins which are now called Galectins,[95] are involved in a range of activities like from inflammation response to a suggested role in cancer. A common trait in galectins is the affinity for *β*-galactosides, preferably as lactose and *N*-acetyl lactosamine, and a significant sequence similarity in the carbohydrate-binding site.

Functions of animal lectins [91]

Animal lectins play a pivotal role in a variety of functions including:

- Self/non-self recognition
- Intracellular routing of glycoconjugates
- Molecular chaperones during glycoprotein synthesis
- Mediation of endocytosis
- Cellular growth regulation
- Extracellular molecular bridging
- Cell –cell interactions for homing and trafficking
- Scavenging of cellular debris; anti-inflammatory action
- Urate transport

- Immune regulation (suppression or enhancement)

Most saccharides bind to the protein receptors with high specificity but weakly, which is not sufficient enough to control the *in-vivo* events mediated by protein–carbohydrate binding. Hence, multiple interactions between carbohydrates and lectins are necessary to achieve strong binding. In nature, carbohydrate–binding proteins are typically aggregated into higher-order oligomeric structures, which suggest that binding limitations can be circumvented by introducing multivalency. Also, most of the multimeric carbohydrates (glycopolymers) which have been synthesized show some enhancement in the activity compared to the corresponding monovalent ligand on a valence-corrected basis. This enhancement is known as the "cluster glycoside effect".[84] The mechanism by which multivalent ligands interact is still not clear, but it is known that the cluster glycoside effect relies on aggregation.

1.9.3. *Lectin Binding assays*

Carbohydrate-lectin binding assays can be conducted through a wide variety of methods, ranging from the earliest hemagglutination inhibition assay (HIA), evaluated by Landsteiner, to the sophisticated surface plasmon resonance (SPR), which uses materials absorbed onto metal.[96,97] The basic principle behind lectin binding assays is the formation of isolated complexes between lectins and their ligands.[98]

HIA is one of the earliest assay methods used for studying the interactions between viruses/viral antigens and their corresponding ligands. Ligand solutions

are initially placed at different concentrations into the microwells, followed by the addition of soluble lectin to allow precipitation of aggregates. After complete precipitation, the minimum concentration of carbohydrate that inhibits the hemagglutination reaction is reported. In order to determine physical parameters, like carbohydrate-lectin binding constants isothermal titration microcalorimetry (ITC) is used, which involves quantification of the heat generated (enthalpy) from the binding.[99] Surface Plasmon Resonance (SPR) is another technique which utilizes the flow of lectin solution over a gold surfaced chip with immobilized ligands resulting in a change in the refractive index at the surface. The binding constant is calculated from the removal of the bound lectin during the flow of buffer solution.[96] Turbidimetric assays carried out using UV-vis spectroscopy is now more frequently used as a method in determining the successful binding of glycopolymers with lectins.[100] Two-dimensional immunodiffusion tests (double diffusion agar, DDA) is also a technique for identifying specific binding between carbohydrates and lectins.[72] There are other complementary techniques, such as using a quartz crystal microbalance (QCM), measuring the weight of the attached lectin, and electrophoresis which determines the molecular size of proteins adhered. The binding assay solution should also be chosen with care. Narain and Xu found that in their system, the use of a certain concentration of Ca^{2+} and Mn^{2+} salts with the same anion (Cl^-) greatly enhanced the aggregation upon interaction of glycopolymer with proteins.[101, 102]

The quantification of binding constant can be done by fluorescence spectroscopy using Scatchard equation (1.8).[103]

$$\frac{[S]}{\Delta F} = \frac{1}{\Delta F_{max}\,[S]} + \frac{1}{\Delta F_{max}\,K_a} \qquad (1.8)$$

Where [S] is the glycopolymer concentration, ΔF the fluorescence intensity, and Ka the association constant. ΔF_{max} is the maximum fluorescence intensity.

1.10. Aggregation induced emission

Aggregation of luminophores will lead to two competing effects of photoluminescence (PL): aggregation-caused quenching (ACQ) and aggregation-induced emission (AIE). The ACQ or AIE effect exhibited by luminogens depends on the molecular structure as well as the intermolecular packing. When aggregation reduces luminescence the effect is called ACQ, which is a major obstacle reducing the applicability of most of the luminescent materials. On the other hand if aggregation enhances fluorescence it is AIE. In ACQ phenomena, addition of a poor solvent in to the solution of the luminescent molecule makes it less emissive. Whereas in AIE addition of a poor solvent makes the system more emissive.

ACQ is an effect common to most aromatic hydrocarbons and their derivatives The structural reason for this is that, conventional luminophores are made up of planar aromatic rings (e.g., perylene, figure 1.9), since electronic conjugation and π-π stacking is an important structural strategy to be fulfilled for luminescence.

But at higher concentrations the chances of formation of excimers or exciplexes are more leading to quenching.[104]

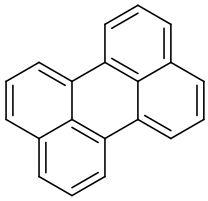

Figure 1.9: Structure of perylene

Hexaphenyl silole (HPS) was the first AIE molecule to be investigated. In the aggregates, the HPS molecules cannot pack through a π–π stacking process due to its propeller shape, while the intramolecular rotations of its aryl rotors are greatly restricted owing to the physical constraint. This restriction of intramolecular rotations (RIR) blocks the non-radiative pathway and opens up the radiative channel. As a result, the HPS molecules become emissive in the aggregated state (Figure 1.10).

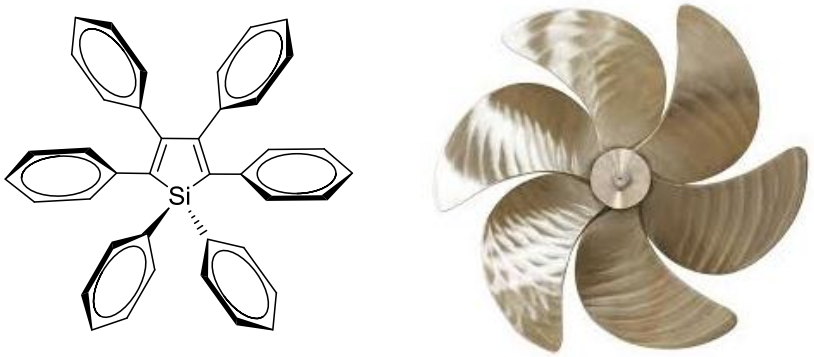

Figure 1.10: Propeller type structure of HPS

Different classes of luminogens which show AIE effect are:

1. Hydrocarbon luminogens
2. Heteroatom containing luminogens
3. Luminogens with cyanosubstituents
4. luminogens with hydrogen bonds
5. Polymeric luminogens
6. Organometallic luminogens

The mechanisms by which the above mentioned materials exhibit luminescence are given below:

1.10.1. *Planarity and rotatability*

The intramolecular rotations of aromatic rotors in an AIE luminogen are faster in solution state and it serves as a relaxation channel for its excitons to decay non radiatively. Whereas in the aggregated state, the intramolecular rotations are restricted due to physical constraint and this blocks the non-radiative pathway and opens the radiative channel.[105]

1.10.2. *Intramolecular restrictions*

One can tune the emission performance of a molecule by modulating its conformational stability. A covalent linkage can lock or stabilize molecular conformation, hinder intra-molecular rotation and thus enhance the emission intensity. For example, in case of biphenyl based luminogens (Figure 1.11) the methylene bridge makes the conformation more planar and restricts the intramolecular rotations.

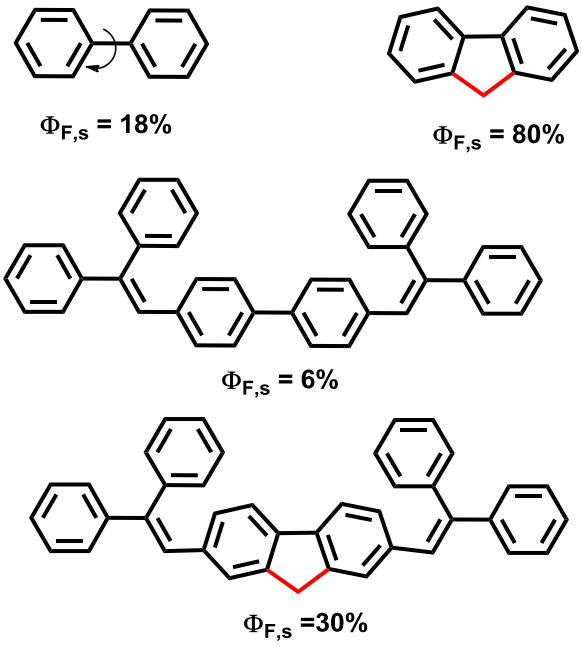

Figure 1.11: RIR effect on luminescence behaviours of biphenyl-based luminogens.

Like the covalent chemical bonds, non-covalent physical interactions such as charge-transfer complexation can also trigger molecular RIR processes.[103]

1.10.3. *Intermolecular interactions*

Conformation of a molecule can also be influenced by intramolecular forces. The molecular conformations can be affected by changes in the surrounding environments like increasing viscosity; decreasing temperature and elevating pressure. These variations may lead to enhancement in the photoluminescence intensity. Luminescence behaviors can be influenced by rigidification of structure by intermolecular processes. For eg: the phenyl ring in tetra phenyl ethylene (TPE) is twisted out of the central ethane plane by ~50^{o} (Figure 1.12).

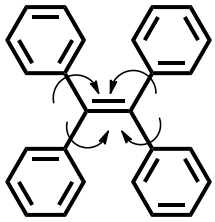

1,1,2,2-Tetraphenylethene (TPE)

Figure 1.12: Structure of AIE active TPE molecule

In crystalline state, the propeller shape of TPE molecule prevents π-π stacking and excimer formation. The multiple C-H….π hydrogen bonds formed between the phenyl rings of one TPE molecule with phenyl rings of other adjacent TPE molecule, stiffen the conformation and enhance their light emission. Many such molecules are known to show enhanced emission by such intermolecular interactions.

1.11. Technological applications

Wherever a RIR phenomenon is involved, AIE effect can be utilized. Various applications of AIE based luminogens are:

1. Electroluminescence: AIE luminogens covering the whole range of visible light spectra have been designed and prepared. The performance of conventional OLEDs (Organic Light Emitting Diodes) based on flat luminogens are unsatisfactory because of ACQ problem. Therefore AIE materials which are emissive in aggregated state are promising materials for manufacture of highly efficient OLEDs.
2. Fluorescence sensors: Conventional fluorescent sensors are fluorescence turn off type, i.e. the emission of these molecules is quenched when they form aggregates with some chemical species or biological analytes.

Whereas AIE effect facilitates the development of sensing systems which work on fluorescence turn on phenomena. These sensors are more effective than turn off type because of high sensitivity and are less likely to develop positive false signals. AIE luminogens have been designed for sensing explosives, pollutants like Hg^{2+}, CN^{-} etc., and also for studying various sugar - lectin interactions.

3. Cell imaging: Most of the luminophores especially ionic luminophores, which are used for cellular imaging face a major problem of photobleaching at low concentration and perturbation of membrane potential as well as cellular physiology at higher concentration. During cell division process, the cellular dyes may diffuse into the extracellular media leading to a concentration gradient which leads to decrease in emission of the stained cells

AIE luminogens can overcome many of these problems as they can be used in higher concentrations in cell imaging processes and the nanoaggregates formed cannot escape from the cellular compartment. Also they remain internalized for a long period of time so that we can monitor the processes like growth of a specific cell line.

CHAPTER 2

EXPERIMENTAL AND TECHNIQUES

2.1. Introduction

Silver nanoparticles loaded hydrogels, glycopolymeric hydrogels, drug loaded polysaccharide glycopolymer composite beads and self assembled fluorescent nanoparticles have been synthesized for various biomedical applications like wound dressings, drug delivery, cell imaging etc. This chapter deals with the methodologies used for synthesis of these material and different techniques used for their characterization as well as studying their applications in biomedical field.

2.2. Materials

Silver nitrate (Merck), gum acacia (S D Fine Chemicals), polyvinyl alcohol (Molecular weight approximately 125,000, S D Fine Chemicals), were of analytical grade, and were used, without further purification. LB agar, used for antibacterial studies, was obtained from Hi Media Laboratories. Methanol, dichloromethane, pyridine, triethylamine, were purified and dried before use for the synthesis of glycoacrylamides. The n-hexane used was the fraction distilling between 40–60 ºC. All the other chemicals including acryloyl chloride, Chitosan (CS) (Molecular weight ~ 1,25,000 Da and 85% deacetylation**)**, succinic anhydride (SA) and doxorubicin hydrochloride (DOX) were procured from either Sigma-Aldrich or Fluka. MTT (3-(4,5-dimethyl thiazol-2-yl)-2,5-diphenyl tetrazolium bromide), Staurosporine, lyophilized powders of Concanavalin A (Con A) from *Canavalia ensiformis*, Peanut Agglutinin (PNA) from *Arachis hypogaea*, FITC conjugates of both Concanavlin A (FITC-Con A) as well as Peanut agglutinin (FITC-PNA) and Bovine Serum Albumin (BSA) were

purchased from Sigma-Aldrich and were used directly. 0.01 M phosphate-buffer saline (PBS) at pH 7.4 was prepared by diluting 10 X concentrated PBS purchased from sigma into distilled water with 150 mM NaCl, 1 mM NaN_3, 1 mM $CaCl_2$ and 1 mM $MnCl_2$. DMEM cell culture medium, penicillin and streptomycin were purchased from Hi Media, Mumbai, India. Fetal Bovine Serum (FBS) was procured from Invitrogen BioServices India Pvt. Ltd. γ–irradiation was carried out in 1 cm diameter closed glass vials under nitrogen atmosphere, using an indigenous Cobalt-60 γ-irradiator (dose rate 0.75 kGy/h). Water, with conductivity 0.6 μS cm^{-1} or lower, obtained from Millipore Milli-Q system, was used for the preparation of aqueous solutions, and was purged with nitrogen, wherever required. Glassware's were cleaned, using chromic acid, followed by rinsing with distilled water, and then, with water, purified by Millipore Milli-Q water purification system and dried in an oven at 110 ^oC.

2.3. Synthetic strategies for hydrogels and polymeric beads

2.3.1. *Synthesis of hydrogels by γ-radiation induced technique*

Many methods are known for the synthesis of hydrogels out of which the greener and cleaner technique is the radiation induced one. Even some of the degrading type of polymers which cannot crosslink upon irradiation, can be utilized for making hydrogels by irradiating along with crosslinking type polymers. The crosslinking density can be controlled by varying the radiation dose and relative concentration of the two types of polymers. This strategy was utilized for the synthesis of PVA/gum acacia hydrogels wherein AgNPs were also generated *in*

situ by the reducing radicals formed during γ-radiolysis. This technique helps in synthesizing sterile nanoparticles - loaded hydrogels in a single step. Purely synthetic hydrogels were also synthesized by γ-radiation induced method. This method was also employed for production of biocompatible glucose based sterile hydrogels from the synthesized non-cytotoxic mono- and bisacrylamide derivatives. The details of the procedures and experimental parameters will be discussed in chapter 3 and 4. The synthesized hydrogels were characterized by different techniques, as discussed in the subsequent sections.

2.3.2. *Synthesis of glycopolymer stabilized N-succinyl chitosan beads*

The *N*-succinyl chitosan beads were synthesized by ionic crossslinking method. But these beads are not stable at high ionic strength of body fluids which makes them unsuitable for controlled drug delivery purposes. Hence the synthesized beads were stabilized by glycopolymer, which forms an interpenetrating network in the bead thereby stabilizing it. The succinyl units in the beads facilitate the loading of the cationic drug doxorubicin and also pH dependent delivery of the drug. The appropriate swelling kinetics of the hydrogel network in the beads also helps in slow and sustained delivery of the drug. The experimental parameters will be discussed in detail in the respective chapters.

2.3.3. *Synthesis of self assembled fluorescent glycoacrylamide nanoparticles*

Glycoacrylamides, both mono and bisacrylamide were synthesized, in a high yielding reaction sequence starting with D-glucose. The synthesis was designed in such a way that these molecules become emissive upon aggregation in aqueous

media. The extensive hydrogen bonding of the hydrophilic sugar units makes the hydrophobic acrylamide side chain to align in a position with restricted motion, leading to π –π stacking. The stacking of the π electrons makes them emissive and thus exhibit Aggregation Induced Emission (AIE) phenomenon. The characterization of the size of the self assembled particles, pH dependency, emission characteristics etc. is described in detail in chapter 6.

2.4. Analytical Methods

2.4.1. *Scanning electron microscopy (SEM)*

SEM technique unlike optical microscopy provides insight into the surface morphology, particle size, magnetic domains and surface defects of materials. SEM can achieve higher magnifications as it uses a focused electron beam to scan the surface. In a typical SEM, a source of electrons is focused into a beam of a very fine spot size of ~5 nm having energy ranging from a few hundred eV to 50 keV, to examine a very small area of an object.

Accelerated electrons originating from a filament in an electron gun are focused to the specimen in a vaccum chamber. These accelerated electrons interacts with samples and generate signals which includes secondary electrons, back scattered electrons (BSE), differential back scattered electrons, characteristic X-rays, visible light and heat. Secondary electrons (SE), with energies between 0 and 50 eV, are easy to collect, and can be used over a wide range of incident beam energies. The secondary electrons (SE) are ejected from the specimen, and have energies lower than that of primary electrons. SEs are created near the surface,

and give idea about the morphology and topography of the sample. BSEs are generated when the primary electrons interact with the nucleus of a sample atom, and get scattered in any direction with little loss of energy. These BSEs are more energetic than SEs and therefore can emerge out from a greater depth within the sample. Hence unlike SEs, the BSEs will neither carry much information about sample topography nor will it be highly resolved in space. The contrast in the BSE image depends on atomic number as well as magnetic and crystallographic nature of the sample. BSEs illustrate contrast in composition of multiphase samples.

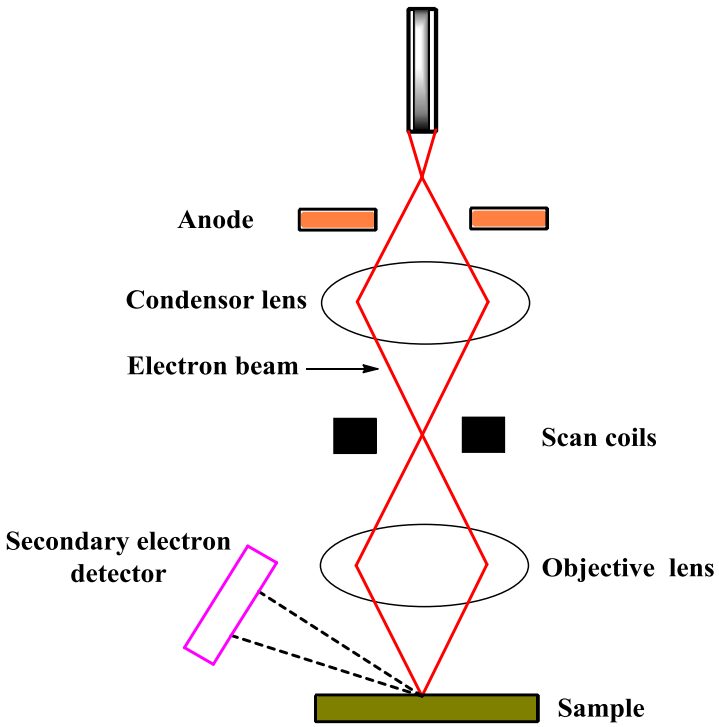

Figure 2.1: Various components of a typical SEM

Recording SEM images of the organic or non conductive samples, faces a major problem of destruction of sample due to build-up of charges, or the strong electric currents produced by the electron beam. Hence, such samples should be coated with a thin layer of conductive material, before recording the image. Depending on the type of interactions, the emitted rays are detected by a silicon-lithium (Si (Li)) detector. Each signal is collected, amplified and corrected for absorption and other effects to give an image. The schematic of a typical SEM is shown in figure 2.1. The porosity and the crosslinking density of the hydrogels as well as hydrogel beads were studied using MECK-FEI Model NOVA Nanosem 450 scanning electron microscope.

2.4.2. *Transmission electron microscope (TEM)*

TEM is a technique which operates on the same basic principles as that of a light microscope, but uses electrons instead of light. The lower wavelength of electrons compared to that of light, results in better resolution of the TEM image compared to a light microscope image. TEM uses electromagnetic lenses rather than glass lenses to focus the electrons into a very thin beam. The electron beam then travels through the specimen, depending on the density of the material, out of which some are scattered and disappears from the beam.

At the bottom of the microscope the unscattered electrons hit a fluorescent screen, which gives rise to a "shadow image" of the specimen with its different parts displayed in varied darkness according to their density. The image can be studied directly by the operator or photographed with a camera. The structures of the self

assembled particles were studied using Zeiss-Carl (Libra-120) transmission electron microscope at an accelerating voltage of 120 kV. The schematic of a typical TEM is shown in figure 2.2.

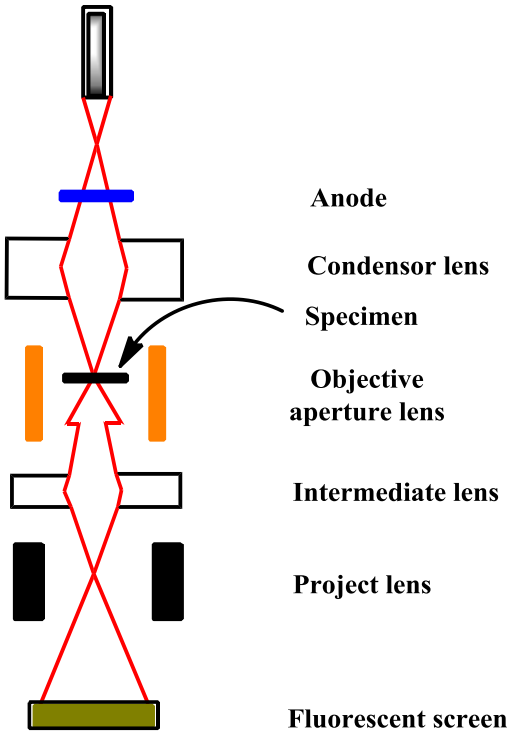

Figure 2.2: Schematic diagram of TEM.

2.4.3. *Confocal fluorescence microscopy*

Confocal fluorescence microscopy is a microscopic technique that provides true three-dimensional (3D) optical resolution. In microscopy, 3D resolution is generally realized by designing the instrument so that it is primarily sensitive to a specimen's response coming from an in-focus plane, or by subsequently removing the contributions from out-of-focus planes. Several techniques have been developed to achieve this. True 3D resolution is accomplished by actively

suppressing any signal coming from out-of-focus planes. This is achieved by using a pinhole in front of the detector as schematically depicted in figure 2.3.

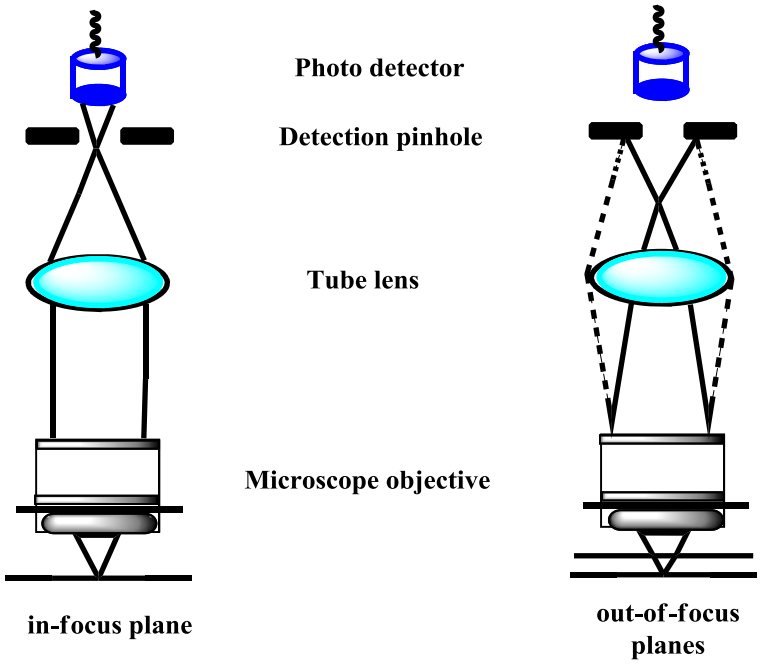

Figure 2.3: Picture depicting the principle of confocal fluorescence microscopy. Light coming from out-of-focus planes is largely blocked by a pinhole in front of the detector.

Light originating from an in-focus plane is imaged by the microscope objective such that it freely passes the pinhole, whereas light coming from out-of-focus planes is largely blocked by the pinhole. In a confocal fluorescence microscope (Figure 2.4), the specimen is generally illuminated by a laser. The light coming from the laser passes through an (excitation) pinhole, is reflected by a dichroic mirror, and focused by a microscope objective to a small spot in the specimen. A fraction of the fluorescence emitted by the fluorophores in the specimen is collected by the microscope objective and imaged onto the detection pinhole in

front of a photo-detector. The dichroic mirror reflects light of a shorter wavelength while transmitting that of a longer wavelength. Specific dichroic mirrors can be made for the relevant wavelength regions of excitation and fluorescence. By having a confocal pinhole, the microscope is really efficient at rejecting the out of focus fluorescent light.

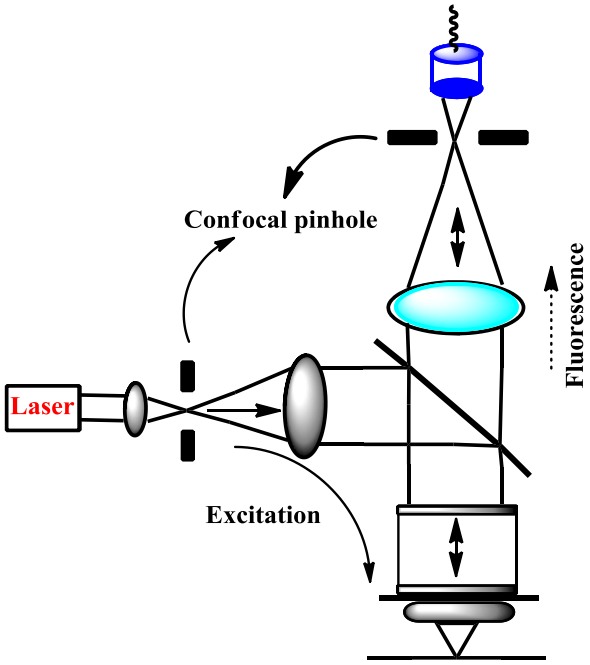

Figure 2.4: Schematic of excitation of the specimen in confocal fluorescence microscopy by a laser.

2.4.4. *Fourier transform infra-red (FT-IR) spectroscopy*

When IR radiation passes through the sample a part of it is absorbed and the remaining is transmitted. The resulting spectrum is due to the molecular absorption and transmission, creating a molecular fingerprint of the sample. Two unique molecular structures do not produce the same infrared spectrum like fingerprints. It can identify different functional groups present in organic and

inorganic materials. For example, double and single bonds associated with carbon oxygen and carbon hydrogen (associated with sp^2 and sp^3 carbon) bonding (=C-H,-C-H, C-O and C=O) can be distinguished by IR absorption.

When IR radiation is illuminated on a sample, the vibrating bonds in the molecule absorb energy of the incoming radiation which leads to either bending or stretching of a molecule or functional group.

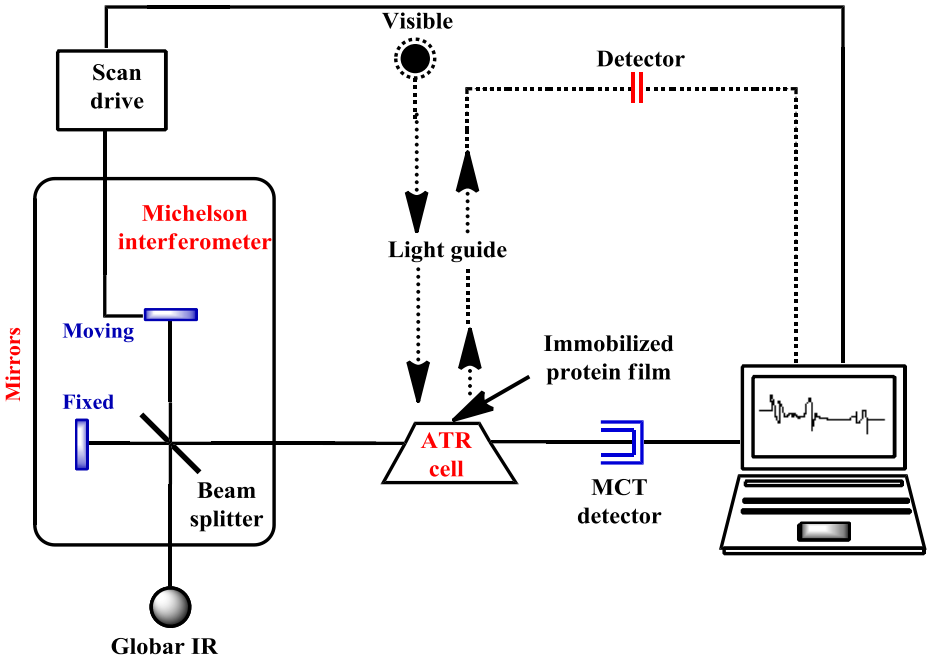

Figure 2.5: Schematic of FT-IR spectrometer equipped with ATR-cell.

The main part of the FT-IR spectrometer is a Michelson interferometer composed of a beam-splitter and two mirrors: one is fixed- and other is moving which produce the interference pattern. Infra red spectroscopy measures the absorption of this incident infra-red radiation as it passes through the vibrating atoms of a molecule. Only those vibrations are IR active which are associated with changes

in dipole moments. A typical instrumentation of IR is shown in figure 2.5. The IR spectra of the polymer samples were recorded using diamond attenuated total reflectance (ATR) with IR Affinity, Shimadzu spectrophotometer.

2.4.5. *UV-visible absorption spectroscopy*

UV-vis spectrophotometers are commonly used to determine the concentration of an absorbing species in a solution/solid and to study the molecular structure and electronic excitations. When the energy of the excited state of any atom/molecule/radical/ion resonates with the photon energy, absorption occurs and the intensity of the transmitted light is decreased which gives rise to an absorption band.

The principle of UV-visible absorption spectroscopy is based on the "*Beer-Lambert's Law"*. It states that "*A beam of light passing through a solution of absorbing molecules transfers energy to the molecules, as it proceeds, and, therefore decreases progressively in intensity. The decrease in the intensity, or irradiance, dI, over the course of a small volume element is proportional to the irradiance of the light entering the element, the concentration of absorbers (C) and the thickness of the absorbing element, dl*.

Mathematically it can be expressed as

$$-dI/dl \propto Ic \qquad (2.1)$$

or

$$dI/I = kcdl \qquad (2.2)$$

where, k is the constant of proportionality and is called absorption coefficient.

The integrated form is given as

$\ln I_0/I = kcl$ (2.3)

or

$\log I_0/I = (k/2.303)cl$ (2.4)

$k/2.303 = \varepsilon$ (Extinction coefficient)

For any absorbing substance (solution/solid) absorbance 'A' is defined as

$A = \log I_0/I$ (2.5)

From eqn. 2.4 and 2.5, the absorbance can be written as

$A = \varepsilon cl$ (2.6)

UV-visible spectra were recorded using Jasco V-650 spectrometer. A typical instrumentation of a double beam UV-vis spectrophotometer is shown in figure 2.6.

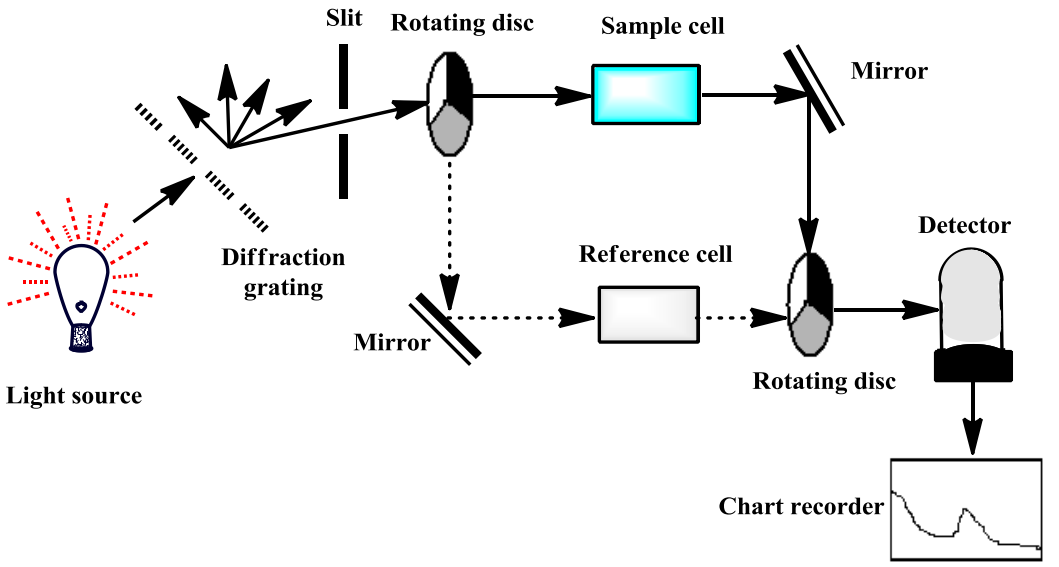

Figure 2.6: A schematic of the UV-visible spectrophotometer

2.4.6. *Fluorescence spectrophotometry*

Fluorescence spectrophotometry is a fast, simple and inexpensive method to determine the concentration of an analyte in solution based on its fluorescent properties. In fluorescence spectroscopy, a beam with a wavelength varying between 180 and ~800 nm passes through a solution in a cuvette. The light that is emitted by the sample is measured from an angle. In fluorescence spectrophotometry both an excitation spectrum (the light that is absorbed by the sample) and/or an emission spectrum (the light emitted by the sample) can be measured. The concentration of the analyte is directly proportional to the intensity of emission.

Intensity and shape of the spectra while recording emission spectra is dependent on various factors like:

- Excitation wavelength
- Concentration of the analyte solvent
- Path length of the cuvette
- Self-absorption of the sample

The schematic of a fluorimeter shown in figure 2.7 depicts that the light source and the detector are at 90^{o} angle and the sample cuvette is at the intersection of the two beam paths. The 90^{o} angle is maintained to prevent interference from the transmitted excitation light. Fluorescence spectroscopy is primarily concerned with electronic and vibrational states of molecules. The species under study is first excited, by absorbing a photon, from its ground electronic state to one of the

various vibrational states in the excited electronic state. Intermolecular collisions cause the excited molecule to lose vibrational energy until it reaches the lowest vibrational state of the excited electronic state.

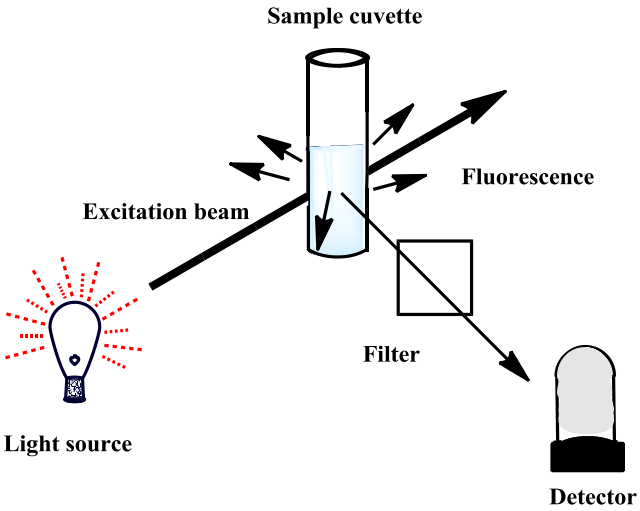

Figure 2.7: Schematic diagram of a fluorescence spectrophotometer

This can be visualized with a Jablonski diagram as shown in figure 2.8. As molecules may drop down into any of several vibrational levels in the ground state, photons are emitted with different energies, and thus frequencies. Therefore, by analyzing the different frequencies of light emitted in fluorescence spectroscopy, along with their relative intensities, the structure of the different vibrational levels can be determined. In a typical fluorescence (emission) measurement, the excitation wavelength is fixed and the detection wavelength varies, while in fluorescence excitation measurement the detection wavelength is fixed and the excitation wavelength is varied across a region of interest.

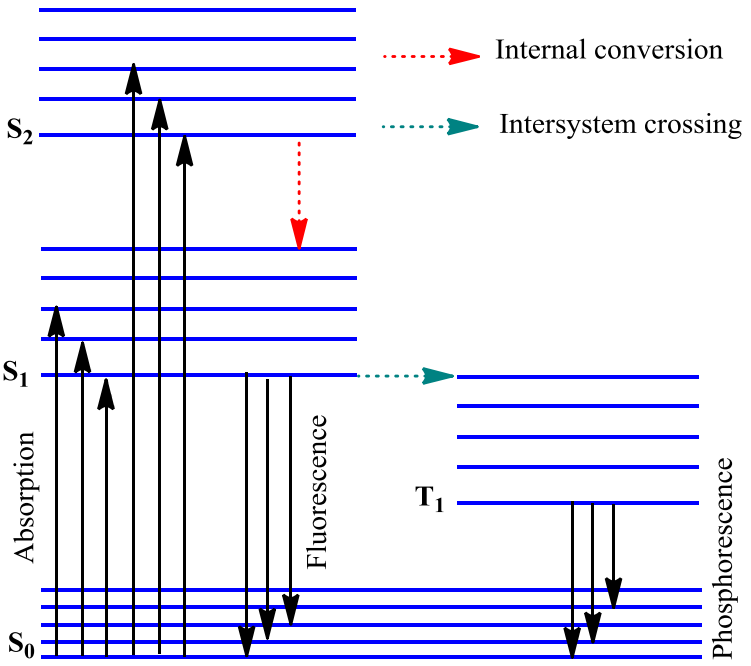

Figure 2.8: Jablonski diagram

The fluorescence measurements were carried using Jasco Spectrofluorometer FP-8500.

2.4.7. *Nuclear magnetic resonance spectroscopy*

Nuclear Magnetic Resonance (NMR) spectroscopy is a powerful and theoretically complex analytical tool. The information obtained from the NMR spectra about the nuclei, can be utilized to deduce the chemical environment of a specific nuclei.

Subatomic particles (electrons, neutrons and protons) are imagined to be spinning about their own axis. The nuclei of an atom are like a charge particle, which generates a magnetic field because of its spin. In many atoms (such as ^{12}C) these spins are paired against each other, such that the nucleus of the atom has no overall spin. However, in some atoms (such as ^{1}H and ^{13}C) the nucleus does

possess an overall spin. The rules for determining the net spin of a nucleus are as follows;

1. If the number of neutrons **and** the number of protons are both even, then the nucleus has **NO** spin.
2. If the number of neutrons **plus** the number of protons is odd, then the nucleus has a half-integer spin (i.e. 1/2, 3/2, 5/2)
3. If the number of neutrons **and** the number of protons are both odd, then the nucleus has an integer spin (i.e. 1, 2, 3)

Quantum mechanics tells us that a nucleus of spin I will have $2I + 1$ possible orientations. A nucleus with spin 1/2 will have 2 possible orientations. In the absence of an external magnetic field, these orientations are of equal energy (Figure 2.9). The nucleus which is spinning on its own axis, in the presence of a magnetic field, will precess around the magnetic field. The frequency of precession is termed the larmor frequency, which is identical to the transition frequency. If energy is absorbed by the nucleus, then the angle of precession will change.

In case of ½ spin nucleus, the magnetic moment "flips", so that it opposes the applied field. This generates two spin states +1/2 and -1/2 as shown in figure 2.9. Each level is given a *magnetic quantum number, m*. When the nucleus is in a magnetic field, the initial populations of the energy levels are determined by thermodynamics, as described by the Boltzmann distribution.

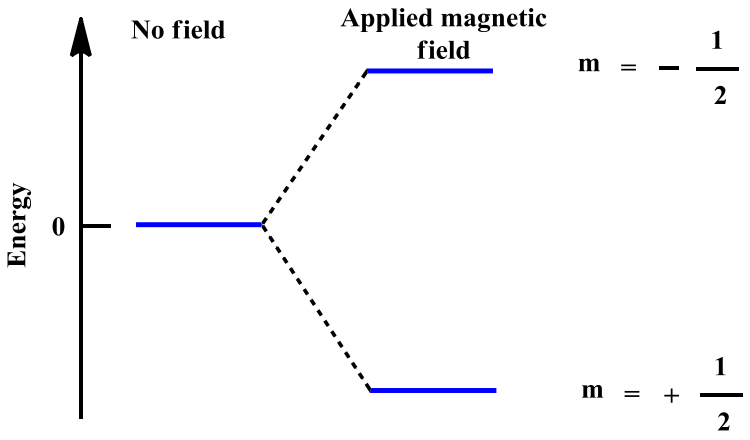

Figure 2.9: Energy levels of a nucleus with spin quantum number ½.

This is very important, and it means that the lower energy level will contain slightly more nuclei than the higher energy level. It is possible to excite these nuclei into the higher energy level with electromagnetic radiation. The frequency of radiation needed is determined by the difference in energy between the two levels. The nucleus has a positive charge and is spinning. This generates a small magnetic field. The nucleus therefore possesses a magnetic moment, μ, which is proportional to its spin, *I*.

$$\mu = \frac{\gamma I h}{2\pi} \qquad (2.7)$$

The constant, γ, is called the *magnetogyric ratio* and is a fundamental nuclear constant which has a different value for every nucleus, *h* is the Planck's constant.

The energy of a particular level is given by;

$$E = -\left(\frac{\gamma h}{2\pi}\right) mB \qquad (2.8)$$

Where *B* is the strength of the magnetic field at the nucleus.

The difference in energy between the levels (the transition energy) can be found from equation 2.9.

$$\Delta E = -\frac{\gamma h B}{2\pi} \qquad (2.9)$$

This means that if the magnetic field, *B*, is increased, so is ΔE. It also means that if a nucleus has a relatively large magnetogyric ratio, then ΔE is correspondingly large. The magnetic field experienced by the nucleus is not equal to the applied magnetic field, as the electrons around the nucleus shield it from the applied field. The difference between the applied magnetic field and field at the nucleus is termed as nuclear shielding. The precise resonance frequency of the energy transition is dependent on the extent of nuclear shielding, which is in turn dependent on the chemical environment. The chemical shift of a nucleus is the ratio of the difference between the resonance frequency of the nucleus and a standard and the resonance frequency of the standard. This quantity is reported in ppm and is given by the symbol δ.

$$\delta = \frac{(\nu - \nu_{ref}) \times 10^6}{\nu_{ref}} \qquad (2.10)$$

In NMR spectroscopy, the standard often used is tetramethylsilane, $Si(CH_3)_4$, abbreviated TMS. The chemical shift is a very precise metric of the chemical environment around a nucleus. The NMR spectrometer must be tuned to a specific nucleus, like the ^1H, ^{13}C etc. The actual procedure for obtaining the spectrum varies, but the simplest is referred to as the continuous wave (CW) method. A typical CW-spectrometer is shown in the following figure 2.10.

A solution of the sample in a uniform 5 mm glass tube is oriented between the poles of a powerful magnet, and is spun to average any magnetic field variations, as well as tube imperfections. Radio frequency radiation of appropriate energy is broadcast into the sample from an antenna coil (colored red). A receiver coil surrounds the sample tube, and emission of absorbed rf energy is monitored by dedicated electronic devices and a computer.

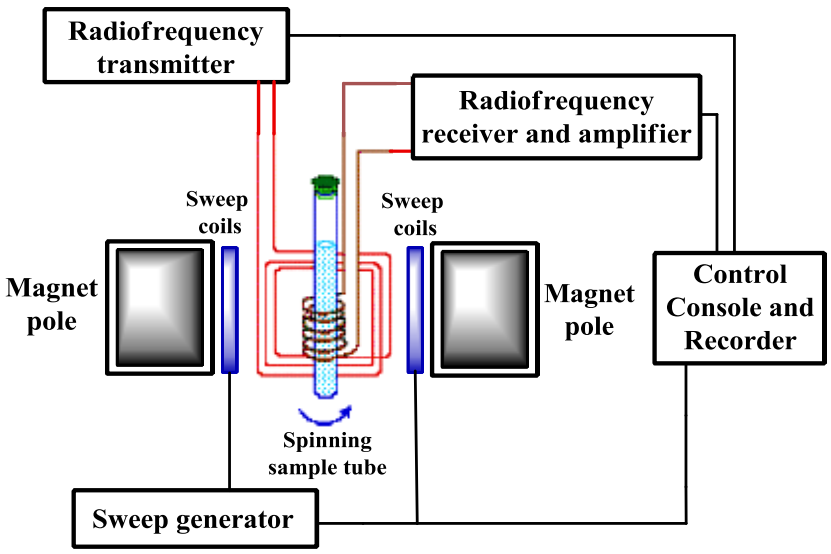

Figure 2.10: Schematic representation of NMR spectrometer

A NMR spectrum is acquired by varying or sweeping the magnetic field over a small range while observing the rf signal from the sample. An equally effective technique is to vary the frequency of the rf radiation while holding the external magnetic field constant. The ^{1}H and ^{13}C (500 MHz) NMR spectra were recorded with a Brüker Oxford or Varian instrument, for characterizing the synthesized compounds, the details of which are given in the respective chapters.

2.4.8. *Thermal analysis*

Thermal analysis involves a variety of techniques in which a particular property of a sample is monitored when it is subjected to a predetermined temperature profile. Recently there have been major advances in the thermal analysis technique through improved furnace technology, microcomputer-based electronics and the addition of microcomputer data handling systems. There are multiple methods in thermal analysis depending on the type of properties of the sample that are to be measured. The most commonly used techniques of thermal analysis are given in table 2.1.

Name of the technique	Measurement Object	Unit	Uses
Differential thermal analysis (DTA)	Temperature difference	^{o}C µV	Phase changes different reactions
Differential scanning calorimetry (DSC)	Thermal flow	J/sec	Heat capacity Phase changes Reactions
Thermogravimetry (TG)	Mass	mg	Decompositions Oxidation
Thermomechanical analysis (TMA)	Deformations	µm	Softening Expansion
Dynamic thermomechanical measurements (DTM)	Elasticity	Pa, dyn/cm^2	Phase changes Polymer curing

Table 2.1: Thermal analysis techniques

2.4.8.1. *Thermogravimetric analysis (TGA)*

TGA is a technique in which the sample specimen is subjected to a controlled temperature program and mass of the substance is monitored as a function of temperature or time. Any physical or chemical process (evaporation, sublimation,

oxidation, thermal degradation etc.) involving mass loss or gain of the material can be studied by this technique. TGA can be carried out by using either a heating ramp (dynamic mode) or a constant test temperature (isothermal mode).The decomposition of a substance can be studied under inert, oxidizing or reducing conditions by changing the test atmosphere by gas switching. The major components of TGA are: a precision balance, a programmable furnace and a recorder or a computer. In addition provisions are also made for surrounding the sample with air, nitrogen or an oxygen atmosphere. A schematic layout of TGA instrument is shown in figure 2.11.

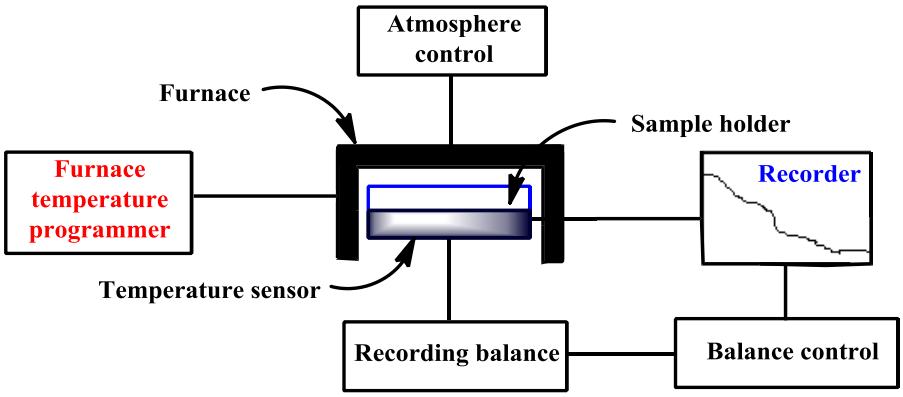

Figure 2.11: Block diagram of thermogravimeter

In the present studies, thermogravimetric analysis measurements have been carried out, using Mettler Toledo TG/DSC star^{e} system. The details of thermal programming, used in studying the individual systems will be discussed in the relevant sections.

2.4.8.2. *Differential Scanning Calorimetry (DSC)*

Differential scanning calorimeter (DSC) is a fundamental tool in thermal analysis which can be used in many industries – from pharmaceuticals and polymers, to

nanomaterials and food products. The information these instruments generate is used to understand amorphous and crystalline behavior, polymorph and eutectic transitions, curing and degree of cure, and many other material properties used to design, manufacture, and test products. DSC, is a thermal analysis technique that looks at how heat capacity of a material (Cp) is changed with temperature. A sample of known mass is heated or cooled and the changes in its heat capacity are tracked as changes in the heat flow. This allows the detection of transitions such as melts, glass transitions, phase changes, and curing.

In the 1960s, Mike O'Neill of Perkin-Elmer developed the first double-furnace, or power controlled DSC in order to measure heat flow, the movement of heat in and out of a sample, directly. This instrument uses a feedback loop to maintain the sample at a set temperature while measuring the power needed to do this against a reference furnace. This allows for very precise control of temperature, hence very accurate enthalpy and heat capacity measurements, and true isothermal performance. Because of its direct measurement of heat flow, it is often called heat flow DSC. DSC technique can be used for measuring temperature difference between sample and reference or heat flux. This is called heat flux DSC. It measures the temperature difference and calculates heat flow from calibration data. Because of their single furnace design, heat flux DSCs are less sensitive to small transitions, heat and cool at slower rates than heat flow DSC and give less accurate values for Cp and enthalpy. A pictorial representation of heat flux DSC and heat flow DSC are given in figure 2.12.

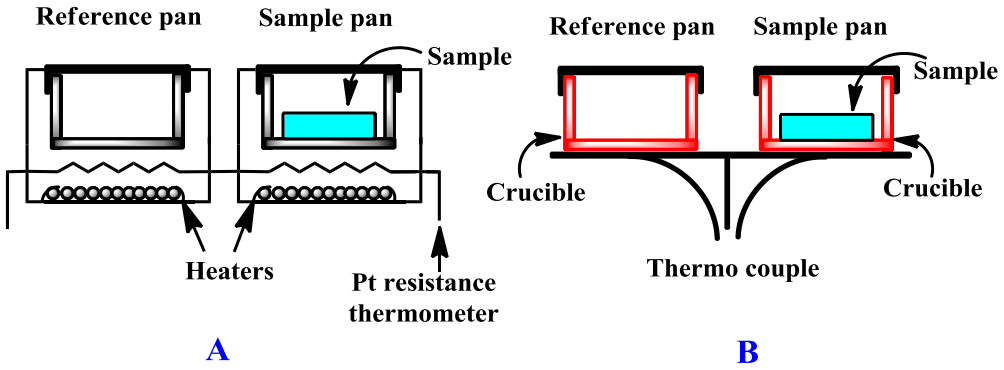

Figure 2.12: Pictorial representation of (a) heat flow and (b) heat flux DSC.

In a heat flow DSC, the endothermic peaks – those events which require energy, point up – because the instrument must supply more power to the sample, to keep the sample and reference furnaces at the same temperature. In a heat flux DSC, these same events cause the sample to absorb heat and be cooler than the furnace, so they point down. The reverse logic applies to exothermic events where energy is released. Modulated Temperature DSC (MT-DSC) is the general term for DSC techniques, where a non-linear heating or cooling rate is applied to the sample to separate the kinetic from the thermodynamic data. This is done by applying a series of heating (or cooling) micro-steps followed by an isothermal hold. This technique removes kinetic noises from transitions, such as enthalpic overshoot or curing exotherm, from an overlapping Tg.

Mettler Toledo DSC star^{e} system was utilized for determination of states of water in the synthesized hydrogel samples, the details of the experiment is given in the respective chapters.

2.4.9 *Dynamic light scattering (DLS)*

DLS is most commonly used to analyze nanoparticles. A monochromatic light source, usually a laser, is shot through a polarizer and into a sample. The scattered light then goes through a second polarizer where it is collected by a photomultiplier and the resulting image is projected onto a screen. All of the molecules in the solution, being hit with the light, diffract the light in all directions. The diffracted light from all of the molecules can either interfere constructively (light regions) or destructively (dark regions). If the light source is a laser, which is monochromatic and coherent, the scattering intensity fluctuates over time. This fluctuation is due to the fact that the small molecules in solutions are undergoing Brownian motion, and so the distance between them is constantly changing with time. This scattered light then undergoes either constructive or destructive interference and we get information about the scale of motion of small molecules in solution from this intensity fluctuation.

It is very important to remove dust and artifacts from the solution during the sample preparation either by filtration or centrifugation. The dynamic information of the particles is derived from an autocorrelation of the intensity trace recorded during the experiment. Once the autocorrelation data have been generated, different mathematical approaches can be employed to determine particle size information from it. Analysis of the scattering is facilitated when particles do not interact through collisions or electrostatic forces between ions which can be suppressed by dilution, and charge effects are reduced by the use of salts to

collapse the electrical double layer. The simplest approach is to treat the first order autocorrelation function as a single exponential decay, which is appropriate for a monodisperse population.

$$g^1(q;\tau) = e^{-\Gamma\tau} \quad (2.11)$$

where $g^1(q;\tau)$ is the autocorrelation function at a particular wave vector, q, and delay time, τ, Where Γ is the decay rate**.** The translational diffusion coefficient Dt may be derived at a single angle or at a range of angles depending on the wave vector q.

$$\Gamma = q^2 Dt \quad (2.12)$$

Where

$$q = \left(\frac{4\pi n_0}{\lambda}\right) \mathrm{Sin}\theta/2 \quad (2.13)$$

Where λ is the incident laser wavelength, n_0 is the refractive index of the sample and θ is angle at which the detector is located with respect to the sample cell.

Dt is used to calculate the hydrodynamic radius of the particles using Stokes-Einstein equation (2.14) which is as follows:

$$Dt = \frac{K_B T}{6\pi\eta r} \quad (2.14)$$

Where, K_B = Boltzmann constant

T = Absolute temperature

η = Dynamic viscosity

r = Radius of the spherical particle

It is important to note that the size determined by dynamic light scattering is the size of a sphere that moves in the same manner as the scatterer. So, for example, if the scatterer is a random coil polymer, the determined size is not the same as the radius of gyration determined by static light scattering. The obtained size will include any other molecules or solvent molecules that move with the particle.

2.5.0. ***Cobalt-60 gamma irradiator***

The radionuclide cobalt-60 (Co-60 or $^{60}Co_{27}$) is the most commonly used source of gamma radiation for radiation technology, both for industrial and medical purposes. Production of radioactive cobalt starts with natural cobalt (metal), which is an element with 100% abundance of the stable isotope cobalt-59. Cobalt-rich ore is rare and this metal makes up only about 0.001% of the earth's crust. Slugs (small cylinders) or pellets made out of 99.9% pure cobalt sintered powder are generally welded in Zircaloy capsules and placed in a nuclear power reactor, where they stay for a limited period (about 18–24 months) depending on the neutron flux at the location.

While in the reactor, a cobalt-59 atom absorbs a neutron and is converted into a cobalt-60 atom. During the two years in the reactor, a small percentage of the atoms in the cobalt slug are converted into cobalt-60 atoms. Specific activity is usually limited to about 120 Ci/g of cobalt. After irradiation, the capsules containing the cobalt slugs are further encapsulated in corrosion resistant stainless steel to finally produce the finished source pencils in a form such that gamma radiation can come through but not the radioactive material (cobalt-60) itself. The

source pencils are arranged in the form of a cylinder, over the source rack of the industrial irradiator. Cobalt-60 ($^{60}Co_{27}$) decays (disintegrates) into a stable (non-radioactive) nickel isotope ($^{60}Ni_{28}$) principally emitting one negative beta particle (of maximum energy 0.313 MeV) with a half-life of about 5.27 years. Nickel-60 thus produced is in an excited state, and it immediately emits two photons of energy 1.17 and 1.33 MeV in succession to reach its stable state. The decay scheme is given in figure 2.13.

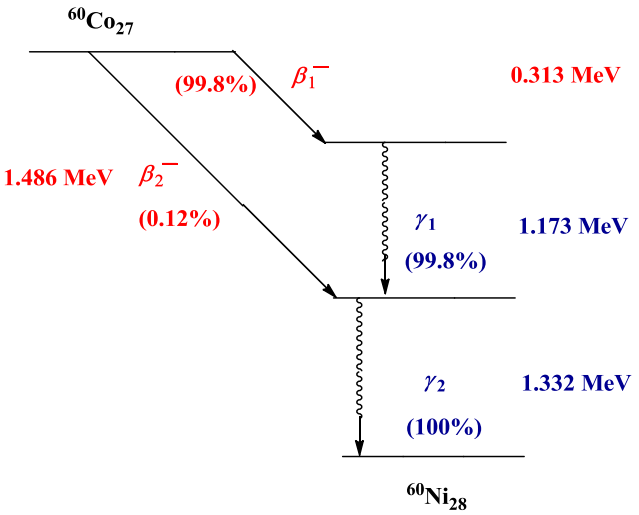

Figure 2.13: Decay scheme of Cobalt-60

These two gamma ray photons are responsible for radiation processing in the cobalt-60 gamma irradiators. With the decay of every cobalt-60 atom, the strength or the radioactivity level of the cobalt source is decreasing, such that the decrease amounts to 50% in about 5.27 years, or about 12% in one year. Additional pencils of cobalt-60 are added periodically to the source rack to maintain the required capacity of the irradiator. Cobalt-60 pencils are eventually removed from the

irradiator at the end of their useful life, which is typically 20 years. Cobalt-60 gamma irradiator was used for synthesis of sterilized hydrogels and also glycopolymers, the dose rate of which was determined by Fricke dosimetry.

2.5.1. *Rheometer*

A rheometer is a laboratory device used to measure the way in which a liquid, suspension or slurry flows in response to applied forces. There are two distinctively different types of rheometers. Rheometers that control the applied shear stress or shear strain are called rotational or shear rheometers, whereas rheometers that apply extensional stress or extensional strain are extensional rheometers. Rotational or shear type rheometers are usually designed as either a native strain-controlled instrument (control and apply a user-defined shear strain which can then measure the resulting shear stress) or a native stress-controlled instrument (control and apply a user-defined shear stress and measure the resulting shear strain). Different types of rotational or shear type rheometers are:

1. *Dynamic shear rheometer*: Dynamic shear rheometer commonly known as (DSR) is used for studying the viscoelastic behavior of thick liquids or gels. This is done by deriving the complex modulus (G*) from the storage modulus (elastic response, G') and loss modulus (viscous behaviour, G") yielding G* as a function of stress over strain.
2. *Rotational cylinder type shear rheometer*: This set up contains liquid placed within the annulus of one cylinder inside another. One of the cylinders is rotated at a set speed. This determines the shear rate inside the annulus. The

liquid tends to drag the other cylinder round, and the force it exerts on that cylinder (torque) is measured, which can be converted to a shear stress.

3. *Cone and plate shear rheometer*: The liquid is placed on horizontal plate and a shallow cone placed into it. The angle between the surface of the cone and the plate is around 1 to 2 degrees but can vary depending on the types of tests being run. Typically the plate is rotated and the force on the cone is measured. Cone and plate rheometers can also be operated in an oscillating mode to measure elastic properties, or in combined rotational and oscillating modes.

Rheological characterization is based on a response to an applied load, force or deformation and substances can thus be rheologically classified as, elastic (ideal solids), viscous (ideal fluids) or viscoelastic. Viscoelastic materials like rubbers, paints, gels etc. exhibit a combination of elastic and viscous effects simultaneously. These materials are characterized by parameters such as phase angle (δ), elastic (G′) and loss moduli (G″). Ideal solids (elastic) and ideal fluids (viscous) represent extremes for rheological analyses, and substances between the two extreme scenarios are called viscoelastic materials. Ideal solids store energy gained during deformation and following the removal of the load return to an original shape using the stored energy. Hooke's law is observed in such solids which state that the load applied to a body is directly proportional to the imposed deformation. In rheological terms, stress and strain are related linearly to each other,

$$\sigma = G\,\gamma \qquad (2.15)$$

The degree of viscoelasticity is characterized by parameters which are generally obtained through dynamic or oscillatory testing. In such tests, a stress or strain varying in a sinusoidal fashion is allowed into the material, and the resulting strain or stress respectively, is assessed. The amplitude of the input stress or strain is the peak stress (σ_a) or strain (γ_a) during oscillation.

Viscoelastic parameters include the complex modulus (G*), the phase angle (δ), elastic (or storage) modulus (G′), and viscous (or loss) modulus (G″).

Complex modulus is the ratio of the amplitude stress and strain determined in the linear viscoelastic region

$$G^* = \sigma_a/\gamma_a \qquad (2.16)$$

Phase angle can be defined as the ratio of the viscous effects to the elastic effects. In the linear viscoelastic region, when a strain is input into a material, phase angle is the angle with which the responding shear stress deviates from the input strain. For a perfectly elastic solid, the stress is in phase with the strain without any lag, and hence the phase angle is 0°. For a perfectly viscous liquid, the strain and stress are totally out of phase, and the phase angle is 90°. Mathematically, phase angle is determined as

$$\delta = \tan^{-1}(G''/G') \qquad (2.17)$$

Thus, a large value of elastic modulus, G′, in comparison with loss modulus, G″, indic7ates a more elastic material, while a larger value of G″ indicates a more viscous material. A material with a phase angle between 0°and 90°is deemed viscoelastic in nature. The elastic modulus or the storage modulus (G′) represents the energy stored within the material and corresponds to the elastic behavior of the sample. Mathematically, storage modulus is computed as the product of complex modulus and the cosine of the phase angle (equation 2.18).

$$G' = G^* \operatorname{Cos} \delta = \frac{\sigma_a}{\gamma_a} \operatorname{Cos} \delta \tag{2.18}$$

The loss modulus (G″) is used as a measure of the energy lost through dissipation and accordingly describes the viscous behavior of the sample. Loss modulus is the product of complex modulus and sine of the phase angle (equation 2.19).

$$G'' = G^* \operatorname{Sin} \delta = \frac{\sigma_a}{\gamma_a} \operatorname{Sin} \delta \tag{2.19}$$

Consequently, complex modulus can be re-written as a combination of the elastic and loss modulus which form the real and imaginary parts defined as,

$$G^* = G' + iG'' \tag{2.20}$$

CHAPTER 3

SILVER NANOPARTICLE LOADED ANTIBACTERIAL PVA/GUM ACACIA HYDROGEL

3.1. Introduction

Metal nanoparticles-embedded hydrogels, wherein the three dimensional, hydrophilic polymeric network stabilizes the nanoparticles, have attracted attention mainly due to their wide range of applications in the field of catalysis, biomedicine, optics, pharmaceuticals, etc.[106] Most of the synthetic routes for the formation of metal nanoparticles employ chemical reduction methods, using hydrazine hydrate, dimethyl formamide, ethylene glycol, etc., which causes toxicity and biological hazards.[107] Recent research efforts in this area are directed more towards developing new approaches, to incorporate metal nanoparticles into polymeric hydrogel matrices, without involving any toxic chemical reductants, or using any complicated physical techniques, such as sputtering, plasma deposition, etc. Radiation technology is one such method, by which it is now possible to synthesize nanoparticles incorporated hydrogel matrices *in situ*.

The advantage of using radiation-induced synthesis of hydrogels is that, the process can be optimized to form a sterilized gel matrix, which can be used, without further purification, for various biomedical applications. This makes it one of the best methods for hydrogel synthesis. Also, radiation-induced method of synthesis of nanoparticles has a better control over the size.[106] Hence, radiation technique can be used as a cleaner and simpler method, to form a hydrogel matrix, with nanoparticles embedded in it. While considering the synthesis of hydrogels for biomedical applications, its biocompatibility is an important parameter. Synthesis of biocompatible hydrogel matrix from a nontoxic, economical, and

easily available material such as polysaccharides, is usually more advantageous than that from synthetic polymers.[108] Gum acacia (GA) is a well-known polysaccharide, obtained from the stems and branches of acacia Senegal tree.[109-111] According to the recent structural studies, it is known to be composed of (i) arabinogalactan, (ii) arabinogalactan-protein (AGP) complex fraction, and (iii) minor glycoprotein fraction.[110,111] The high molecular weight protein part in GA is attached to polysaccharide through hydroxyproline and serine residues. Uronic acid (16%) is present in low quantities in different components of the gum, which makes it a weakly charged polyelectrolyte.[110] But, GA cannot be cross-linked by gamma irradiation, whereas poly vinyl alcohol (PVA) is well known to form hydrogels induced by gamma, as well as electron irradiation. In the present work, gum acacia and PVA was an obvious choice for the synthesis of a composite hydrogel matrix, due to its biocompatible, economical and environmental friendly nature.

Thus a combination of water soluble biopolymer GA and synthetic polymer PVA with silver nanoparticles can produce new hydrogel matrix, with antimicrobial property. Recent studies have shown that, silver in the form of nanoparticles, is very effective as antimicrobial agent, both *in vivo* and *in vitro*, compared to bulk silver or silver ions, due to their enhanced permeation and retention effects (EPR).[112-115] Their antimicrobial activity is due to its interaction with sulphur containing proteins present in bacterial cell membrane as well as with phosphorous containing DNA. The size and the rate of leaching of the silver

nanoparticles also play a major role in antimicrobial activity of such hydrogels, especially for wound dressing applications. For such applications, a hydrophilic environment is necessary, to facilitate the release of silver from the polymer matrix, and also to maintain a moist environment around the wound bed, which is essential for optimal wound healing. The polysaccharides, like gum acacia, carrageenan, agar, etc., can improve the water retention properties, and hence are suitable for such hydrogel synthesis.

In the present work, in view of the advantages of radiation induced technique and biocompatibility of the hydrogel matrix, radiolytic synthesis of silver nanoparticle loaded PVA-GA hydrogel (Ag/PVA-GA hydrogel) was carried out, and its antibacterial behaviour was studied.

3.2. Experimental

3.2.1. *Preparation of Ag /PVA-GA hydrogel*

Freshly prepared stocks of 10% PVA and 10% GA (W/V) in water were used for preparation of PVA-GA blends. Aqueous solution of 3% PVA containing different concentrations of GA (1%, 3%, and 5%) and 1 mM $AgNO_3$, were prepared by appropriate dilution of these stock solutions. The PVA-GA blends containing $AgNO_3$ were transferred into glass tubes and sealed after bubbling with nitrogen~ (for 30 min at 5 ml/min) to flush out any dissolved oxygen. These tubes were irradiated in Co-60 gamma source at a dose rate of 1.44 kGy/h, to an absorbed dose of 35 kGy under ambient conditions. Thus, silver nanoparticles

(AgNPs) were produced *in situ* in the hydrogel which were taken out and washed thoroughly with distilled water to remove any unreacted species (Figure 3.1).

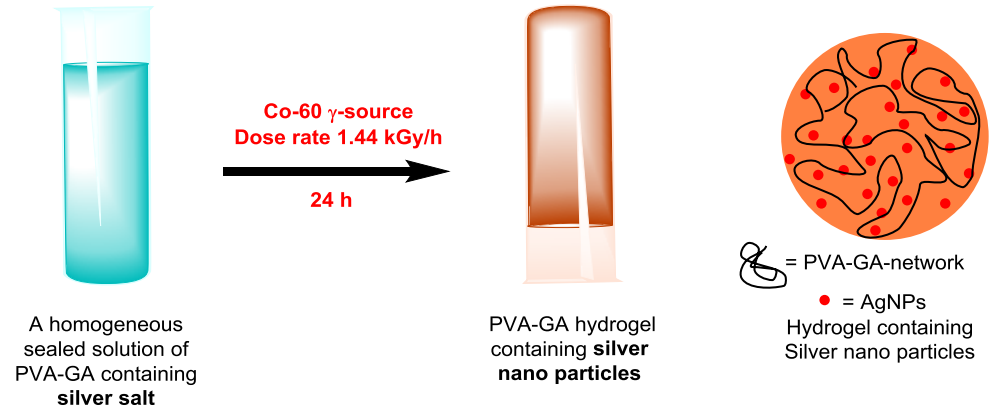

Figure 3.1: Schematic representation of the synthesis of PVA-GA hydrogel containing AgNPs.

These gels were dried to constant weight in vaccum at 40 ^{o}C for further characterization by different techniques. The mechanism of formation of silver nanoparticles in the hydrogel matrix can be explained as follows.

Gamma irradiation of an aqueous solution mainly produces $^{\cdot}$OH, $^{\cdot}$H radicals and hydrated electrons (e_{aq}^{-}), along with some molecular products, due to radiolysis of solvent as shown in equation 1.1 (Chapter 1).

Among these $^{\cdot}$OH is oxidizing in nature, while $^{\cdot}$H and e_{aq}^{-} are of reducing nature. The $^{\cdot}$OH and $^{\cdot}$H radicals are mainly responsible for crosslinking of the PVA chains, whereas $^{\cdot}$H and e_{aq}^{-} reduce Ag^{+} ions to AgNPs. The initially formed neutral Ag^{o} atoms can combine with themselves or with the Ag^{+} ions trapped in the polymer chains, to form dimeric clusters of silver (equation (3.1-3.3)).[9]

$$Ag^{+} + e_{aq}^{-} / H^{\bullet} \longrightarrow Ag^{0} \quad (3.1)$$

$$Ag^{0} + Ag^{0} \longrightarrow Ag_2^{0} \quad (3.2)$$

$$Ag^{0} + Ag^{+} \longrightarrow Ag_2^{+} \quad (3.3)$$

These dimeric clusters can further react with excess silver cations to form trimeric, tetrameric and higher order silver ion clusters which simultaneously get reduced by e^{-}_{aq} and H atoms.[112, 116] These higher nanometallic clusters grow with time and get stabilized in the nanolevel domains of gum acacia/PVA matrix. These nano level domains are formed due to inter and intramolecular H-bonds between –COOH and –OH groups of gum acacia and –OH groups of PVA and radiation induced crosslinks between the polymeric chains, resulting in a hydrogel network system. Upon continuous irradiation the clusters trapped in these domains are converted into nanoparticles. The 'O' atom of the functional groups on the network chains anchor the AgNPs, resulting in a surface charge which leads to electrostatic repulsive force, and the steric effects of the polymer chains, stabilize the nanoparticles.[117]

Generally polymers may crosslink or degrade upon irradiation depending on its chemical structure. PVA is known to be a crosslinking polymer, while GA is of degrading nature. Therefore along with crosslinking of PVA, degradation of polysaccharide GA is also taking place in the reaction medium, and the overall behavior will depend up on the relative concentration of the two polymers.

The rate constants for reaction of ˙OH and ˙H radicals with both PVA and GA are very similar and are of the order of 10^9 dm^3 mol^{-1} s^{-1} while the rate constants for the reaction of e_{aq}^- with both these polymers are much lower. On the contrary, reactivity of both ˙H and e_{aq}^- with Ag^+ ions are about an order of magnitude higher (i.e 10^{10} dm^3 mol^{-1} s^{-1}). The concentration of the solutes are appropriately chosen so that the ˙OH and ˙H radicals preferentially react with the polymers and the e_{aq}^- reacts mostly with Ag^+ ions, leading to a cross-linked hydrogel network containing AgNPs. Thus an aqueous solution of PVA, GA and silver nitrate of appropriate concentrations upon gamma irradiation, form covalently crosslinked yellow colored hydrogel with AgNPs trapped in the network. The parameters like gel strength, water absorption capacity, thermal strength, adhesion, etc. depend on the concentration of PVA, GA, crosslinking density, gamma dose, irradiation conditions etc.[106]

3.2.2. *Characterization of the synthesized Ag /PVA-GA hydrogels*

The synthesized hydrogel samples were vacuum dried to constant weight and then utilized for characterization techniques like FT-IR, swelling studies, thermal analysis, and particle size measurements.

3.2.2.1. *FT-IR analysis*

The FT-IR spectra of PVA/GA and AgNPs/PVA-GA hydrogel samples were recorded in order to identify the functional groups involved in the synthesis of AgNPs.

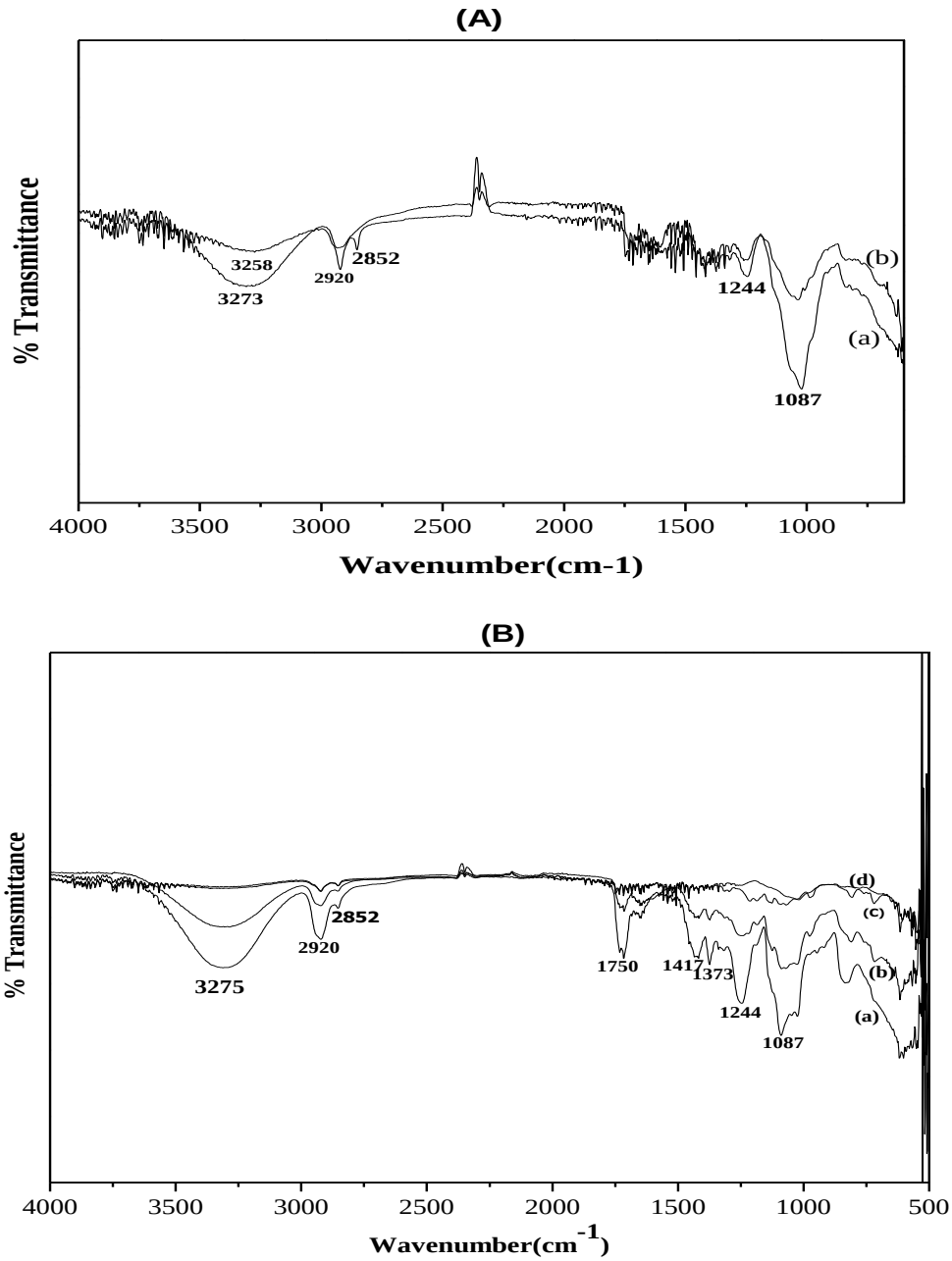

Figure 3.2: FT-IR spectra of vaccum dried hydrogel samples: (A) (a) without AgNPs (b) with AgNPs. (B) Synthesized using variable GA concentrations ((a) 0%, (b) 1%, (c) 3%, (d) (5%) with 3% PVA, 1 mM $AgNO_3$, at an applied radiation dose of 35 kGy).

In the presence of silver the oxygen atom of -OH and -COOH groups gets associated with silver clusters.[116] This leads to broadening and shifting of O-H stretching from 3273 cm^{-1} (silver unloaded) to 3258 cm^{-1}(silver loaded). The C-H stretching peak at 2920 cm^{-1} in silver unloaded sample is slightly broadened and also split into two peaks upon silver loading (Figure 3.2A). This indicates the interaction of silver with -OH groups, which leads to a shift in the stretching of the C-H groups associated with these hydroxyl groups.

FT-IR spectra of silver loaded hydrogel samples containing different concentrations of GA (1%, 3% and 5%) were also recorded to understand the variation in the interaction between GA, PVA and silver (Figure 3.2B). The major peaks are 3275 cm^{-1} (O-H stretching), 2920 cm^{-1}, 2852 cm^{-1} (C-H stretching), 1417 cm^{-1} (O-H deformation), 1244 cm^{-1} (C-O stretching of PVA), 1087 cm^{-1} (C-OH stretching of GA) (Figure 3.2B).[117] The presence of large number of hydroxyl and carboxyl groups and the possible hydrogen bonding between them resulted in broadening of peaks at ~3200 cm^{-1} and ~1000 cm^{-1}. With increase in concentration of GA more hydroxyl groups are involved in hydrogen bonding and this leads to further peak broadening and slight shift in the C-O stretching frequency at 1244 cm^{-1} of PVA as well at 1087 cm^{-1} of GA (Figure 3.2B).

3.2.2.2. *Thermogravimetric analysis*

Thermogravimetric analysis was performed using Mettler Toledo TG/DSC star^{e} system. About 5-10 mg of the dried hydrogel samples were heated in an alumina crucible and the profiles were recorded from 30-750 ^{o}C, at a scan rate of 10

^{o}C/min, under nitrogen atmosphere, with a flow rate of 50 ml/min. The thermal stability of the matrix and the silver loading in the hydrogel matrix was studied from the thermogravimetric data. Figure 3.3 illustrates the thermogram of silver loaded and unloaded dry hydrogel samples. The weight loss observed for PVA/GA hydrogel sample was 72.7% at 500 °C whereas Ag/PVA-GA composite hydrogel showed only 64.3% at the same temperature. This weight loss difference indicates the presence of AgNPs and its possible matrix stabilization due to its interaction with the matrix.

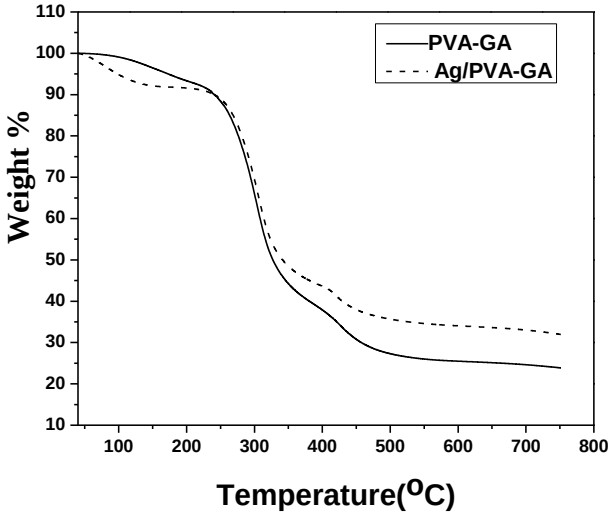

Figure 3.3: Thermogravimetric curves showing the weight loss in (Ag/PVA-GA) and (PVA-GA) vaccum dried hydrogel samples**.**

3.2.3. *Swelling studies of the hydrogels*

Equilibrium degree of swelling (EDS) was determined gravimetrically. The hydrogel samples dried to constant weight were immersed in double distilled water at room temperature for ~ 24 h. The excess water was removed with a filter

paper and the samples were weighed. The EDS was calculated using equation 3.4.[118]

$$\% \text{ EDS} = \frac{(We - Wd)}{Wd} \times 100 \qquad (3.4)$$

Where,

W_e = weight of the swollen hydrogel at equilibrium

W_d = initial weight of the dried hydrogels.

The % EDS values were determined at different pH as well as at different compositions of hydrogels. The pH was adjusted to desired value by using 0.1 M HCl and 0.1 M NaOH solutions and the ionic strength was maintained to 0.1 M with NaCl.

3.2.3.1. *Equilibrium degree of swelling as a function of PVA and GA concentration*

The % EDS was determined for the hydrogels containing different concentrations of PVA and GA, keeping concentration of silver nitrate and applied radiation dose constant, to study the effect of this variation, on the network structure of the hydrogels (Table 3.1). The % EDS was found to decrease with increase in relative concentration of PVA (Table.3.1). This is because at higher PVA concentrations cross linking density is more, hence results in a tighter 3D-structure which will swell less compared to the hydrogels with lower concentration of PVA. The % EDS of the resultant hydrogels increased from 984% to 1826% with increase in GA fraction from 0 to 0.63 (Table.3.1). This may be due to the hydrophilic nature of GA which can lead to more hydrogen bonding between GA and water.

Sample (Dose = 35 kGy)**	
GA fraction	**% EDS***
0.00	984
0.29	1170
0.38	1390
0.50	1553
0.63	1826

*Average of three measurements

**Gel formation was not observed when the PVA concentration was below 3% or GA concentration was above 5% at an applied radiation dose of 35 kGy.

Table 3.1: Variation in % EDS at different PVA and GA concentrations in the presence of 1 mM $AgNO_3$.

The increase in % EDS can also be explained in terms of decrease in crystallinity of PVA segments, due to the bulky units of GA. In fact, the hydrogen bonding due to –OH groups crystallize PVA through physical cross linking but the steric hindrance of the bulky GA groups disturbs the chains and decreases the crystallinity. Also, the presence of GA in polymer solution reduces the probability of radical recombination during irradiation, which ultimately reduces the crosslinking density of the gel leading to more free volumes in the polymer network and consequently more water can be absorbed.[119]

3.2.3.2. *Equilibrium degree of swelling as a function of pH*

The pH sensitivity of the matrix was analyzed by determining % EDS at different pH of the absorbing medium. It was observed that the % EDS does not vary significantly with variation in the pH of the medium (Table.3.2). This behavior

may be because, the pH dependent –COOH groups of GA are very less compared to the –OH groups present in PVA and GA together. So the pH variation doesn't significantly affect % EDS of the hydrogels.

pH	% EDS*
1	1424
4	1485
7	1466
10	1489
12	Gel disintegrated

* Average of three measurements

Table 3.2: Effect of pH on the % EDS of the hydrogel formed by gamma irradiation of aqueous solution containing 3% PVA, 5% GA, and 1 mM $AgNO_3$ for 35 kGy dose.

3.2.4. *Release of silver from hydrogels*

The antimicrobial activity of silver containing hydrogels is dependent on the release of silver from the polymeric matrix to the pathogenic environment. UV-vis spectroscopic technique was utilized to study the leaching of silver. A freshly prepared Ag/PVA-GA hydrogel samples with different initial GA contents 1%, 2%, 3%, 5% (w/v) and 5% (w/v) PVA were used for the analysis. The *in vitro* release profiles of silver from hydrogel matrices were obtained by measuring the optical density (O.D) at different time periods. Briefly, hydrogels of 1.0 g was stored in a flask containing 10 ml of distilled water at 37 ^{o}C and the flask was

oscillated at a frequency of 60 rpm in a rotary shaker. The amount of silver released was determined by measuring the O.D at the λ_{max}, due to the silver nanoparticles released in the aqueous medium.

As shown in figure 3.4, in the case of 5% GA sample the release of silver was rapid in the beginning and became almost constant.

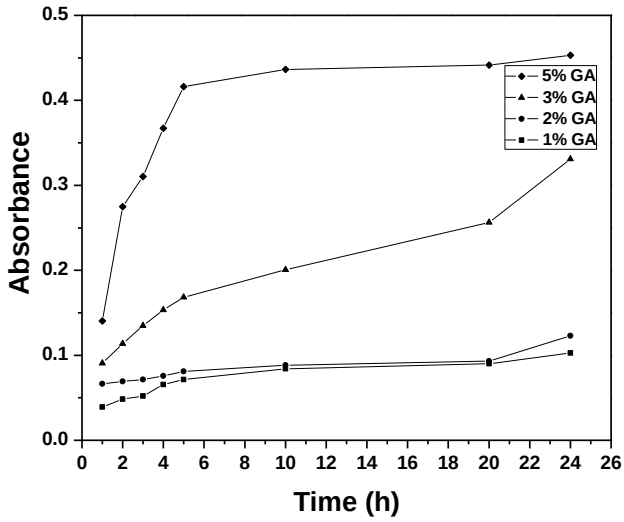

Figure 3.4: Graph showing the silver release profiles of hydrogels prepared with different GA concentrations, at 5% PVA, 1 mM $AgNO_3$ and applied radiation dose of 35 kGy.

This is probably due to higher silver loading as well as higher hydrophilicity of the matrix with increasing GA concentration. But at lower concentration (1%, 2% and 3% GA) the initial release was not so rapid; it increases gradually and a considerable increase can be observed only after long incubation period of ~ 20 h. The longer time for the release of silver may be the result of slow swelling nature of the matrix with low GA content *vide supra* (3.2.3.1).

3.2.5. *Particle size analysis*

Particle size analysis was carried out by dynamic light scattering (DLS) method using VASCO $^{\gamma}$ particle size analyzer at 25 ^{o}C (laser wavelength 658 nm). DLS method measures the Rayleigh scattering. Based on the assumptions (monomodal particle size distribution, spherical particles) it is possible to compute particle size distributions by intensity, by volume, and by number.[120]

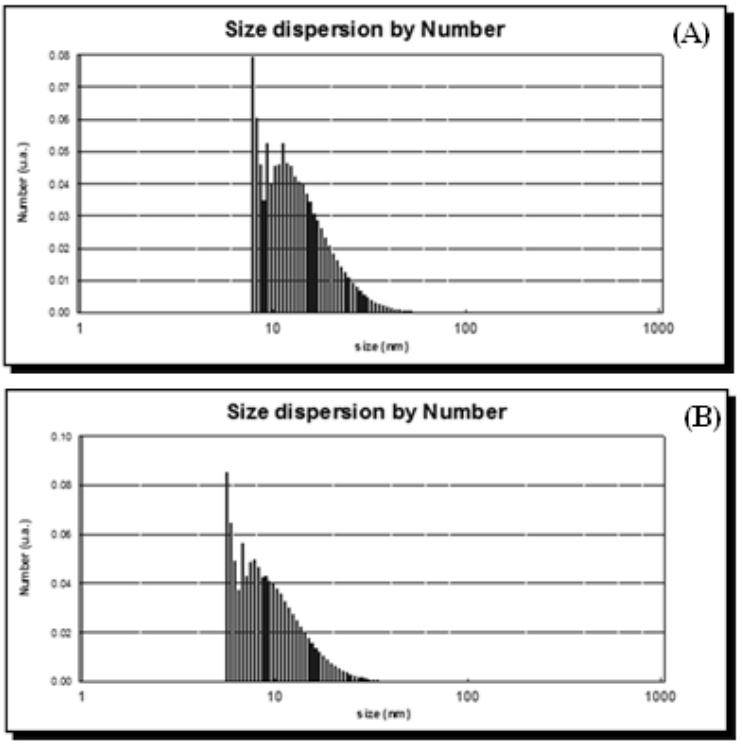

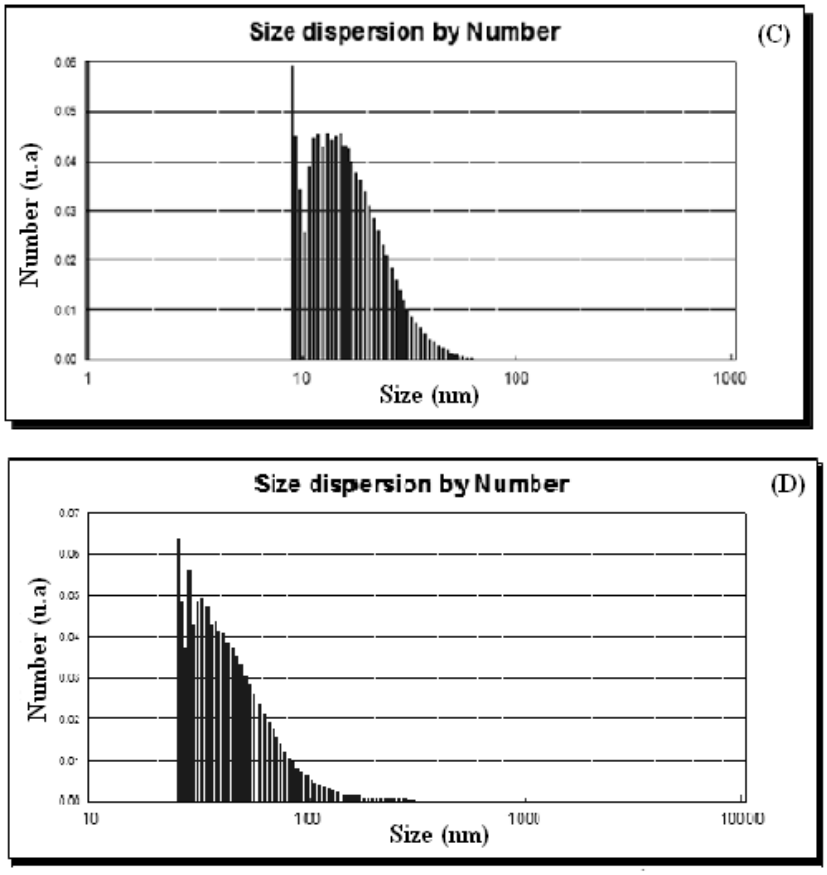

Figure 3.5: Variation in particle size at different GA concentration keeping all other parameters constant (a) 1% GA (b) 2% GA (c) 3% GA (d) 5% GA.

The variation in particle size distribution as a function of GA concentration was studied keeping the radiation dose (35 kGy), PVA (3%) and silver ion concentration (1 mM) constant. The mean particle diameters when GA concentration was 1%, 2%, 3% and 5%; was obtained as 9.8 nm, 13.7 nm, 16.9 nm, 42.0 nm (Figure 3.5). This may be because with increase in GA concentration the possibility of inter- and intra-molecular crosslinking in PVA decreases because of steric effects due to GA and hence the crosslinking density

decreases. So there is more probability of aggregation of silver nanoparticles in the matrix resulting in larger clusters of nanoparticles.

3.2.6. *Gel point determination*

Gelation is a process which involves change from liquid to solid like behavior. This can be studied by rheological experiments. The storage modulus G' (ω) and the loss modulus G" (ω) can be measured by applying an oscillatory shear field to the sample. The phase difference (δ) between the externally applied stress σ and strain γ inside the sample describes the viscoelastic properties of the material. The condition of G'<G" indicates liquid like behavior and while that of G'>G" indicates more of solid like behavior.[121]

Determination of gel point can be done by different rheological methods out of which the most reliable and generally valid is the one based on Chambon-Winter (CW) criterion. According to CW criterion, the gel point is indicated by the independence of the viscoelastic function, tan (δ) on frequency (ω).[122] The crossover of G' and G" has been suggested as a criterion for gelation, however it is frequency dependent in most polymer systems and is only observable in polymer fluids, where there are permanent molecular entanglements, extending throughout the system. Also due to 'weak gel' characteristics of the present system observing a crossover is perhaps not expected. Such crossovers in weak gels can be expected at lower frequencies (ω), however the experiments become unfeasible at very low frequencies because the measurement time, t_{exp} is inversely proportional to ω_{min}, where ω_{min} is the lowest investigated frequency.[123] Hence to

determine gel point T_g accurately, it is most appropriate to consider the point at which tan (δ) exhibits frequency independence or alternatively the frequency independence can be shown by the power law (equation 3.5),

$$\tan(\delta) = K\,\omega^{q} \qquad (3.5)$$

Where, q = 0 at the gel point and K is a constant which is characteristic of the gel.[124]

3.2.6.1. ***Conditions of rheology experiments***

The composition of the samples used for irradiation was 5% (w/v) GA, 3% (w/v) PVA and 1 mM $AgNO_3$, which was kept constant. The samples were irradiated under the same conditions at different radiation doses to study the viscoelastic properties. All measurements were done in the linear viscoelastic region so that the storage moduli (G') and the loss moduli (G") were independent of the applied strain. Therefore, a strain sweep test was conducted for each sample. For the study of gelation, the storage and loss moduli were measured, from a constant strain-frequency sweep experiments over frequency range of 100-0.1 rad/s.

3.2.6.2. ***Evolution of the modulus G' and G" with applied radiation dose and determination of the gel point***

Initially, with the samples obtained at lower radiation doses G'(ω) was smaller than G"(ω) and remained small during the frequency sweep test. Then, with increase in applied radiation dose, both moduli were found to increase and finally G' (ω) became larger than G"(ω).[125] It was observed that above ~30 kGy

radiation dose the G' (ω) was larger than G"(ω) indicating solid like behavior.[126] Also there is congruency of G'(ω) and G"(ω) values above ~30 kGy (Figure 3.6).

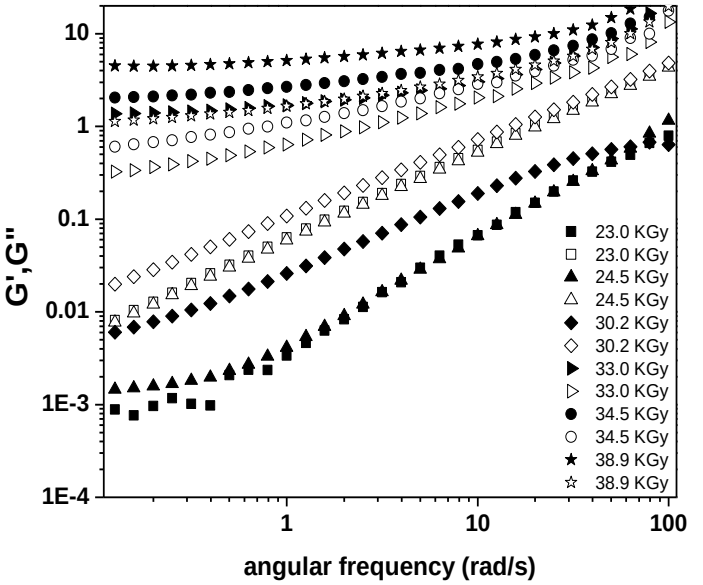

Figure 3.6: Frequency dependence of storage modulus G' (closed symbols) and loss modulus G" (open symbols) at different applied radiation dose**.**

But this observation cannot give us the exact gel point. To consider the applicability of the gel point determination method proposed by Winter and Chambon, it is necessary to take a power law fit of tan (δ) over a range of frequencies. Figure 3.7 illustrates the frequency dependence of tan (δ), for each applied dose to the system described. Below the gelation dose, G' increases more rapidly than G" and thus tan (δ) decreases rapidly with dose. Initially at lower doses the tan (δ) value is higher at lower frequencies, which is typical for a viscoelastic liquid. This indicates that the networks are not interconnected to a macroscopic scale.

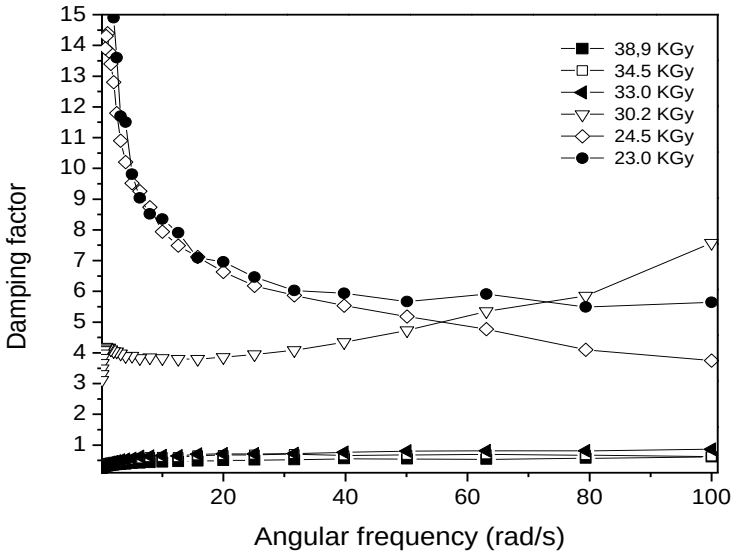

(For clarity only necessary datas are incorporated.)

Figure 3.7: Frequency dependence of damping factor at different applied radiation doses.

After the gel point, the clusters form three dimensional interconnected networks which is reflected by the less rapid increase of G' over G". As a result tan (δ) decreases gradually with dose and increases smoothly with frequency, indicating the formation of a visco elastic solid. After 30.2 kGy, the tan(δ) values become almost independent of frequency, suggesting the post gel point region.[127] A power law fit to the data in figure 3.7 was observed over two decades of frequency with a correlation coefficient $R^2 \geq 0.95$.

Fitting tan (δ) to a power law relationship, yields a power law coefficient (q), for each radiation dose, the relationship of which, with irradiation time is described in figure 3.8 The time of irradiation, at which the power law coefficient (q), passes through zero represents a frequency independent measure of tan(δ) and thus congruency in the behavior of G' and G", fulfilling the requirements for the gel

point.[111] From the figure 3.8 it can be concluded that gel point occurs at 19.2 hours of irradiation i.e. 25.34 kGy of radiation dose.

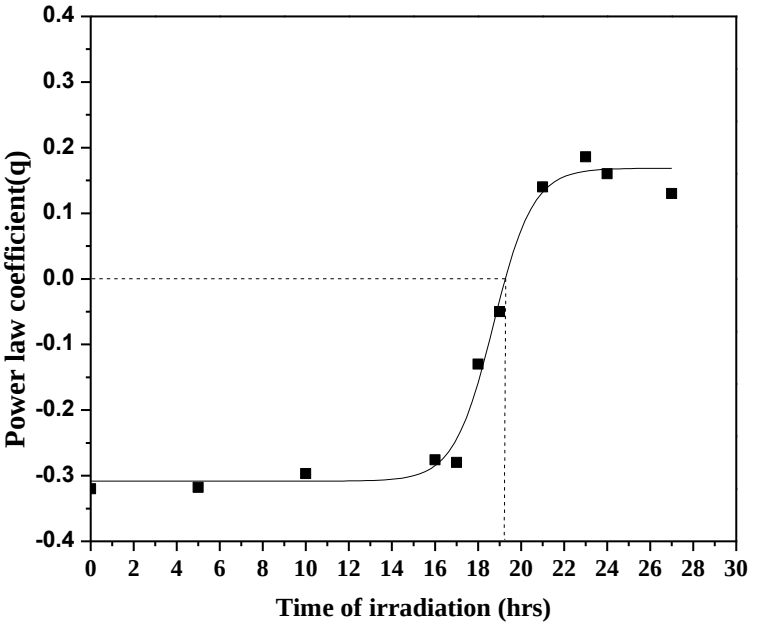

Figure 3.8: Power law coefficient (q) *vs* irradiation time for samples synthesized with 5 % PVA, 3 % GA and 1 mM $AgNO_3$. All correlation coefficients for power law fit $R^2 \geq 0.95$.

3.2.7. *Antibacterial Studies*

Antibacterial activity of the Ag/PVA-GA blend hydrogels against wild type *Escherichia coli* W1103 (*E.Coli*) (Gram negative) was evaluated using the disc diffusion method. Overnight grown culture of *E.Coli* was diluted and plated on LB agar. Equally weighed hydrogel samples consisting of 1%, 2%, 3% and 5% GA; keeping silver nitrate and PVA concentration unchanged, were kept on the plates which were incubated at 37 ºC for 24 h, then the plates were taken out and the inhibition area was observed. The incubation zone was observed in each of the

samples, which decreased with increase in GA concentration (Figure 3.9). Hydrogel samples with 1% and 2% GA concentration, showed an inhibition zone around the sample. But for 3% and 5% GA concentration, the gels were found to be just contact active. This is in agreement with the particle size data given in section 3.2.5. So it can be observed smaller the particle size better is the antibacterial activity.

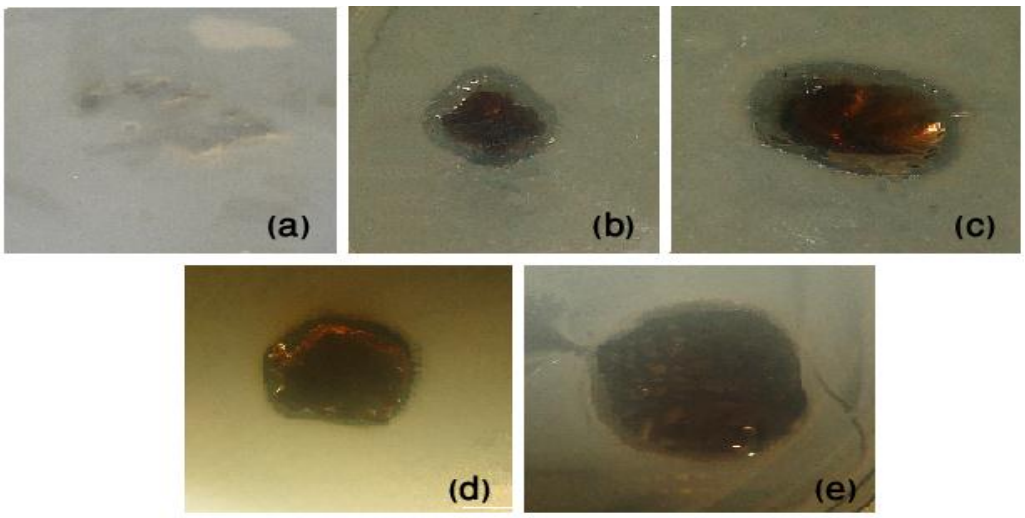

Figure 3.9: Antibacterial activity picture of hydrogel samples, against *E.Coli* bacteria (a) no silver loading (b) 1% GA (c) 2% GA (d) 3% GA (e) 5% GA. All samples were prepared with 1 mM $AgNO_3$, 3% PVA and radiation dose of 35 kGy.

3.3. Conclusions

In the present work, a simple one-pot synthesis of silver nanoparticle loaded PVA/GA hydrogel with varying size distribution (average 10-20 nm) of nanoparticles, depending on the concentration of GA, through gamma irradiation route was accomplished. The addition of GA improved the biocompatibility as

well as the swelling properties of the hydrogels. The FT-IR analysis suggested that the hydroxyl and carboxylic acid functional groups present in GA and PVA, interact with AgNPs during their formation. The silver loaded hydrogel network was found to be more thermally stable than unloaded one, reveals the TG analysis. The results of the study showed that this method has a good control over the size of the AgNPs for producing hydrogels with appropriate antibacterial activity. The swelling studies showed that, the % EDS increases with increase in GA concentration and decreases with increase in PVA concentration. Also % EDS of the hydrogels were independent of pH. The silver release profiles showed an increase with increase in GA concentration. The gel point determination using CW criterion gives the gel point at 25.34 kGy with highest GA concentration. It was observed that nano silver containing hydrogels had good antibacterial performance against gram negative E.*Coli* bacteria.

CHAPTER 4

SYNTHESIS AND STUDY OF BIOCOMPATIBLE GLYCOPOLYMERIC HYDROGELS

4.1. Introduction

A new class of biocompatible and biodegradable materials containing sugar moieties called as glycopolymers has received great attention in the scientific community. This is largely due to their wide range of applications, which include, the synthesis of macromolecular drugs, matrices for cell culture, model biological systems, surface modifiers, chromatographic purposes and so on.[128] The advanced polymerization techniques have facilitated the synthesis of glycopolymers of different types required for specific applications. In general, the application of polymers widens, with the scope of achieving it in different forms like gels.

The last three decades saw a vast and more creative development in the field of hydrogels directed towards a more precise/selective application.[129] The most attractive and important aspect of hydrogel is its bio-compatibility and bio-degradability which ensures its application in biomedical field.[130] This is largely promoted by its high water content and a similar physiochemical nature of hydrogels to the native extracellular matrix.[131] Even though extensive work have been carried out in the area of glycopolymers,[132] very little is known about the synthesis and study of purely sugar based hydrogels.[133] The significance of carbohydrate based polymers/hydrogels in the biomedical field is owing to the glycotargeting ability of carbohydrate pendants present in the polymer network.[134] The carbohydrate pendants in the glycopolymeric framework can be recognized by the cell surface carbohydrate binding proteins-lectins [135] and this makes them a unique class of materials for targeted drug delivery applications.[136]

Generally, sugar based hydrogels are synthesized from low molecular weight gelators (LMWG).[137] However, it has been reported that hydrogels derived from LMWG possess several disadvantages that include aggregation, crystallization or precipitation with time.[137d] One way to overcome this is to synthesize hydrogel from low molecular weight carbohydrate derivative by radiation polymerization. This technique has the potential to overcome most of the limitations that arises from LMWG, as the radiation crosslinked hydrogels possess more lifetime stability due to covalent crosslinking. An added advantage of radiation induced synthesis is that, a sterilized hydrogel can be achieved in a single step process by applying appropriate radiation dose.

Recently, studies towards the synthesis of biodegradable materials revealed that incorporation of biodegradable crosslinkers into a non-biodegradable but biocompatible polymer could transform the latter to a biodegradable material.[14] This observation triggered efforts to make biodegradable crosslinkers based on peptides/saccharides. In this context, it is of interest to have a crosslinker with functional groups like that on the monomer, so that the functional homogeneity is maintained throughout the polymeric network. Currently, for the synthesis of glycopolymeric hydrogels, commercially available crosslinking agents with non-sugar residue are being used.[138c] It was Dordick and coworkers who demonstrated for the first time a chemoenzymatic method for the synthesis of sugar containing polyacrylate hydrogels.[138d] To the best of our knowledge there exists only one report on the chemical synthesis of a sugar based cross linker *i.e.*,

bis(methacrylamido) derivative of D-glucose **1 (**Figure 4.1). The utility of **1** to form hydrogel has been tested successfully by synthesizing PHEMA based biocompatible hydrogel.[138c]

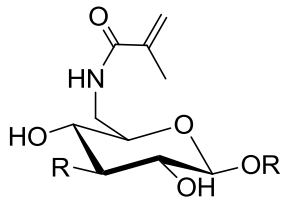

1, R = $(CH_2)_2NHC(O)C(Me)=CH_2$

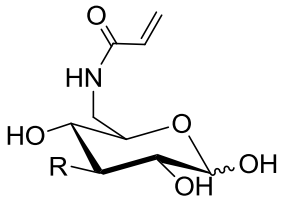

2a, R = $NHC(O)CH=CH_2$
2b, R = OH

Figure 4.1: Acrylamides derived from D-glucose

Citing the significance of glycopolymeric hydrogels and the relevance of having a sugar based crosslinker, we here by describe the synthesis of a D-glucose based bisacrylamide cross linker substituted at C-3 and C-6 carbon of sugar (Glc-bis) **2a**, (Figure 4.1) with hemiacetal functionality. To check the feasibility of Glc-bis to form homogeneous glycopolymeric gel (Glc-gel), a related monoacrylamide substituted at C-6 position (Glc-acryl) **2b** was also synthesized and their gelation was studied using radiation polymerization. The targets selected are also interesting by the fact that D-glucose derived polymers substituted at C-6 position showed specific binding to the asialoglycoprotein receptor of mouse primary hepatocytes.[139]

The synthesized Glc-bis and Glc-acryl were characterized by ^{1}H and ^{13}C-NMR. The molecular structure, water content, viscoelasticity, thermal stability, cytotoxicity and lectin recognition of the synthesized hydrogels (Glc-gel) were studied using the techniques like Fourier Transform Infra-Red (FT-IR)

spectroscopy, oscillatory rheology, Thermogravimetric-Differential Scanning Calorimetric (TG-DSC) analysis, MTT assay and UV-vis spectroscopy.

4.2. Experimental

The details of synthesis procedures followed for achieving the required intermediates and targets are given below.

4.2.1. ***3-Azido-3-deoxy-5-hydroxy-1,2-O-isopropylidene-6-O-tosyl-α-D-gluco-furanose (4).***

To a stirred solution of the azido diol **3** (3.50 g, 14.27 mmol) and pyridine (1.38 mL, 17.12 mmol) in CH_2Cl_2 (50 mL) at 0 ºC, was added tosyl chloride (2.91 g, 15.27 mmol) dissolved in CH_2Cl_2 (15 mL) dropwise and DMAP (4-Dimethyl aminopyridine) (0.08 g, 0.71 mmol). The reaction mixture was stirred at same temperature for 1 h, slowly brought to 25 ºC and stirred for additional 2 h. After completion of reaction (*cf.* TLC), water (50 mL) was added and extracted with CH_2Cl_2 (100 mL). The organic layer was washed, sequentially, with cold 1N HCl (2 x 20 mL), saturated $NaHCO_3$ (1 x 20 mL), brine (1 x 20 mL), water (1 x 50 mL), and dried over anhydrous Na_2SO_4. Filtration and evaporation in vacuum gave a residue, which on column chromatography afforded **4** (4.96 g, 87%) as a thick liquid: R_f = 0.48 (30% EtOAc/hexane); $[\alpha]_D^{25}$ –7.27 (c 1.1, $CHCl_3$); ν_{max}/cm^{-1} 1176, 1367; δ_H(600 MHz; $CDCl_3$) 7.81 (d, *J* = 8.2 Hz, 2H), 7.36 (d, *J* = 8.2 Hz, 2H), 5.81 (d, *J* = 3.4 Hz, 1H), 4.61 (d, *J* = 3.4 Hz, 1H), 4.31 (d, *J* = 8.8 Hz, 1H), 4.17 (s, 1H), 4.11 – 4.07 (m, 3H), 2.74 (d, *J* = 3.7 Hz, 1H, exchangeable

with D_2O), 2.46 (s, 3H), 1.47 (s, 3H), 1.31 (s, 3H) (Figure 4.2); δ_C(50 MHz; $CDCl_3$) 145.8, 132.9, 130.7, 128.7, 113.1, 105.6, 83.8, 78.1, 73.1, 68.2, 66.8, 27.2, 26.9, 22.3 (Figure 4.3). Elemental Analysis Calculated for $C_{16}H_{21}N_3O_7S$: C, 48.11; H, 5.30. Found: C, 48.15; H, 5.37; ESI-MS: Calculated for $[C_{16}H_{21}N_3O_7S+Na]^+$: 422.01 Da, Observed: 421.85 Da.

4.2.2. ***3,6-Diazido-3,6,-dideoxy-5-hydroxy-1,2-O-isopropylidene-α-D-gluco-furanose (5)***.

Sodium azide (1.83 g, 28.25 mmol) was added to a solution of tosylate (**4**) (4.51 g, 11.29 mmol) in DMF (20 mL) and heated at 80 ^oC for 3 h. After completion of reaction (*cf*. TLC), DMF was removed under vacuo, and the residue was extracted with EtOAc (3 x 50 mL). The combined organic layer was dried over anhydrous Na_2SO_4, concentrated and purified using column chromatography to give diazide (**5**) as a thick liquid (2.63 g, 86%): R_f = 0.49 (25% EtOAc/hexane); $[\alpha]_D^{25}$ –40.05 (c 1.2, $CHCl_3$); ν_{max}/cm^{-1} 2100; δ_H(700 MHz; $CDCl_3$) 5.87 (d, *J* = 3.5 Hz, 1H), 4.65 (d, *J* = 3.5 Hz, 1H), 4.12 – 4.17 (m, 2H), 4.03 – 3.96 (m, 1H), 3.67 (dd, *J* = 12.6, 2.8 Hz, 1H), 3.51 (dd, *J* = 12.6, 6.3 Hz, 1H), 2.38 – 2.32 (m, 1H, exchangeable with D_2O), 1.51 (s, 3H), 1.33 (s, 3H) (Figure 4.4.); δ_C(176 MHz, $CDCl_3$) 113.1, 105.6, 83.9, 79.8, 69.3, 66.8, 55.5, 27.2, 26.8 (Figure 4.5). Elem. Anal. Calcd. for $C_9H_{14}N_6O_4$: C, 40.00; H, 5.22. Found: C, 40.07; H, 5.18.

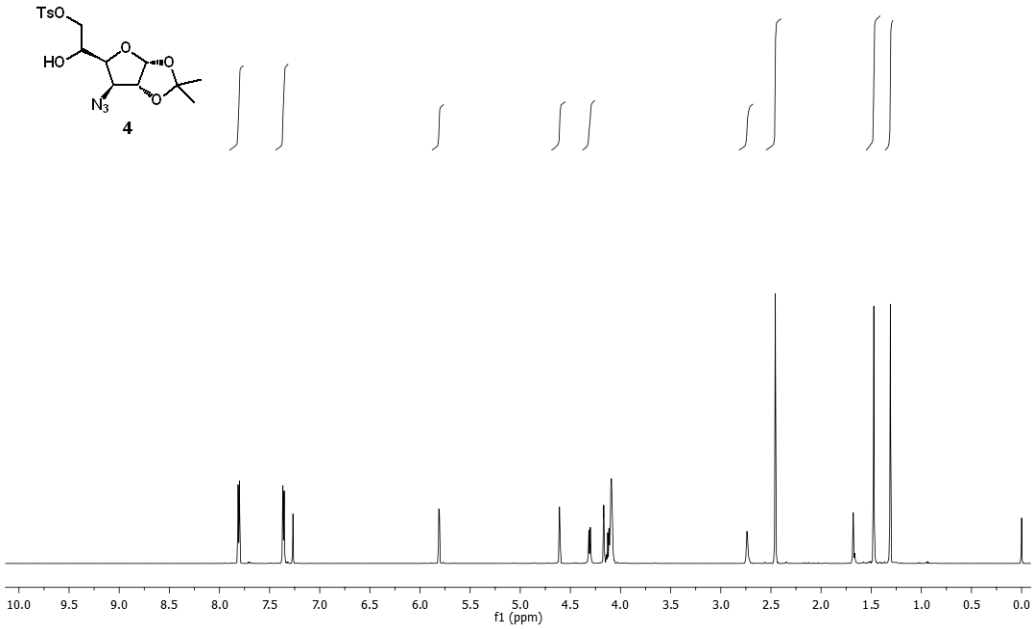

Figure 4.2: ^{1}H NMR (600 MHz, $CDCl_3$) spectrum of compound **4**

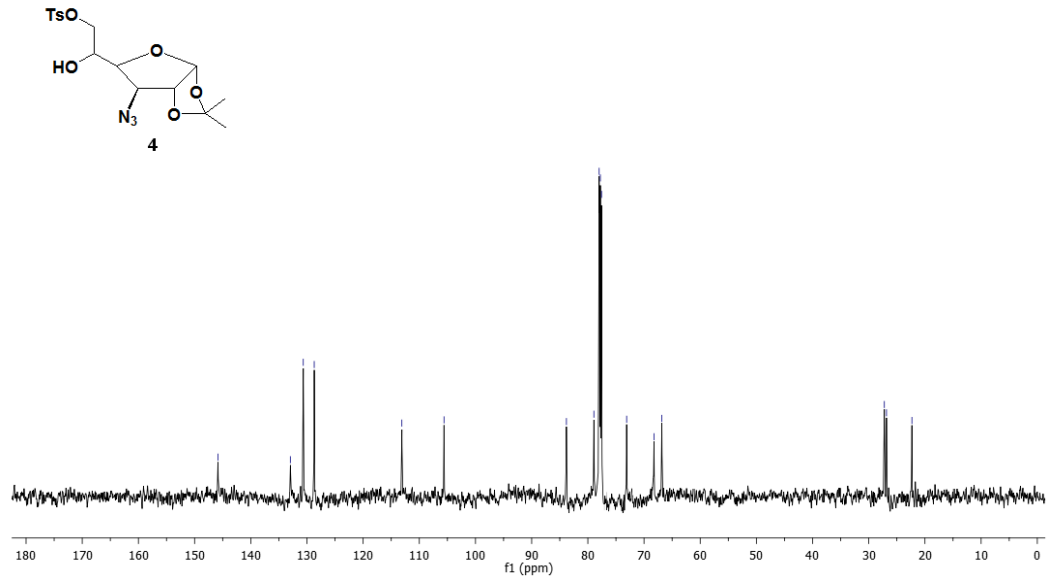

Figure 4.3: ^{13}C NMR (151 MHz, $CDCl_3$) spectrum of compound **4**

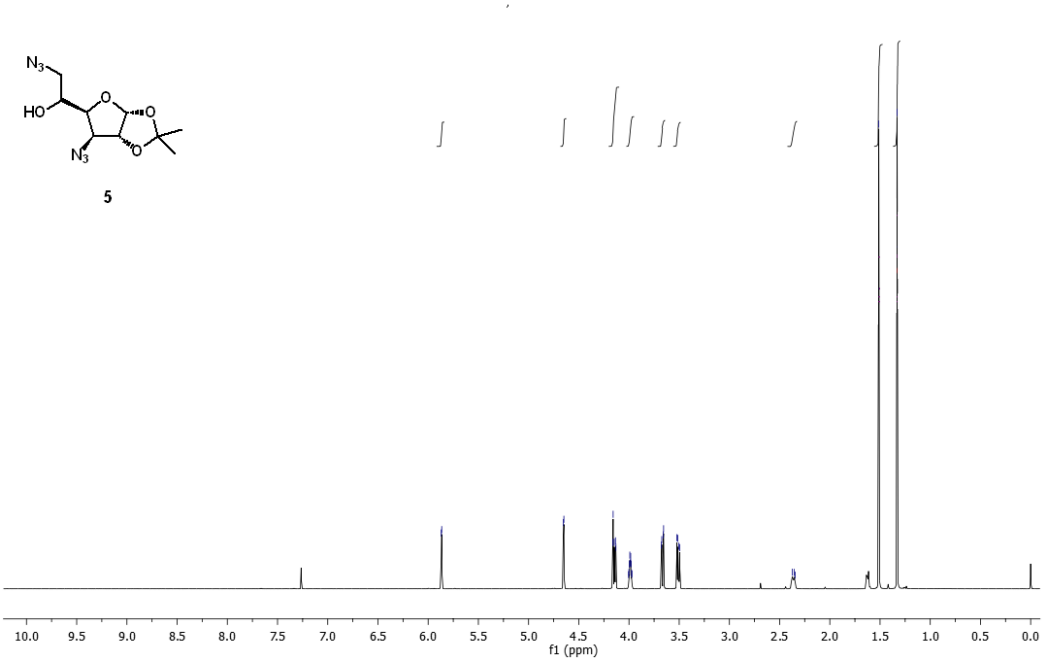

Figure 4.4: ^{1}H NMR (700 MHz, $CDCl_3$) spectrum of compound **5**

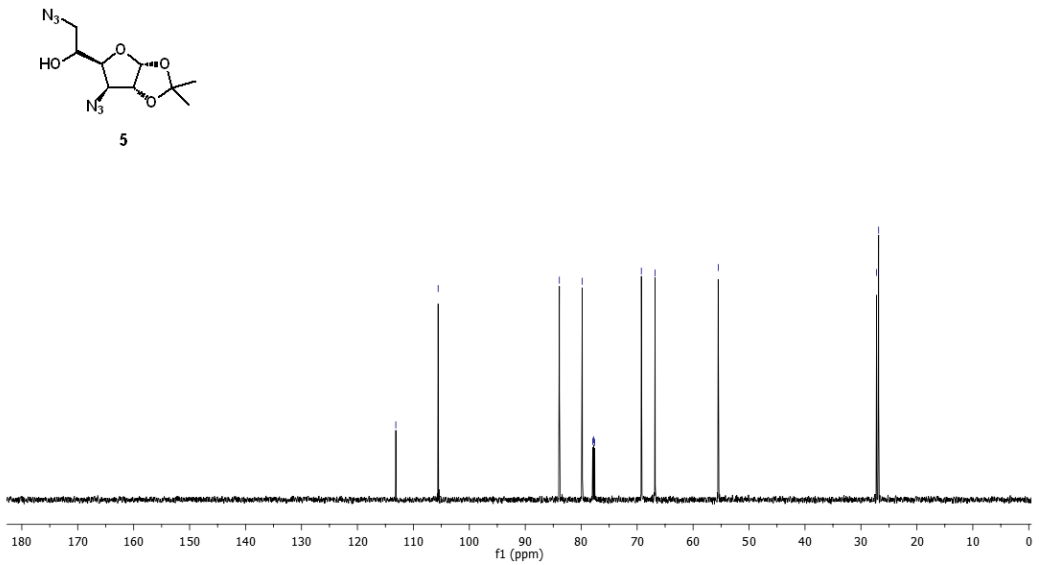

Figure 4.5: ^{13}C NMR (176 MHz, $CDCl_3$) spectrum of compound **5**

4.2.3. *3,6-Bisacrylamido-3,6,-dideoxy-5-hydroxy-1,2-O-isopropylidene-α-D-gluco-furanose (6)*.

To a solution of diazido alcohol (**5**) (2.45 g, 9.06 mmol) in MeOH (30 mL), was added 10% Pd/C (0.17 g) and hydrogenated (80 psi) for 12 h at 25 ºC. The catalyst was filtered through a pad of Celite 545 using MeOH (4 x 10 mL). The filterate was concentrated and dried under vaccum. The vaccum dried diamine was dissolved in CH_2Cl_2 (35 mL) and DIEA (Diisopropylethylamine) (7.89 mL, 45.30 mmol), cooled to –40 ºC, acryloyl chloride (1.64 mL, 20.11 mmol) was added and stirred at same temperature for 20 min. After completion of reaction (*cf.* TLC), reaction mixture was diluted with cold water (5 mL), and extracted using CH_2Cl_2 (3 x 30 mL). The combined organic layer was kept over anhydrous Na_2SO_4, concentrated under vacuo, and purified using column chromatography to afford (**6**) as a thick liquid (2.36 g, 79% (over two steps)): R_f = 0.15 (80% EtOAc/hexane); $[\alpha]_D^{25}$ +90.35 (c 1.50, $CHCl_3$); ν_{max}/cm^{-1} 1685, 1665, 1551; δ_H(600 MHz; CD_3OD) 7.85 (s, 1H, exchangeable with D_2O), 6.30 – 6.12 (m, 4H), 5.84 (d, *J* = 3.6 Hz, 1H), 5.66 (dd, *J* = 8.4, 3.5 Hz, 1H), 5.59 (dd, *J* = 10.1, 1.8 Hz, 1H), 4.48 (d, *J* = 3.6 Hz, 1H), 4.43 (d, *J* = 3.3 Hz, 1H), 3.98 (dd, *J* = 8.6, 3.3 Hz, 1H), 3.70 – 3.62 (m, 2H), 3.27 (s, 1H, exchangeable with D_2O), 3.15 (dd, *J* = 14.4, 8.6 Hz, 1H), 1.44 (s, 3H), 1.26 (s, 3H) (Figure 4.6); δ_C(126 MHz; CD_3OD) 167.1, 167.0, 130.6, 129.9, 126.7, 125.5, 111.7, 104.7, 84.0, 79.8, 67.2, 55.8, 42.9, 25.5, 25.1(Figure 4.7). Elem. Anal. Calcd. for $C_{15}H_{22}N_2O_6$: C, 55.21; H, 6.79. Found:

C, 55.19; H, 6.85; ESI-MS: Calcd. for $[C_{15}H_{22}N_2O_6 + Na]^+$: 349.12 Da, Obsd: 348.98 Da.

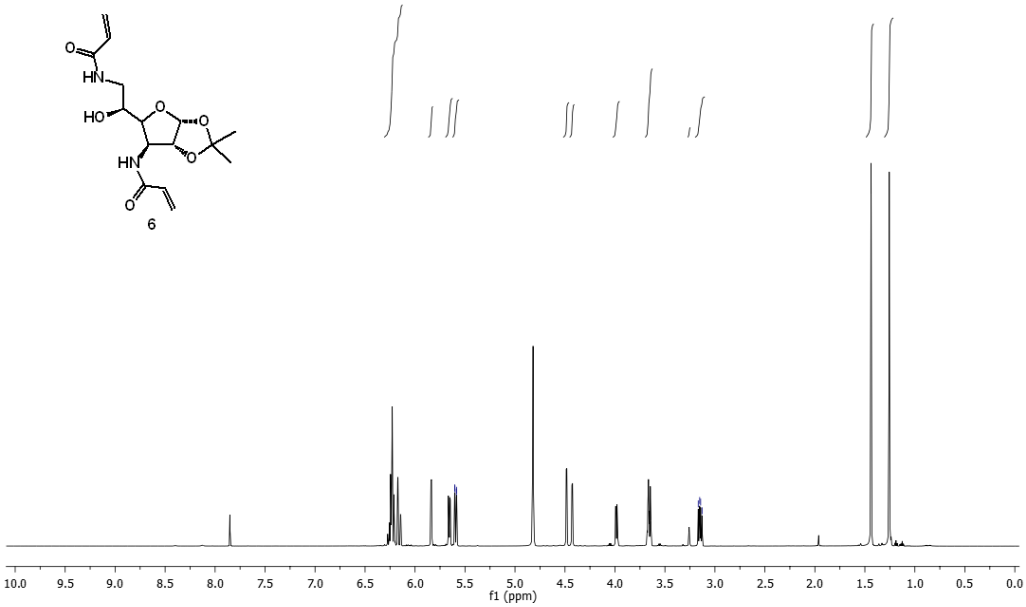

Figure 4.6: ^{1}H NMR (600 MHz, CD_3OD) spectrum of compound **6**

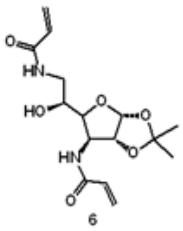

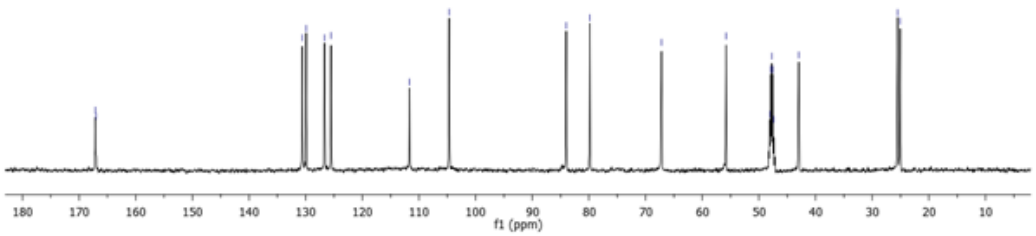

Figure 4.7: ^{13}C NMR (126 MHz, CD_3OD) spectrum of compound **6**

4.2.4. *(2R,3S,4S,5S)-4-acrylamido-6-(acrylamidomethyl)-tetrahydro-2H-Pyran-2,3,5-triol (Glc-bis, 2a)*

A pre-cooled solution of TFA-H_2O (3:2, 10 mL) was added dropwise to a RB flask charged with bisacrylamide **6** (1.30 g, 3.98 mmol) (synthesized as shown in scheme 4.1) at 0 ^oC. The reaction mixture was stirred at same temperature for 30 min, slowly brought to 25 ^oC and stirred for additional 10 h. After completion of reaction (*cf*. TLC) TFA was evaporated along with toluene and dried under vaccum. The residue was precipitated using dry EtOAc (20 mL) and washed well with EtOAc (5 x 10 mL). The residue was vaccum dried, redissolved in double distilled water, filtered through Millex (25 mm, 5 µm) and lyophilized to afford bisacrylamide **2a** as a white amorphous powder (0.78 g, 68%). In the ^1H NMR spectrum of **2a** (Figure 4.8) the anomeric protons H_{1e} and H_{1a} appeared as two distinct doublets at δ 5.27 and 4.76 with $J_{1e,2a}$ = 3.6 Hz, and J_{1a2a} = 7.8 Hz, respectively. The three sets of multiplets at δ 6.41 – 6.31, 6.29 – 6.21, and 5.88 – 5.78 were due to protons attached to the olefinic carbons. The ^{13}C NMR spectrum confirmed the presence of two amide bonds with the appearance of peaks at δ 169.5, 168.8, while peaks at δ 129.9, 129.7, 127.7, 127.5, accounted for four olefinic carbons of the bisacrylamide moiety (Figure 4.9).

4.2.5. *{[1,2,],[5,6]}-Di-O-isopropylidene-3-O-tert-butyldiphenylsilyl-α-D-gluco-furanose (8)*

To a cooled (0 ^oC) solution of diacetone D-glucose (**7**) (5.00 g, 19.21 mmol) and imidazole (2.61 g, 38.42 mmol) in DMF (25 mL) was added TBDPSCl (*tert*-butyl

(chloro) diphenyl silane) (6.16 mL, 24.01 mmol) dropwise, followed it with DMAP (*N*,*N*-Dimethyl amino pyridine) (0.12 g, 0.96 mmol). The reaction mixture was slowly brought to 30 ^{o}C, and stirred for additional 24 h. After the completion of reaction (*cf*. TLC), DMF was evaporated under pressure and then extracted using EtOAc (200 mL) afforded a thick residue which on coloumn purification afforded (**8**) as a thick liquid (8.30 g, 86%): R_f = 0.55 (10% EtOAc/hexane); $[\alpha]_D^{25}$ –10.08 (c 1.0, $CHCl_3$); ν_{max}/cm^{-1} 1211, 1093; δ_H(600 MHz; $CDCl_3$) 7.98 – 7.64 (m, 4H), 7.52 – 7.32 (m, 6H), 5.81 (d, *J* = 3.2 Hz, 1H), 4.48 – 4.42 (m, 2H), 4.19 – 4.15 (m, 1H), 4.06 (d, *J* = 3.1 Hz, 1H), 4.05 – 3.97 (m, 2H), 1.42 (s, 3H), 1.39 (s, 3H), 1.33 (s, 3H), 1.09 (s, 9H), 1.08 (s, 3H) (Figure 4.10); δ_C(176 MHz; $CDCl_3$) 136.7, 136.4, 134.7, 133.2, 130.6, 130.2, 128.5, 128.3, 112.3, 109.8, 105.7, 85.2, 83.2, 77.3, 72.9, 68.6, 27.6, 27.5, 27.3, 26.7, 25.9, 20.1 (Figure 4.11). Elem. Anal. Calcd. for $C_{28}H_{38}O_6Si$: C, 67.44; H, 7.68. Found: C, 67.47; H, 7.62.

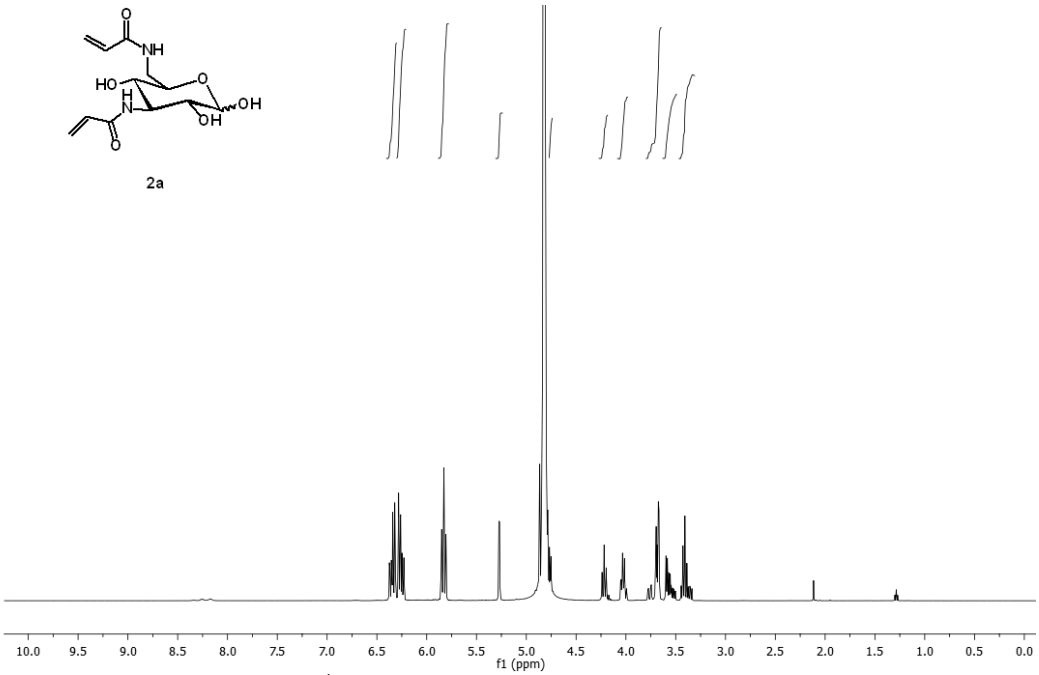

Figure 4.8: ^{1}H NMR (500 MHz, D_2O) spectrum of compound **2a**

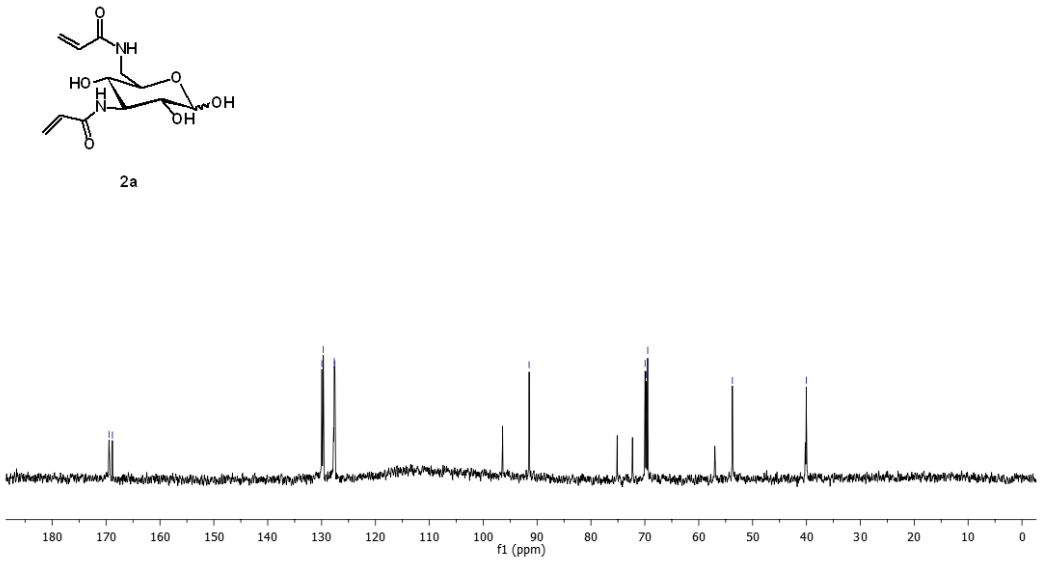

Figure 4.9: ^{13}C NMR(126 MHz, D_2O) spectrum of compound **2a**

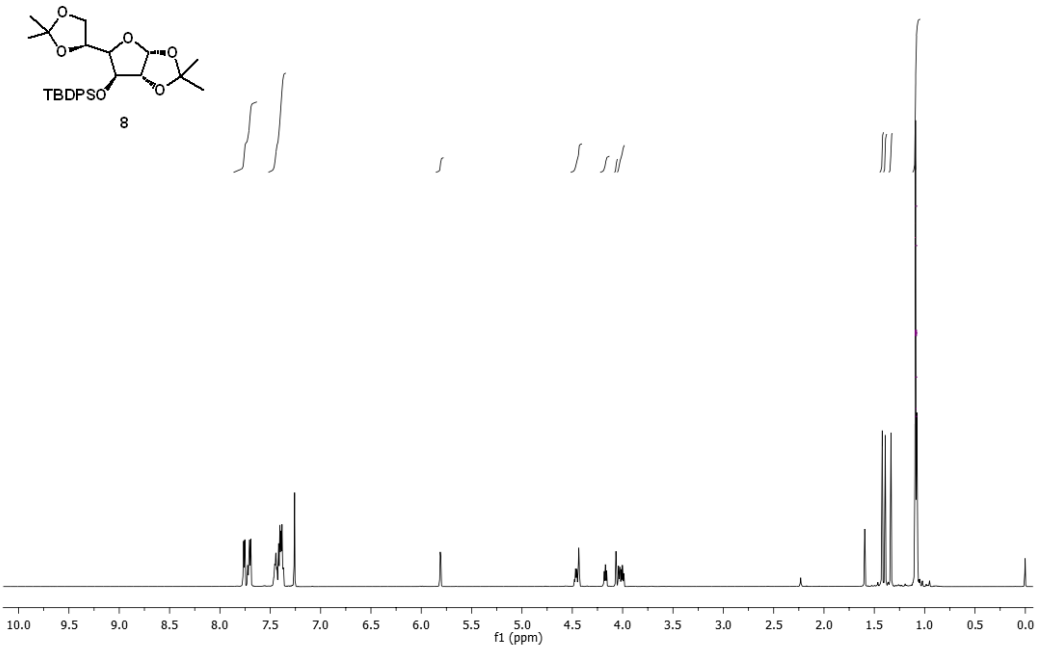

Figure 4.10: ^{1}H NMR (600 MHz, $CDCl_3$) spectrum of compound **8**

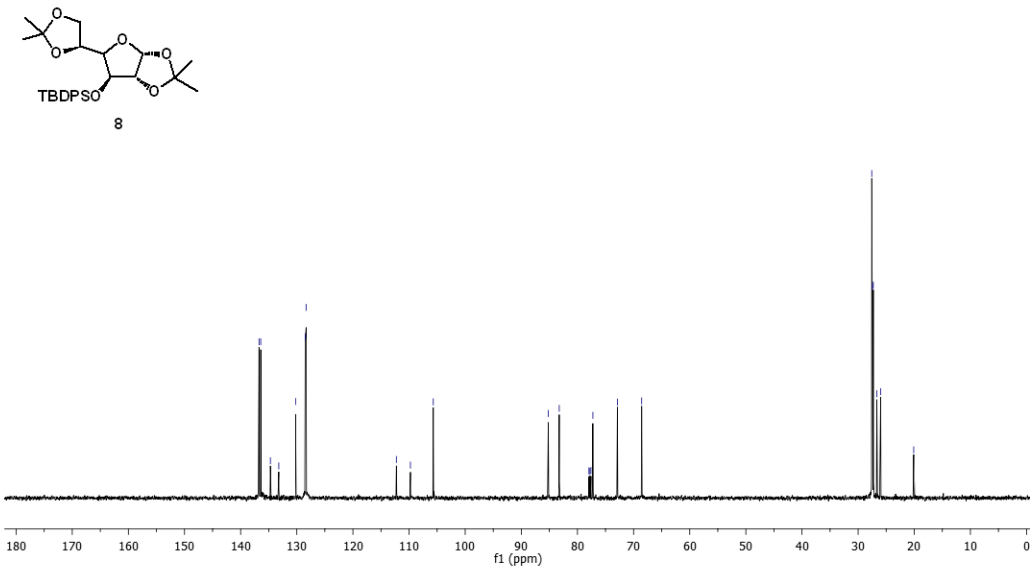

Figure 4.11: ^{13}C NMR (176 MHz, $CDCl_3$) spectrum of compound **8**

4.2.6. *5,6-Dihydroxy-1,2-O-isopropylidene-3-O-tert-butyldiphenylsilyl-α-D-gluco-furanose (9)*

30% Perchloric acid (8 mL) was slowly added to a solution of (**8**) (8.00 g, 16.04 mmol) in THF (20 mL) at 0 ^{o}C. The reaction mixture was stirred at same temperature until it showed complete conversion (*cf*. TLC), neutralized using K_2CO_3 (saturated) solution, concentrated, and extracted using EtOAc (3 x 50 mL). The combined organic layer was dried over anhydrous Na_2SO_4, concentrated, to afford a thick liquid which was purified using column chromatography to yield diol (**9**) as a white solid (5.72 g, 77%): Mp 120 ^{o}C; R_f = 0.30 (30% EtOAc/hexane); $[\alpha]_D^{25}$ –17.50 (c 1.1, $CHCl_3$); ν_{max}/cm^{-1} 3355br, 1227, 1064; δ_H(700 MHz; $CDCl_3$) 7.73 (d, *J* = 7.7 Hz, 2H), 7.68 (d, *J* = 7.7 Hz, 2H), 7.47 (t, *J* = 7.3 Hz, 2H), 7.42 (t, *J* = 7.3 Hz, 4H), 5.84 (d, *J* = 3.5 Hz, 1H), 4.48 (s, 1H), 4.28 (d, *J* = 3.5 Hz, 1H), 4.06 – 3.97 (m, 2H), 3.88 – 3.78 (m, 1H), 3.73 (dd, *J* = 11.2, 5.3 Hz, 1H), 1.67 – 1.61 (m, 2H, exchangeable with D_2O), 1.40 (s, 3H), 1.14 (s, 3H), 1.10 (s, 9H) (Figure 4.12); δ_C(176 MHz; $CDCl_3$) 136.5, 136.4, 134.5, 133.2, 130.9, 130.8, 128.7, 128.6, 112.4, 105.5, 85.1, 81.9, 77.4, 69.2, 65.2, 27.7, 27.3, 26.7, 20.2 (Figure 4.13). Elem. Anal. Calcd for $C_{25}H_{34}O_6Si$: C, 65.47; H, 7.47. Found: C, 65.44; H, 7.45; ESI-MS: Calcd. for $[C_{25}H_{34}O_6Si + Na]^+$: 481.19 Da, Obsd: 481.02 Da.

4.2.7.6-Azido-6-deoxy-5-hydroxy-1,2-O-isopropylidene-3-O-tert butyldiphenylsilyl-α-D-gluco-furanose (10)

To a solution of diol (**9**) (5.52 g, 12.03 mmol) in CH_2Cl_2 (60 mL) at 0 ^oC was added triethyl amine (TEA) (2.01 mL, 14.42 mmol) followed it with dropwise addition of methane sulfonyl chloride (0.98 mL, 12.63 mmol) in CH_2Cl_2 (15 mL) over 30 min. The reaction was stirred at same temperature for 1 h, then brought to 25 ^oC and stirred for additional 1 h. The reaction was quenched using cold water (20 mL) and extracted using CH_2Cl_2 (3 x 25 mL). The combined organic layers were dried over anhydrous Na_2SO_4, concentrated and dried under vacuum to afford mesylate (crude) as a thick liquid. To the solution of mesylate (crude) in DMF (25 mL), was added sodium azide (5.47 g, 84.21 mmol) and heated at 70-80 ^oC for 3 h. The usual workup and column purification afforded azide (**10**) (3.10 g, 53%) as a thick liquid: R_f = 0.70 (20% EtOAc/hexane); $[\alpha]_D^{25}$ –22.25 (c 1.1, $CHCl_3$); ν_{max}/cm^{-1} 2098, 1215, 1093; δ_H(700 MHz; $CDCl_3$) 7.74 (d, *J* = 7.7 Hz, 2H), 7.70 (d, *J* = 7.7 Hz, 2H), 7.48 – 7.45 (m, 2H), 7.44 – 7.39 (m, 4H), 5.90 (d, *J* = 3.5 Hz, 1H), 4.48 (d, *J* = 3.5 Hz, 1H), 4.32 (t, *J* = 2.7 Hz, 1H), 4.22 (q, *J* = 4.7 Hz, 1H), 4.12 – 4.08 (m, 1H), 3.40 (dd, *J* = 12.8, 4.8 Hz, 1H), 3.33 (dd, *J* = 12.8, 4.0 Hz, 1H), 3.19 (d, *J* = 3.5 Hz, 1H, exchangeable with D_2O), 1.49 (s, 3H), 1.31 (s, 3H), 1.09 (s, 9H) (Figure 4.14); δ_C(176 MHz; $CDCl_3$) 136.4, 136.3, 134.2, 133.1, 131.0, 130.9, 128.8, 128.7, 112.5, 105.6, 85.2, 81.7, 77.1, 68.5, 55.5, 27.7,

27.4, 26.8, 20.1 (Figure 4.15). Elem. Anal. Calcd. for $C_{25}H_{33}N_3O_5Si$: C, 62.09; H, 6.88. Found: C, 62.15; H, 6.93.

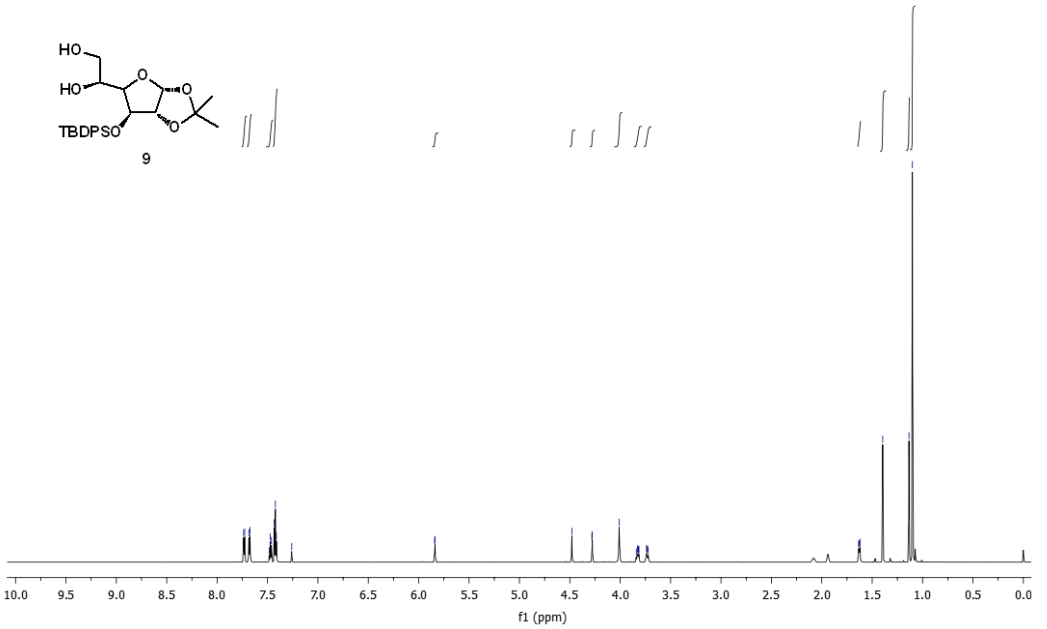

Figure 4.12: ^{1}H NMR (700 MHz, $CDCl_3$) spectrum of compound **9**

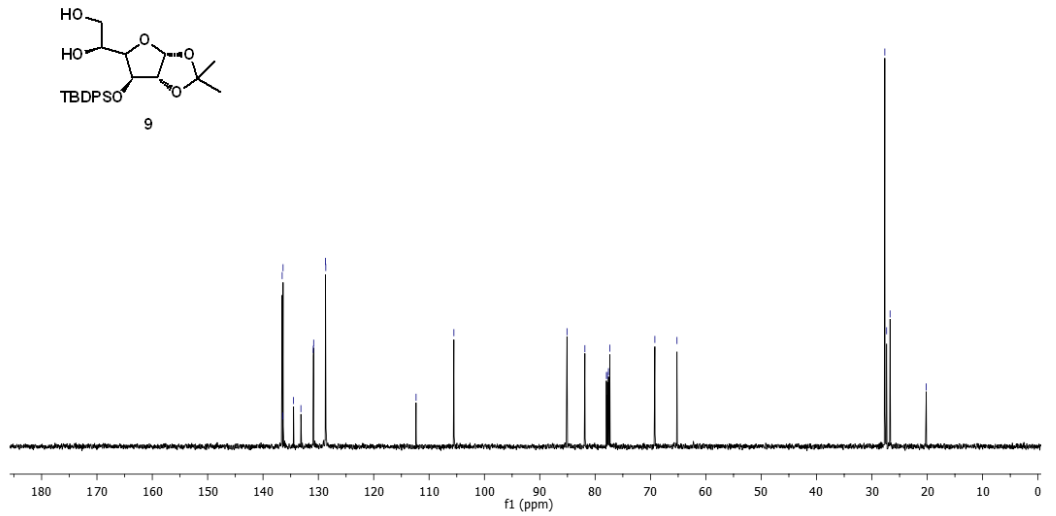

Figure 4.13: ^{13}C NMR (176 MHz, $CDCl_3$) spectrum of compound **9**

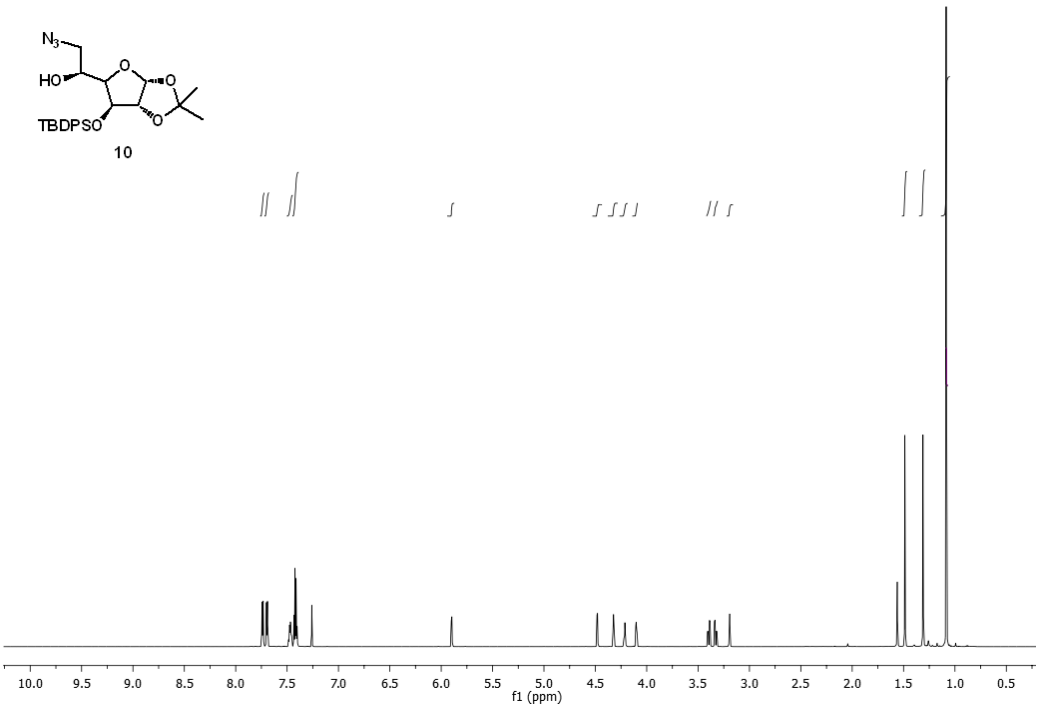

Figure 4.14: ^{1}H NMR (700 MHz, $CDCl_3$) spectrum of compound **10**

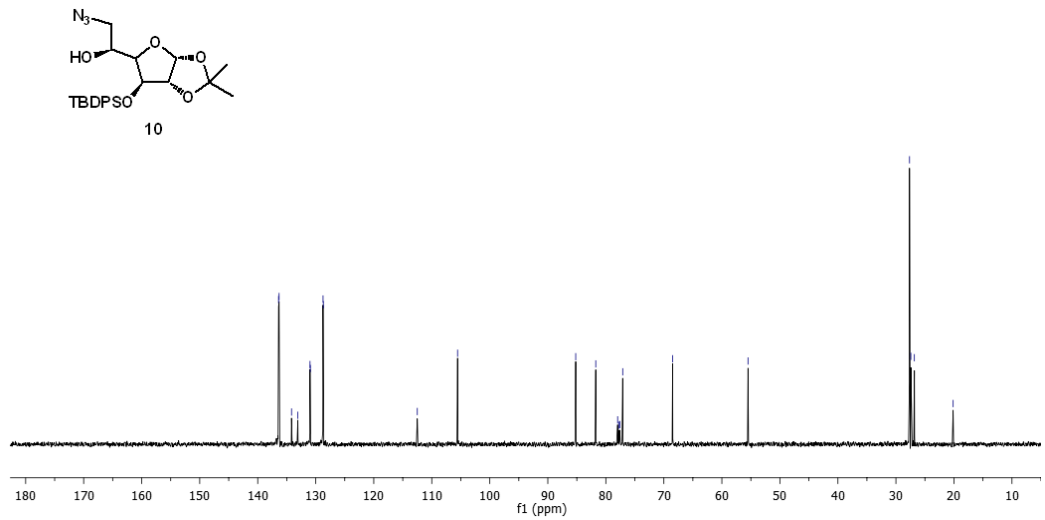

Figure 4.15: ^{13}C NMR (176 MHz, $CDCl_3$) spectrum of compound **10**

4.2.8. *6-Acrylamido-6-deoxy-5-hydroxy-1,2-O-isopropylidene-3-O-tert-butyldiphenylsilyl-α-D-gluco-furanose (11)*

The hydroxyl azide (**10**) (3.30 g, 6.82 mmol) was subjected to hydrogenation (10% Pd/C (0.20 g), H_2 (20 psi), 5 h) and acrylation (acryloyl chloride (0.58 mL, 7.17 mmol), DIEA (1.42 mL, 8.18 mmol) sequentially, as mentioned earlier for the synthesis of bisacrylamide (**6**), to afford acrylamide (**11**) as a thick liquid (2.90 g, 83% (over two steps)): R_f = 0.20 (30% EtOAc/hexane); $[\alpha]_D^{25}$ +24.21 (c 1.2, $CHCl_3$); ν_{max}/cm^{-1} 3490br, 1680; δ_H(700 MHz; $CDCl_3$) 7.76 – 7.74 (m, 2H), 7.70 – 7.67 (m, 2H), 7.48 – 7.42 (m, 2H), 7.40 (q, *J* = 7.2 Hz, 4H), 6.34 – 6.29 (m, 1H), 6.19 (s, 1H, exchangeable with D_2O), 6.13 (dd, *J* = 17.0, 10.3 Hz, 1H), 5.80 (d, *J* = 3.4 Hz, 1H), 5.69 (dd, *J* = 10.3, 1.1 Hz, 1H), 4.50 (d, *J* = 2.2 Hz, 1H), 4.14 – 4.11 (m, 2H), 3.84 (ddd, *J* = 14.4, 6.1, 2.7 Hz, 1H), 3.79 (bs, 1H), 3.46 (dt, *J* = 14.4, 6.1 Hz, 1H), 1.61 (s, 1H, exchangeable with D_2O), 1.36 (s, 3H), 1.09 (s, 12H) (Figure 4.16); δ_C(176 MHz; $CDCl_3$) 168.6, 136.7, 136.4, 134.8, 133.1, 130.9, 130.8, 130.7, 128.7, 128.6, 127.9, 112.3, 105.5, 85.1, 82.6, 77.1, 69.1, 45.5, 27.6, 27.5, 26.8, 20.2 (Figure 4.17). Elem. Anal. Calcd. for $C_{28}H_{37}NO_6Si$: C, 65.72; H, 7.29; Found: C, 65.75; H, 7.36; ESI-MS: Calcd. for $[C_{28}H_{37}NO_6Si + Na]^+$: 534.22 Da, Obsd: 534.09 Da.

4.2.9. *6-Acrylamido-6-deoxy-3,5-dihydroxy-1,2-O-isopropylidene-α-D-gluco-furanose (12)*

To a solution of acrylamide (**11)** (1.00 g, 1.93 mmol) in THF at 0 ^{o}C was added TBAF (Tetra-n- butyl ammonium fluoride) (1M in THF) (2.51 mL, 2.51 mmol). The reaction mixture was stirred for 1.5 h and brought to 30 ^{o}C. After completion of reaction (*cf*. TLC) the reaction mixture was concentrated under vaccum, and extracted using EtOAc (6 x 20 mL). The resultant thick liquid, was purified using coloumn chromatography to afford the diol (**12**) as a thick liquid (0.44 g, 83 %): R_f = 0.25 (EtOAc); $[\alpha]_D^{25}$ +4.00 (c 1.1, MeOH); ν_{max}/cm^{-1} 3500br, 1687, 1671, 1545; δ_H(600 MHz; CD_3OD) 6.34 – 6.19 (m, 2H), 5.87 (d, *J* = 2.1 Hz, 1H), 5.65 (d, *J* = 10.0 Hz, 1H), 4.47 (s, 1H), 4.20 (s, 1H), 3.98 – 3.90 (m, 2H), 3.68 (d, *J* = 13.9 Hz, 1H), 3.32 – 3.27 (m, 2H), 1.44 (s, 3H), 1.29 (s, 3H) (Figure 4.18); δ_C(176 MHz; CD_3OD) 167.4, 130.7, 125.4, 111.3, 105.1, 85.6, 81.4, 73.9, 67.3, 43.4, 25.7, 25.0 (Figure 4.19). Elem. Anal. Calcd. for $C_{12}H_{19}NO_6$: C, 52.74; H, 7.01. Found: C, 52.81; H, 6.97; ESI-MS: Calcd. for $[C_{12}H_{19}NO_6 + Na]^+$: 296.10 Da, Obsd: 295.92 Da.

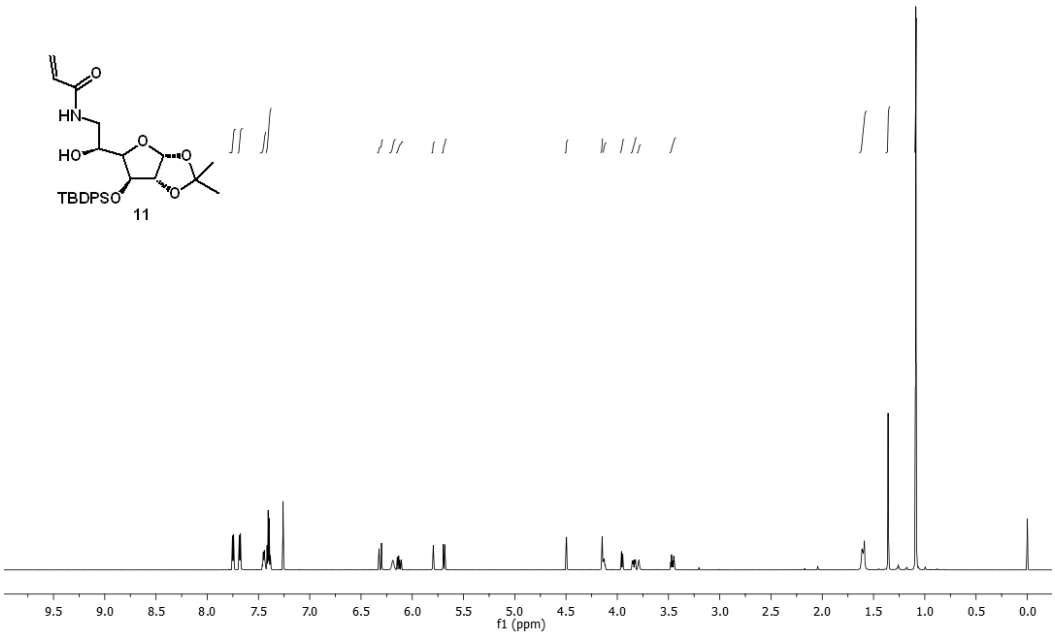

Figure 4.16: ^{1}H NMR (700 MHz, $CDCl_3$) spectrum of compound **11**

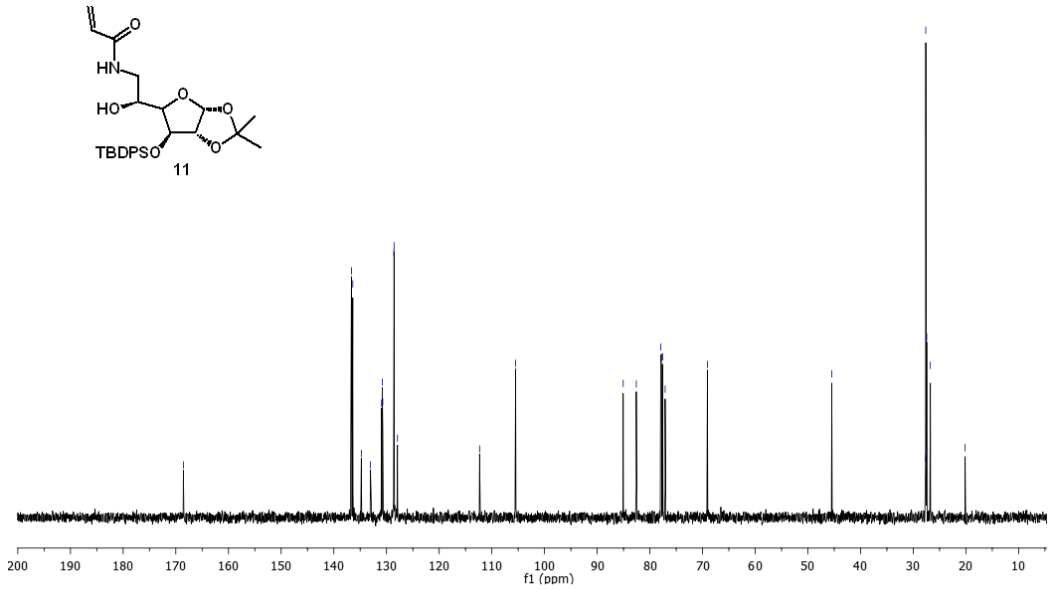

Figure 4.17: ^{13}C NMR (176 MHz, $CDCl_3$) spectrum of compound **11**

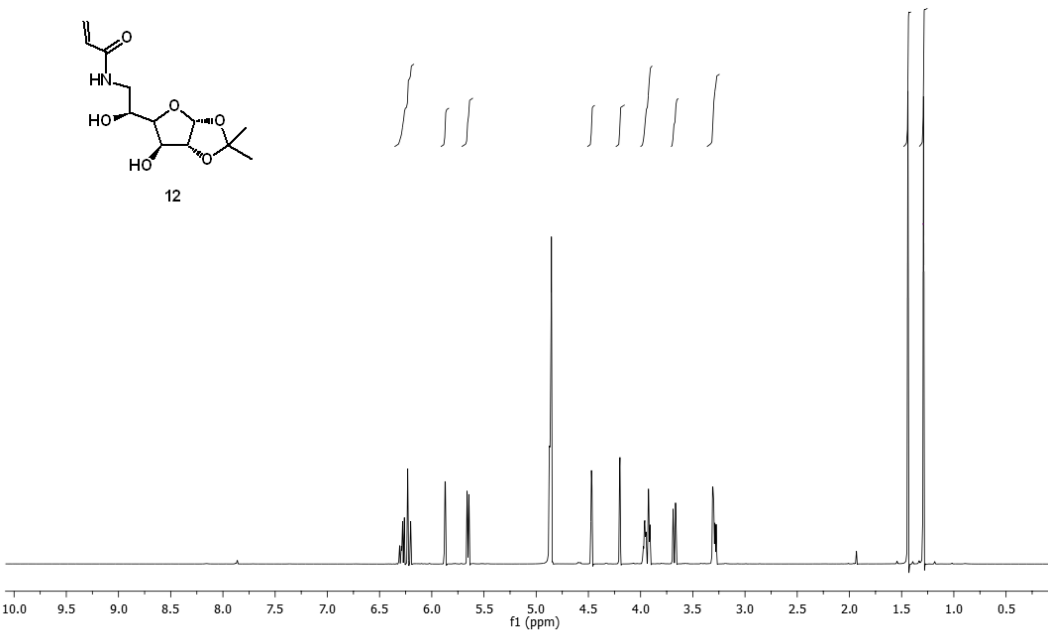

Figure 4.18: ^{1}H NMR (600 MHz, CD_3OD) spectrum of compound **12**

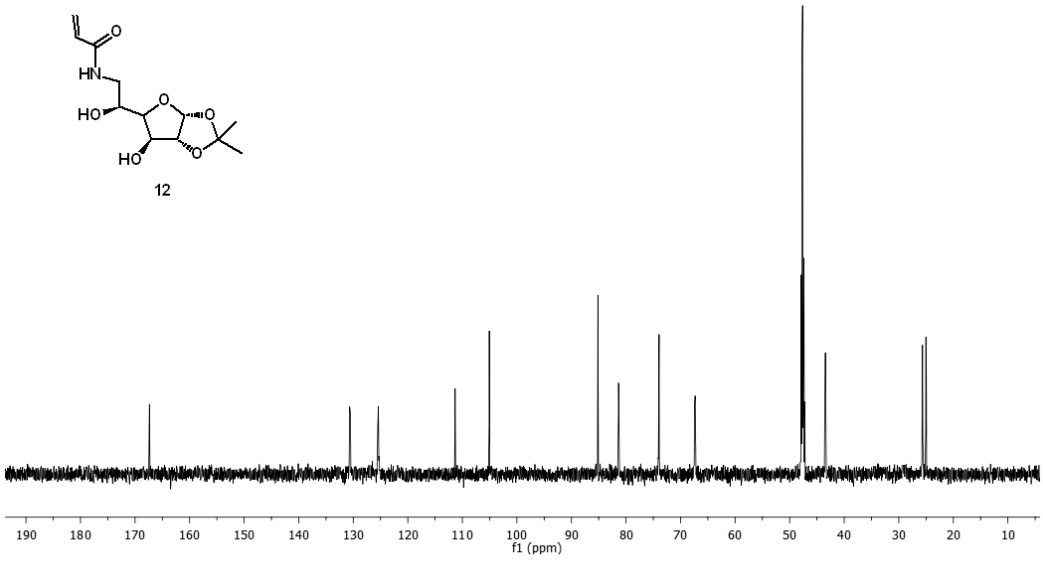

Figure 4.19: ^{13}C NMR (176 MHz, CD_3OD) spectrum of compound **12**

4.3.0. *N-(((3S,4S,5S,6R)-tetrahydro-3,4,5,6-tetrahydroxy-2H-pyran-2-yl)methyl) acrylamide (Glc-acryl, 2b)*

A pre-cooled solution of TFA-H_2O (3:2, 10 mL) was added dropwise to RB charged with acrylamide **12** (1.30 g, 4.75 mmol) (synthesized as shown in Scheme 4.2) at 0 ^oC. The reaction mixture was stirred at same temperature for 30 min, slowly brought to 25 ^oC and was stirred for additional 10 h. After completion of reaction (*cf.* TLC) the reaction was worked up as mentioned for the synthesis of bisacrylamide **2a** to get **2b** as a white amorphous powder (0.73 g, 66%). In the ^1H NMR anomeric protons of **2b** (Figure 4.20), H_{1e} and H_{1a}, appeared as two doublets at δ 5.20 and 4.62 with J_{1e2a} = 3.6 Hz and J_{1a2a} = 7.0 Hz, respectively.

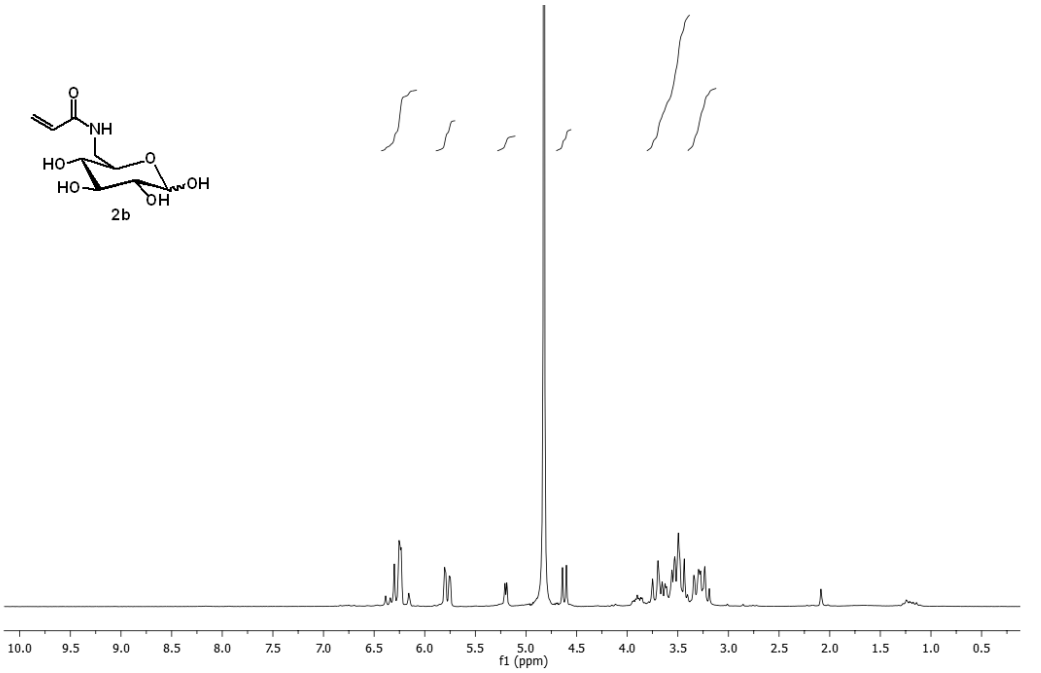

Figure 4.20: ^1H NMR (200 MHz, D_2O) spectrum of compound **2b**

The multiplets at δ 6.61 – 6.42, and 5.85 – 5.73 accounted for three olefinic protons of acrylamide functionality. In the ^{13}C NMR spectrum, the peak appeared

at δ 168.9 was due to the amide functionality and the peaks at δ 129.6, 127.6 were attributed to olefinic carbons of the monoacrylamide **2b** (Figure 4.21).

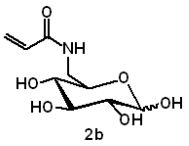

2b

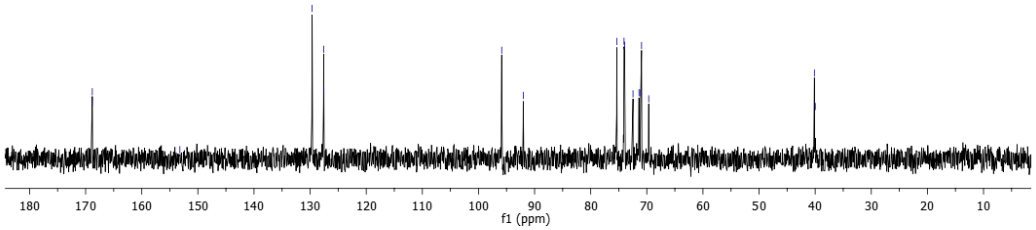

Figure 4.21: ^{1}H NMR (50 MHz, D_2O) spectrum of compound **2b**

4.3.1. *Preparation of Glc-gel*

The aqueous solutions of **2a** and **2b** prepared in different compositions were irradiated upto 29.5 KGy in Co-60 γ-source (dose rate 1.23 KGy/h), under ambient conditions. The synthesized gels were washed thoroughly with deionized water and vacuum dried at 40 ^{o}C to constant weight. These dried gels were used for different studies.

4.3.2. *Characterization of the hydrogels*

4.3.2.1. *Swelling kinetics and equilibrium degree of swelling*

The swelling studies were carried out gravimetrically by immersing the dried hydrogel discs of known weight in 50 mL of double distilled water at 25 ^{o}C. The hydrogel discs were removed from water at regular intervals and weighed after

wiping off the free water on the surface with tissue paper. After weighing, the samples were replaced into the same aqueous medium. The samples were swollen and reweighed until they attained a constant weight. The percentage of swelling at time‘t’ (%S) of the swollen hydrogels was calculated using the relation (4.1):

$$\text{Percentage of swelling (\%S)} = \frac{(W_t - W_d)}{W_d} \times 100 \qquad (4.1)$$

Where, W_t is the weight of swollen gel at time‘t’ while W_d is the weight of dried gel. The values reported are average of three repeated experiments.

The percentage equilibrium degree of swelling (%EDS) of the gel was calculated using the relation (4.2):

$$\text{Percentage equilibrium degree of swelling (\%EDS)} = \frac{(W_e - W_d)}{W_d} \times 100 \qquad (4.2)$$

Where, W_e is the weight of the gel at equilibrium swollen state.

4.3.2.2. *Dynamic rheological analysis*

All the dynamic measurements were performed in the linear viscoelastic region. Viscoelastic properties were measured in 0.1–100 Hz frequency range at a constant deformation strain (5%).

4.3.2.3. *Thermal Analysis of Glc-gel*

Thermogravimetric analysis (TGA)

About 5–10 mg of the dried hydrogel samples were heated in an alumina crucible and the thermogravimetric profiles were recorded from 25 to 900 °C, at a scan

rate of 10 °C/min, under nitrogen atmosphere, with a flow rate of 50 mL/min. The weight loss profiles of the hydrogel samples were studied from the thermogram.

Differential Scanning Calorimetry (DSC)

The biomedical and pharmaceutical activity of the hydrogel is decided by the manner in which the water molecules are associated with the polymer in the matrix. It is well established that water exists in three different physical states in polymeric networks: free water, freezing bound water and non-freezing bound water. The composition of different states of water in the hydrogel matrix can be determined by DSC analysis. For this the vaccum dried hydrogel samples were brought to equilibrium swollen state and then sealed in aluminium crucibles. These samples were initially subjected to a cooling run from 30 ^{o}C to –50 ^{o}C and then a heating run from –50 ^{o}C to 40 ^{o}C at a rate of 5 ^{o}C/min in nitrogen atmosphere. The fractions of the freezing water (free water and freezing bound water (W_f)) within the hydrogels were calculated from the area under the endothermic melting peak (ΔH_m) during the heating run and heat of fusion of pure water (ΔH_w = 333.3 J/g) according to the relation (4.3):[140]

$$\text{Percentage of free water and freezing bound water } (\%W_f) = \frac{\Delta H_m}{\Delta H_w} \text{ X } 100 \quad (4.3)$$

Non-freezing bound water content (W_{nf}) was determined by subtracting W_f from the equilibrium water content of the hydrogel (W_∞) (relation (4.4)), which can be

calculated from the fraction of equilibrium degree of swelling (EDS) of the corresponding hydrogel using the relation (4.5).

$$\text{Percentage of non-freezing bound water } (\%W_{nf}) = \%W_{\infty} - \%W_{f} \quad (4.4)$$

$$\text{Percentage equilibrium water content of the hydrogel } (\%W_{\infty}) = \frac{EDS}{(EDS+1)} \text{ X } 100 \quad (4.5)$$

4.3.3. ***In vitro cell cytotoxicity test***

The cell lines INT407 (human intestinal epithelial cell line) and L929 (mouse fibroblast cell line) were obtained from National Centre for Cell Sciences (NCCS), Pune, India. The cells were grown in DMEM medium with 10% fetal bovine serum, penicillin (100 U/mL) and streptomycin (100 µg/mL). Both the qualitative and quantitative *in vitro* cytotoxicity studies towards the test samples, were performed, respectively by microscopically observing the growth of the cells and by MTT, (3-[4,5-dimethylthiazol-2-yl]-2,5 diphenyl tetrazolium bromide) assay. In the former 15,000 cells were plated per well in a 24 well plate and allowed to adhere overnight. The test samples Glc-acryl, Glc-bis and Glc-gel (obtained directly after gamma irradiation) were added to the appropriate wells next day. Photograph of the cells were taken at regular intervals employing an inverted microscope with an attached camera (Leica EC3 type, Switzerland) at 40X magnification. In the MTT assay the procedure mentioned above was followed and at the end of 48 h of incubation with the test samples, the number of viable cells in each well was quantified by incubation with MTT (0.5 mg/mL) for

4 h, followed by solubilisation buffer (10% SDS in 0.01 N HCl) overnight. The plate was read in a plate reader at 550 nm. In both the experiments the samples were in triplicates and each experiment was conducted twice.

4.3.4. *Lectin recognition studies*

The interaction of Glc-gel with lectin Con A and BSA was studied by measuring the absorbance at λ = 420 nm and 278 nm, respectively, of the corresponding buffer solution before and after treatment with the hydrogel.

4.4. Results and Discussion

4.4.1. *Synthesis of Glc-bis (2a)*

In the synthesis, as shown in Scheme 4.1, easily available and cost effective monosaccharide D-glucose was transformed to azidodiol **3** as reported before.[141] Selective tosylation of primary hydroxyl group in **3,** using TsCl and pyridine, afforded monotosylated product **4** in 87% yield. Heating tosylate **4** with sodium azide in DMF furnished the desired diazide **5** in 86% yield. In the next step, both azide groups in **5** were reduced to diamine under hydrogenation condition which, without purification, was subjected to acrylation using acryloyl chloride and DIEA in CH_2Cl_2 at −40 ^oC to obtain bisacrylamide **6** as a thick liquid. Unmasking of 1,2-hydroxyl group in **6** using TFA-H_2O (3:2) afforded the required fully unprotected Glc-bis **2a** in 68% yield (8% overall yield from azido diol **3**).

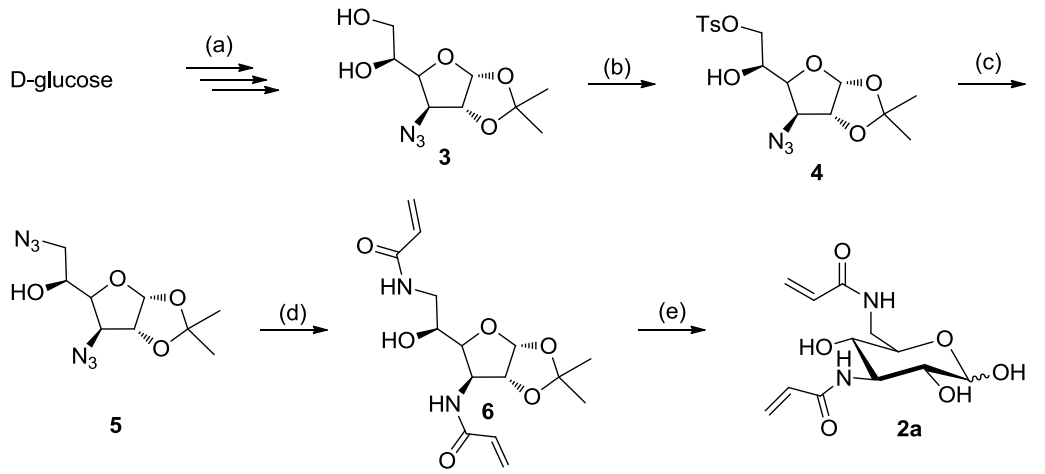

Scheme 4.1: *Synthesis of bisacrylamide*: (a) ref. 138; (b) TsCl, Py, CH_2Cl_2, 0 ^oC-25 ^oC, 3 h; (c) NaN_3, DMF, 80 ^oC, 3 h; (d) i) 10% Pd/C, H_2 (80 psi), 12 h, ii) Acryloyl chloride, DIEA, CH_2Cl_2, -40 ^oC, 20 min; (e) TFA-H_2O (3:2), 0 ^oC-25 ^oC, 10 h.

The Glc-bis **2a** is the only sugar based crosslinker wherein, two hydroxyl groups in the sugar ring are substituted with bis-reactive site in the form of bisacrylamide with the hemiacetal functionality intact, which could find usefulness in further functionalization to make materials of different properties.

4.4.2. *Synthesis of Glc-acryl (2b)*

In order to study and understand the ability of **2a** to function as crosslinker for the synthesis of Glc-gel it is required to have a suitable glycomonomer. Most of the known sugar based monomers have the active group (olefinic) located at the secondary carbon.[142] Since the distance of the sugar pendent from the carbon chain frame work is also an important factor for the glycopolymer to show affinity to lectins, we thought of synthesizing a new C-6 acrylamide derivative of D-glucose, which would place the sugar residue at an optimum distance from the main skeleton without using a spacer.[140]

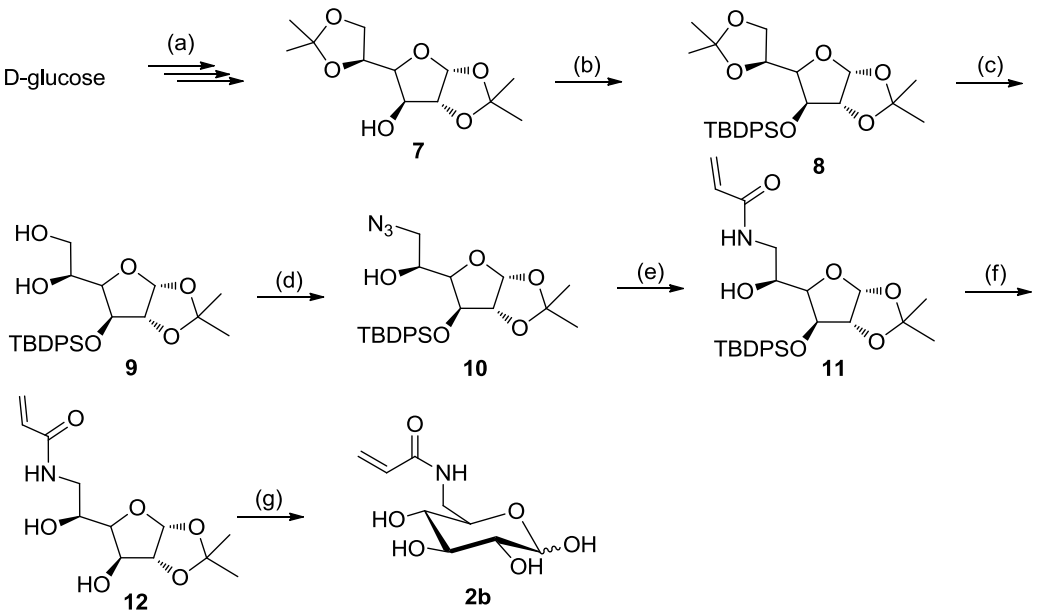

Scheme 4.2: *Synthesis of monoacrylamide*: (a) ref.138a; (b) TBDPSCl, DMF, Imidazole, 0 ^{o}C-25 ^{o}C, 24 h; (c) 30% $HClO_4$, THF, 0 ^{o}C-10 ^{o}C, 2.5 h; (d) i) MsCl, TEA, CH_2Cl_2, 0 ^{o}C-25 ^{o}C, 2 h; ii) NaN_3, DMF, 80 ^{o}C, 3 h; (e) i) 10% Pd/C, H_2 (20 psi), MeOH, 5 h; ii) Acryloyl chloride, DIEA, CH_2Cl_2, –40 ^{o}C, 20 min; (f) TBAF, THF, 0 ^{o}C to 23 ^{o}C, 1.5 h; (g) TFA-H_2O (3:2), 0 ^{o}C-25 ^{o}C, 10 h.

Thus, as shown in scheme 4.2, C-3 hydroxyl functionality in **7** [141a] was protected using TBDPS to yield fully protected furanose **8**. The 5, 6-acetonide in **8** was selectively deprotected using 30% $HClO_4$ in THF to furnish the diol **9** in 77% yield. Mono mesylation of 1^{o} hydroxyl group in diol **9** followed by heating of the resultant mesylate with sodium azide in DMF afforded the azido compound **10** in 53% yield (over two steps). The azide **10** was reduced and acrylated *vide infra* to afford the monoacrylamide **11** in 83% yield, (over two steps). Further, deprotection of TBDPS group in **11** using TBAF in THF yielded the azido diol **12** in 83% yield. Finally, deketalization of monoacrylamide **12** using TFA-water generated the Glc-acryl **2b** in 66% yield. ^{1}H NMR studies of **2a** revealed the predominance of α-anomer over β-anomer, due to anomeric effect, however the

ratio didn't differ (55:45) too much, largely due to the possible H-bonding[144] between anomeric hydroxyl group and ring oxygen, as shown in Figure 4.22. However, in the case of **2b** ^{1}H NMR confirmed the formation of β-anomer as the major product with α to β ratio as 45:55. Glc-acryl and Glc-bis thus obtained were dissolved in water (in suitable proportions) and irradiated with γ-source at a radiation dose of 29.5 KGy to yield transparent Glc-gel (Scheme 4.3 and Figure 4.23).

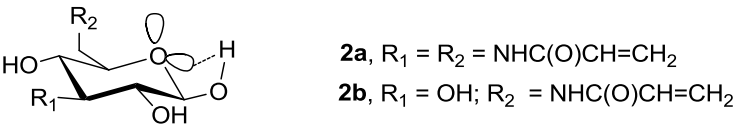

Figure 4.22: Possible H-bonding between anomeric OH and lone pair on ring oxygen

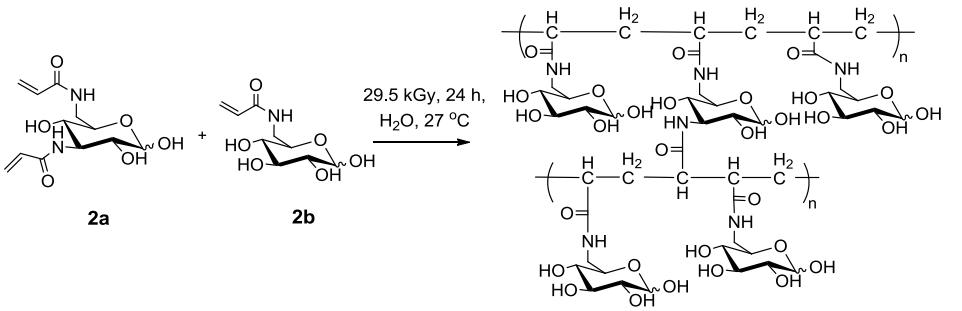

Scheme 4.3: Synthesis of D-glucose derived glycopolymeric hydrogel

Figure 4.23: Photograph of (A) freeze dried Glc-gel (B) swollen Glc-gel formed by radiation induced polymerization.

4.4.3. *FT-IR analysis*

Figure 4.24 shows the FT-IR spectra of Glc-bis (B) and Glc-acryl (C) in the powder form and also of the dry Glc-gel (A). The characteristic peaks of Glc-acryl are slightly broadened due to the hygroscopic nature of the material. The typical peaks of amide I (~1651 cm^{-1}) and amide II (~1552 cm^{-1}) in the monomer (Glc-acryl) and the crosslinker (Glc-bis) remains unaffected in the polymerized dry gel. The peak attributed to $CH=CH_2$ group (~1640 cm^{-1}) in the FT-IR spectra of Glc-acryl and Glc-bis, disappeared in the polymerized gel. This observation suggest that the polymerization has taken place *via* the C=C groups in the Glc-acryl and the Glc-bis.[145]

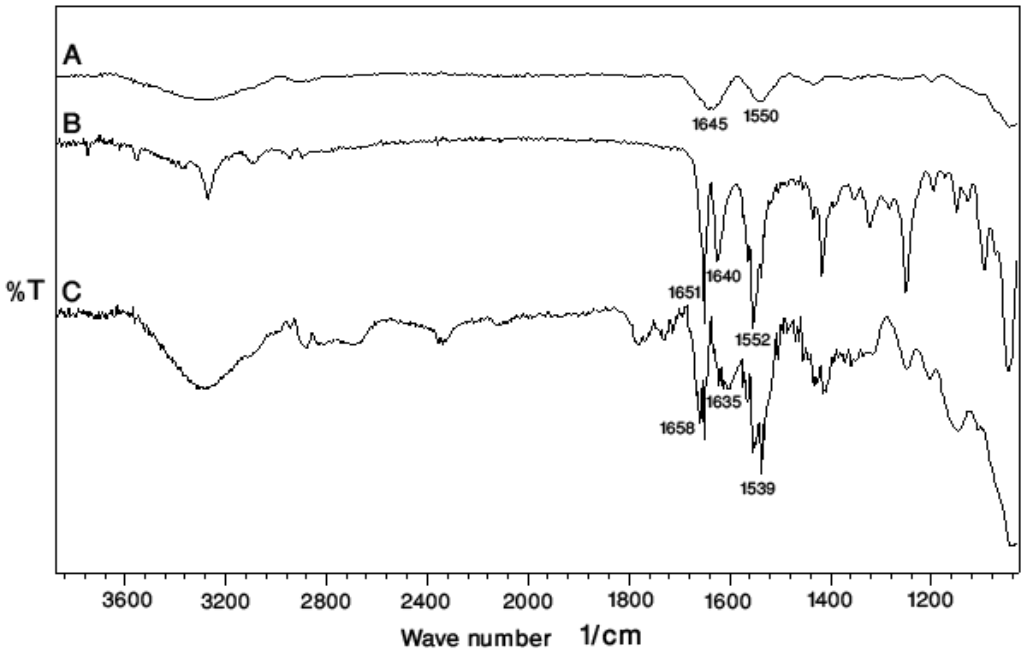

Figure 4.24: FT-IR spectrum of (A) dried Glc-gel, (B) Glc-bis and (C) Glc-acryl powder.

4.4.4. *Swelling studies*

The rate of swelling (Figure 4.25) was found to decrease with the increase in Glc-bis concentration in the hydrogel. This is because as the Glc-bis concentration increases the rigidity of the hydrogel increases and hence the degree of freedom between the chains decreases. Therefore, the polymeric network swells up slowly as compared to the gel with less concentration of Glc-bis. The %EDS (Table in figure 4.25.) calculated using relation **2** shows that the equilibrium swelling is dependent on the Glc-bis content.

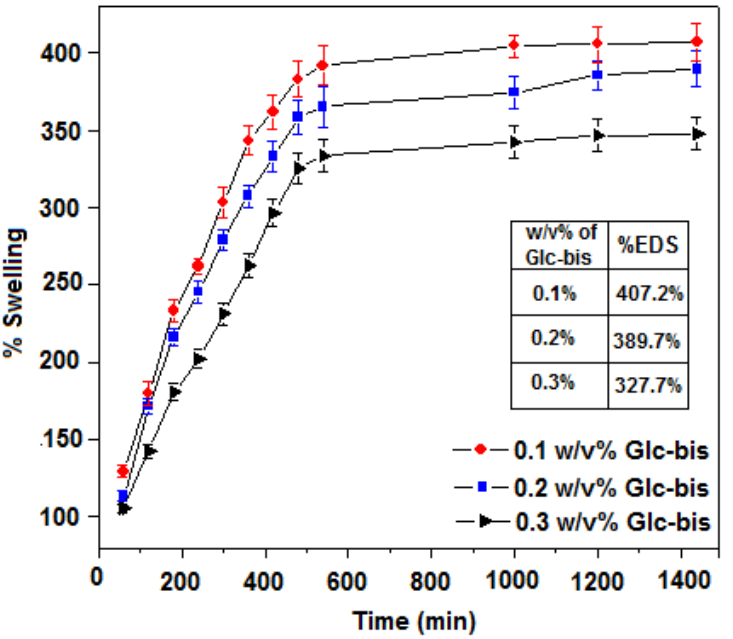

Figure 4.25: The effect of Glc-bis concentration on the rate of swelling of the Glc-gel (8% w/v Glc-acryl at radiation dose of 29.5 KGy) (left). Variation in %EDS at different Glc-bis concentration in the hydrogel formed with, 8% w/v Glc-acryl at radiation dose of 29.5 KGy (right).

4.4.5. *Effect of Glc-bis concentration on viscoelastic properties*

In order to evaluate the effect of crosslinker concentration on the viscoelastic response, the hydrogels derived from different Glc-bis compositions at 8% w/v Glc-acryl and a radiation dose of 29.5 KGy, were used to investigate the viscoelastic parameters in the linear viscoelastic range. The complex viscosity η* is given by the relation (4.6)[146a]:

$$\eta^* = \eta' - i\eta'' = G''/\omega - iG'/\omega \qquad (4.6)$$

Wherein, G' = storage modulus (elastic component) (Pa), G'' = loss modulus (viscous component) (Pa)

ω = angular frequency (rad/sec), η' = Dynamic viscosity (Pa-sec) and η'' = in phase component of dynamic viscosity (Pa-sec).

The complex viscosity (η*) was found to increase with increase in Glc-bis concentration at a fixed Glc-acryl concentration (8% w/v). This indicates the rise in gel strength with crosslinker content. At low frequencies, the rate of molecular rearrangement exceeds the rate of oscillation, hence the entanglement of polymer chains can occur easily during long period of oscillation. However, it was observed that during the frequency sweep the value of complex viscosity decreases with increasing frequency, which could be due to the faster oscillation rate than the rate for entanglement of polymer chains (Figure 4.26).[146] Figure 4.26 also represents the variation of G' with oscillatory frequency. All the Glc-gels

(measured) exhibits a plateau in the range 0.1–10 Hz, which indicates a stable, strong crosslinked gel network. At higher frequencies, all gels showed an increase in G', with the rate of increase highest for the gel with lowest crosslinker concentration (0.1% Glc-bis) and that lowest for the gel with highest crosslinker concentration (0.3% Glc-bis). The loss modulus (G") also exhibited a similar behavior. This is because the magnitude of the viscoelastic response of a polymeric network depends on length of the flexible polymer chains and the nature of the imposed mechanical motion.

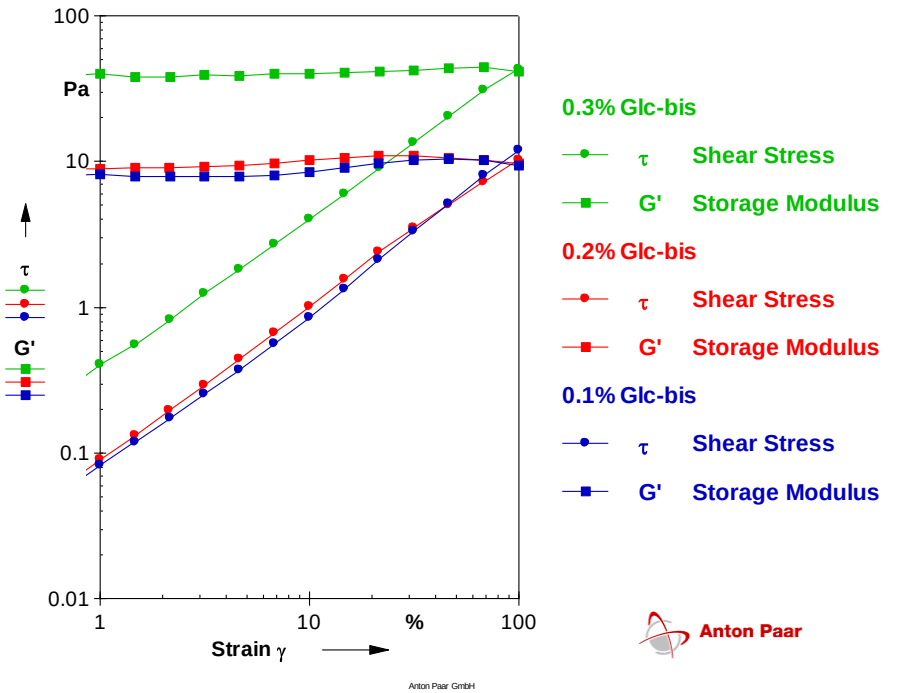

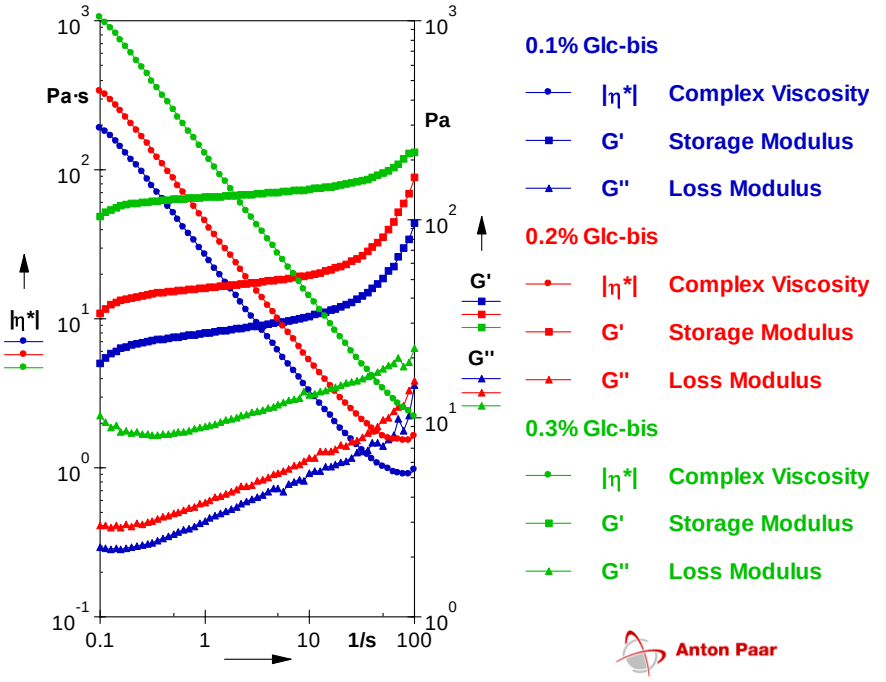

Figure 4.26: Effect of Glc-bis concentration on the complex viscosity of hydrogels at 37 ^{o}C at varying angular frequency.

The relaxation times are longer for longer polymeric chains, which depend on the crosslinker content. In the case of less crosslinked networks the polymeric chain segments between the crosslinks are longer, which gives lower molecular motion frequencies than those arising from highly crosslinked networks. This implies that, at higher frequencies, long chains fail to rearrange themselves at the imposed time scale and they assume more stiff and 'solid- like ' behavior which is characterized by a sharp increase in G' in this region.[147] In other words, for highly crosslinked networks even higher applied frequencies are required for a similar response which is the reason for gradual rise in G' in case of Glc-gel with 0.3% Glc-bis concentration.

4.4.6. *Thermogravimetric analysis*

The thermal degradation profiles of the dried hydrogels at various Glc-bis concentrations (0.1, 0.2, 0.3% w/v) and Glc-acryl concentrations (4, 6, 8, and 10% w/v) at a radiation dose of 29.5 KGy, were studied and were found to be similar. A typical degradation profile is shown in figure 4.27.

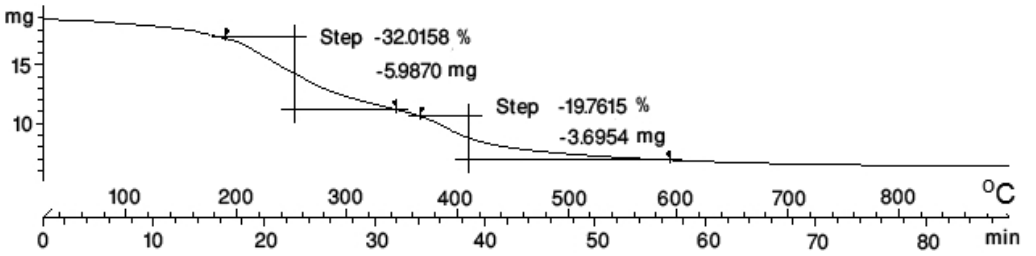

Figure 4.27: Thermal degradation profile of a typical vaccum dried Glc-gel

Degradation takes place in two different steps, first step from 180-320 ^{o}C and second step from 370-520 ^{o}C, which is characteristic of glycopolymers.[145] The effect of Glc-acryl concentration on the thermal stability of Glc-gels, is shown in figure 4.28. From the percentage weight loss at 900 ^{o}C we can deduce that the gels with higher Glc-bis to Glc-acryl ratio are thermally more stable. Thus, the thermal stability of Glc-gel decreases with increase in Glc-acryl concentration keeping all other factors constant, due to the decrease in crosslinking density of the hydrogel.

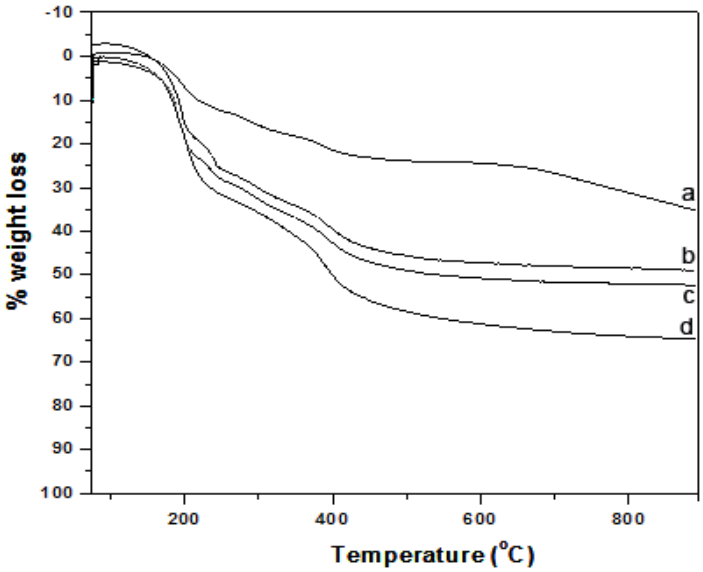

Figure 4.28: Thermal degradation curves for Glc-gel with varying Glc-acryl concentration (**a**) 4 (**b**) 6 (**c**) 8 and (**d**) 10% w/v, at 0.1% w/v Glc-bis and at an applied radiation dose of 29.5 KGy.

4.4.7. *Influence of Glc-bis concentration upon the states of water*

The DSC curves of the swollen hydrogels with varying Glc-bis concentration at equilibrium swelling are shown in figure 4.29. The ΔH_m values were calculated from the area under the corresponding endothermic melting peaks, while the different states of water in the various hydrogel compositions were calculated using the equations (4.3), (4.4), and (4.5). The table in figure 4.29 shows the amount of various states of water in the hydrogels with varying Glc-bis concentration (0.1, 0.2 and 0.3% w/v), at 8% w/v Glc-acryl and 29.5 KGy radiation dose.

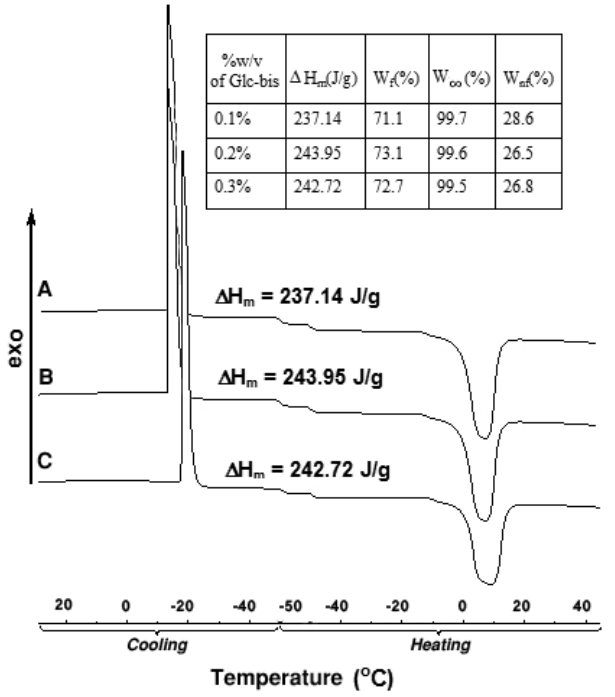

Figure 4.29: DSC curves for determination of states of water in the Glc-gel with varying Glc-bis concentration.

It was observed that the amount of freezing water (W_f) and non-freezing water (W_{nf}) was almost same at all the studied Glc-bis concentrations.

4.4.8. *Influence of Glc-acryl concentration upon states of water*

States of water in the hydrogels were also determined with varying Glc-acryl concentration. It was observed that with an increase in Glc-acryl concentration the amount of freezing water increased, while the proportion of non-freezing water decreased (Figure 4.30). This suggests that the water absorbed by the Glc-gel, with high Glc-acryl concentration, is slightly structured with its freezing occurring in a temperature range close to that of pure water.

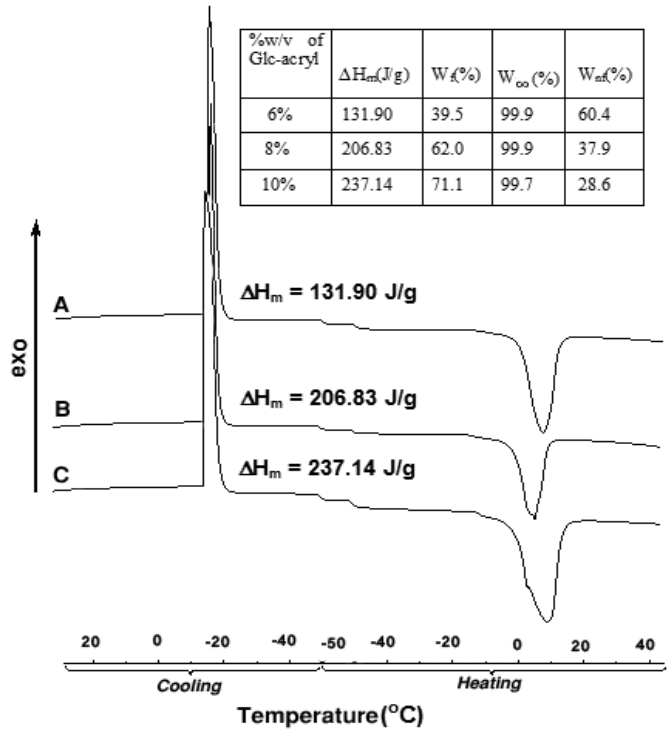

Figure 4.30: DSC curves for determination of states of water in the Glc-gel with varying Glc-acryl concentration.

This could be due to the lower crosslinking density with the increase in Glc-acryl content. Hence unlike Glc-bis the variation in Glc-acryl concentration could decide the amount of various states of water in Glc-gel.

4.4.9. *In vitro cytotoxicity of Glc-acryl, Glc-bis and Glc-gel*

The *in vitro* cytotoxicity of Glc-acryl, Glc-bis and Glc-gel were evaluated qualitatively and quantitatively.[148] At a concentration of 1 mg/mL of Glc-acryl and Glc-bis as well as Glc-gel (20 mg) did not exhibit any toxicity to both the cell lines tested while 1 µM Staurosporine killed both the cell lines completely. As is evident from the figures 4.31, both the cell lines grew normally in the presence of

the test materials without any reduced growth or cell death when observed under a microscope.

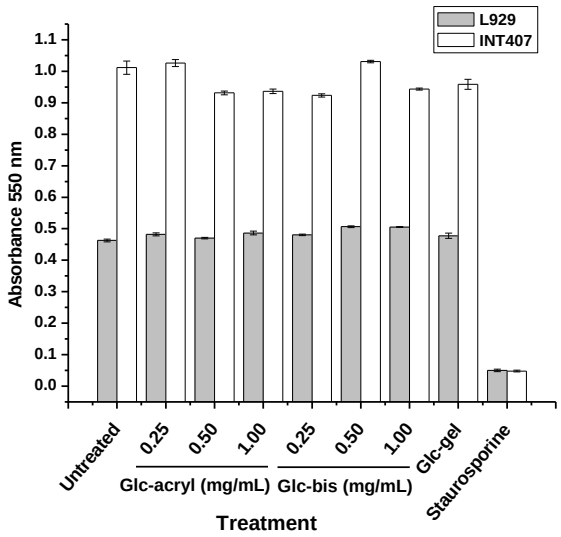

Figure 4.31: Quantification of viable cells by MTT assay after treatment for 48 hrs with different test samples. The test samples were not different from untreated sample ($p < 0.05$) as evaluated by unpaired student's t–test in case of both the cell lines.

A

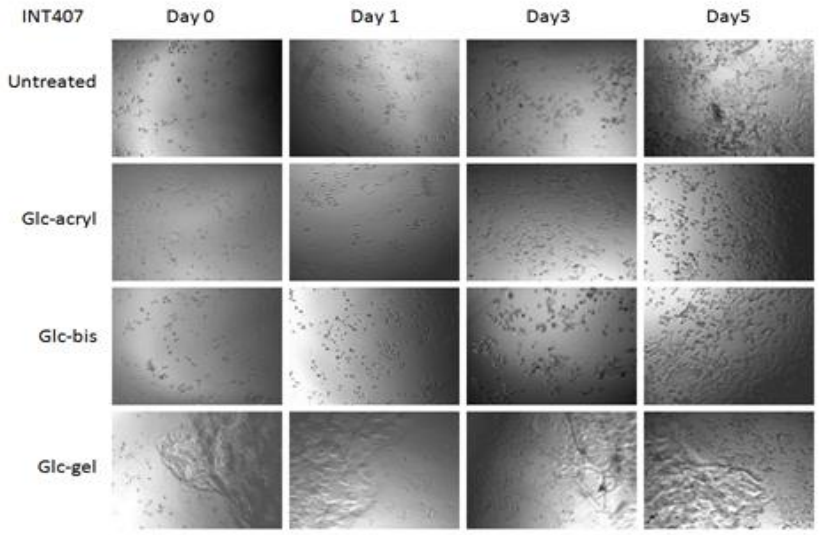

B

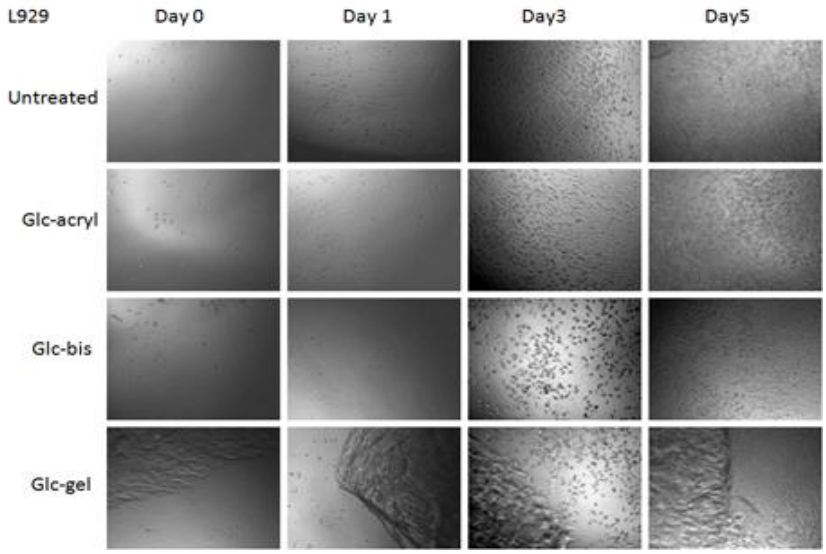

Figure 4.32: Growth of cells monitored in the absence and presence of test samples (1 mg/mL each of Glc-acryl and Glc-bis and 20 mg piece of Glc-gel) under microscope (40 × magnification). (A) INT407 cells and (B) L929 cells

At the end of 5 days all the samples attained confluence and the surface of the well was completely covered with the growing cells (Figure 4.32). In the quantitative MTT assay different concentrations (0.25 to 1 mg/mL) of Glc-acryl, Glc-bis and 50 mg of Glc-gel were tested.[149]

In this assay too both the cell lines grew in a comparable manner to the untreated sample at all the concentrations tested (Figure 4.31). To demonstrate death in the cells 1 μM Staurosporine was used which killed the cells completely. This clearly indicated that the test samples were nontoxic to the cells as they neither retarded the growth nor induced cell death in both the cell lines.

4.4.10. *Recognition study of Glc-gel towards Con A*

To determine the amount of protein that can be precipitated by Glc-gel, UV/vis spectroscopy was performed.[150] Therefore Con A (0.25 mg) in PBS-buffer (1 mL) was mixed with swollen gel pieces (20 mg) and recorded the spectra at regular intervals after separation of the gel pieces. Comparison of UV/vis spectra recorded before and after treatment with gel showed a decrease of peak height at λ = 420 nm of 43.8% after an interaction period of 10 minutes which can be attributed to the protein adsorbed on Glc-gel (Figure 4.33). The amount of protein left in solution is therefore calculated to be 0.14 mg (Δm = 0.11 mg) which means, that 20 mg of swollen Glc-gel is able to precipitate 0.11 mg of Con A. Similar studies in the presence of BSA solution showed a negligible decrement in the absorbance at λ = 278 nm.

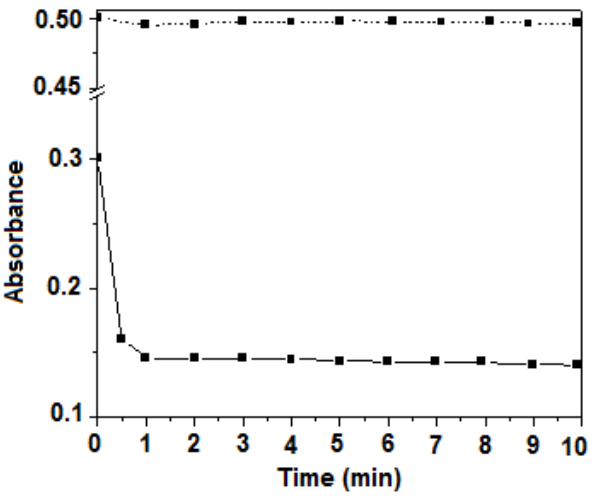

Figure 4.33: Interactions of Glc-gel with Con A (solid line) and BSA (dotted line).

4.5. Conclusion

In summary we have devised for the first time a D-glucose based bisacrylamide (Glc-bis) and monoacrylamide (Glc-acryl) with hemiacetal functionality. The high yielding reaction sequence proves the strategy is good enough to make them in gram quantities. The acrylamides were converted to a sterilized, noncytotoxic and homogeneous Glc-gel using radiation induced polymerization, which also showed strong interaction to lectin Con A. The thermal stability decreased with increase in monomer concentration. The states of water were dependent on Glc-acryl concentration and viscoelastic studies of the gels indicated that the gel strength increased with the Glc-bis content.

CHAPTER 5

GLYCOPOLYMER GEL STABILIZED *N*-SUCCINYL CHITOSAN BEADS FOR CONTROLLED DOXORUBICIN DELIVERY

5.1. Introduction

Cancer therapy has developed at a fast pace in last few decades but still there exist a lot of worries regarding the efficacy of the cancer chemotherapy. This is largely due to the mode of administration of drugs which is mostly done either orally or intravenously.[151, 152] The systemic and cellular transport mechanism of our body restricts bioavailability of the drugs leading to rapid clearance from the body. Also, many anticancer drugs have short plasma life time, low cell membrane permeability, and are highly toxic.[153] In addition, even the advanced drug delivery systems based on liposomes, micelles, polymeric vesicles etc., suffer from non-specific drug delivery and affect the healthy tissues. Hence, there is a strong demand for target-specific, localized vehicles with improved efficacy for sustained drug delivery to reduce the side effects.[154, 155] There has been intense effort to develop improved drug delivery systems which not only provide a sustained release but also control the initial burst release.[156, 159] To address this issue, pilot molecules like sugars, peptides, antibodies, etc. that hold selective interaction with receptors on the cancer cells are being explored. In particular, the sugar-based polymers are very attractive, since the glycopolymeric framework can act as drug carriers, while their constituent sugar pendants can function as pilot molecules as per the principle of "glyco-cluster effect".[156] Also, carbohydrates play significant role in the cell-involved biorecognition events and the glyco-targeting ability of glycopolymers have been proven ideal for cellular specific drug targeting.[160]

Doxorubicin (DOX, **1**) (Figure 5.1) is a highly efficient chemotherapeutic anticancer drug against various types of cancers including breast cancer, urothelial cancer, hematopoietic malignancies, and other solid tumors. But its effectiveness is curtailed by its short life time in the blood stream and toxicity to normal tissues. Its clinical dosage far exceeds the non-toxic cumulative dose that should be limited to 500-600 mg/m^2. [157-164]

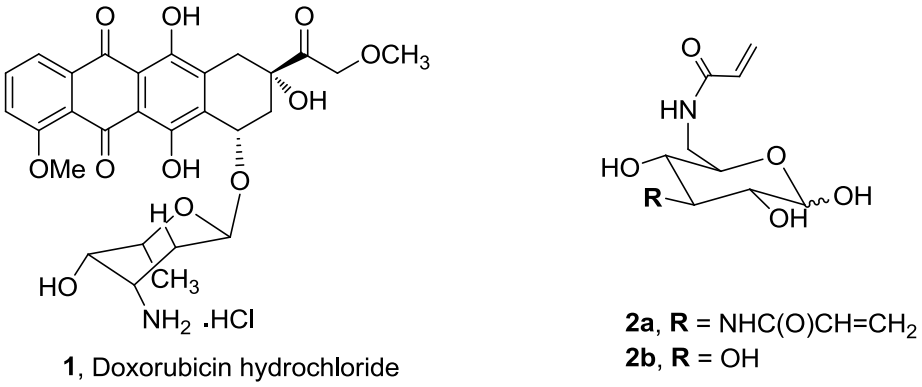

Figure 5.1: Doxorubicin hydrochloride and sugar acrylamides

These emphasize the need for a sustained localized DOX delivery system to increase its activity with least toxicity. It is well established that sustained release of drug at the malicious site is more effective for tumor treatment than the administration of drug in definite doses at specific intervals.[165-170] The development of pH sensitive glycopolymer based drug delivery systems for cancer chemotherapy have attracted tremendous interest owing to the fact that the microenvironment of tumor tissues is mildly acidic (pH 4.5-6.5) in comparison to the healthy tissues. The most common protocol, used so far for efficient loading and delivery of drugs like DOX involves reversible covalent bonding,

electrostatic interaction, as well as attachment of the drugs to a carrier through an acid labile spacer which releases the drug at a definite pH.[171]

In the search for a new drug delivery system based on naturally occurring polysaccharide, we realized that the second most abundant polysaccharide, chitosan (CS) can be a potential candidate. It possesses a C2-amino group that can be easily modified using succinic anhydride (SA) to provide a range of polymers, *N*-succinyl chitosans (NSCs). The plasma half life of NSCs in both normal and tumour cells was earlier found to be higher than the related macromolecules studied, possibly due to the anionic charges that can interact with the blood vessels and tissues.[152, 172-175] Moreover, NSCs can accumulate on malicious tissues by virtue of enhanced permeability and retention (EPR) effects.[176-178] Most importantly, the percentage of $–NH_2$ and –COOH groups in the NSCs can be easily controlled under suitable conditions. This provides a simple option to tune the carrier property of the NSCs for various types of drugs.[179] All these attributes along with the less toxicity of NSCs prompted us to use them as carriers for delivery of DOX.

The present work emphasizes on the synthesis and study of Ca^{2+} cross-linked NSC beads that were stabilized by the interpenetrating network (IPN) of glycopolymeric gel (Glc-gel). We hypothesized that the Glc-gel would provide the required stability for the NSC beads against dissolution upon drug loading, and could control the drug release. The biocompatible Glc-gel used for stabilization of the bead was made from D-glucose based bisacrylamide

crosslinker (Glc-bis, **2a**) and monoacrylamide (Glc-acryl, **2b**) (Figure 5.1) developed in our laboratory.[180] The crosslinker **2a** was used to alleviate the problem of toxicity of crosslinkers, for drug delivery applications.[181, 182]

5.2. Experimental Section

5.2.1. *Synthesis of NSCs*

To a solution of CS powder (2 g) in DMSO (40 mL) was added SA (2 g, 1250 mol eq) in portions, and the mixture stirred at 65 ^{o}C for 6 h/9 h for different extent of substitutions. The pH was adjusted to 10–12 using aqueous 1 M NaOH to obtain the respective precipitates, which were collected by filtration and dissolved in distilled water (90 mL). The solution was dialysed in a dialysis membrane (mol. weight cut off 12,000-14,000 Da) at room temperature for 2-3 days, lyophilised, and the samples stored till further experiments. The synthesized NSCs were characterized using FT-IR spectroscopy, and the degree of substitution (DS) was determined from ^{1}H NMR spectra using equation (5.1).[183, 184]

$$\text{Degree of substitution} = \frac{\text{Integrated area at 2.23-2.48 ppm}}{4 \text{ X } \text{Integrated area at 2.60 ppm}} \text{ X } 100 \qquad (5.1)$$

Further DS was also determined by elemental analysis using equation 5.2 and this value was used to represent the extent of succinylation in CS. Thus, based on CHN analysis NSC-6h was found to have 75% DS (NSC75) while that for NSC-9h was 88% (NSC88).

$$\text{Degree of substitution} = \frac{\text{C/N of substituted chitosan} - \text{C/N of chitosan}}{4} \qquad (5.2)$$

"4" derived from number of carbons in succinyl subtituent

5.2.2. *Synthesis of Glycopolymeric hydrogel (Glc-gel)*

For the synthesis of glycopolymeric hydrogel the aqueous solution of 5 w/v% Glc-acryl **2a** and 0.1 w/v% Glc-bis **2b** were irradiated upto 29.5 kGy in Co-60 γ–source (dose rate 0.75 kGy/h), under ambient conditions. The synthesized gels were washed thoroughly with deionized water and dried to constant weight.

5.2.3. *Synthesis of NSC/Glc-gel beads*

To a gently stirred aqueous saturated solution of $CaCl_2$, was added dropwise, an aqueous solution of 4 w/v% NSC (10 mL) using a microsyringe. The beads, thus formed, were allowed to equilibrate for 3 h, filtered, washed with water (250 mL), and transferred to a solution containing 5 w/v% Glc-acryl and 0.1 w/v% Glc-bis (10 mL). After equilibrating overnight, the mixture was purged with nitrogen for 30 min, sealed tightly and irradiated (total dose 1.68 kGy , dose rate 0.75 kGy/h) with a Co-60 γ-source. The irradiated Glc-gel beads were washed with water, dried under vacuum at 40 ^{o}C to constant weights and used for further studies.

5.2.4. *Determination of glycopolymer content in the bead*

The extent of glycopolymer loading on the Ca^{2+} ions - crosslinked NSC75 and NSC88 beads were gravimetrically determined using the equation (5.3) and the values are the average of three independent measurements.

$$\text{Percentage of glycopolymer loading} = \frac{(W_g - W_d)}{W_d} \times 100 \quad (5.3)$$

where, W_g and W_d are the weights of vacuum dried glycopolymer loaded and unloaded NSC beads, respectively.

5.2.5. *Swelling and weight loss studies of NSC/Glc-gel beads*

The swelling studies were carried out at 37 ^oC at pHs 7.4 and 5 at a physiologically relevant ionic strength (154 mM). The swelling percentage of the gel samples dried to constant weights was determined gravimetrically using equation (5.4) and the values are the average of three independent measurements.

$$\text{Percentage swelling} = \frac{(W_t - W_d)}{W_d} \times 100 \quad (5.4)$$

where, W_t is the weight of swollen bead at time‘t’ and W_d is the weight of dried bead.

5.2.6. *Synthesis of DOX-loaded NSC/Glc-gel beads*

The synthesized swollen beads (1.5 mg) were incubated with 100 µl of DOX solution (500 µg/mL) for 24 h in dark. The absorbances of DOX at 480 nm in the feed solution after loading into the beads were spectrophotometrically measured. The drug encapsulation efficiency of the beads were determined using equation (5.5).[185]

$$\text{Encapsulation efficiency} = \frac{\text{Amount of DOX in hydrogel}}{\text{Amount of DOX in feeding solution}} \times 100 \quad (5.5)$$

5.3. Characterization

5.3.1. *Drug release studies*

The swollen, DOX loaded NSC/Glc-gel bead (2.0 mg) was equilibrated with acetate (pH 5) or phosphate (pH 7.4) buffer (each, 25 mL), with constant stirring at 37 ^{o}C. Aliquots (each, 1 mL) were withdrawn at fixed time intervals and replenished with fresh buffer solution in order to maintain constant sink conditions of the media. The absorbances of the aliquots were measured, and the amount of DOX released was determined using equation (5.6) against the calibration plot prepared under similar conditions using standard DOX solutions.[186] The data are average of three independent measurements.

$$\text{Cumulative release percentage} = \frac{V_t \sum_{1}^{n-1} C_i + V_o C_n}{\text{mDOX}} \text{ X } 100 \qquad (5.6)$$

where, V_t, is the volume taken at time "t" V_0 is the volume of the release medium (V_0 = 25 mL), mDOX represents the amount of DOX in the hydrogel, Ci and C_n are the initial loaded concentration of DOX and that in the n^{th} sample, respectively.

5.3.2. *Morphological studies*

Morphology of the beads was determined with a QX5 DIGITAL BLUE computer microscope, and MECK-FEI Model NOVA Nanosem 450 scanning electron microscope (SEM). The lyophilized beads were coated in vacuo with gold for the SEM characterization.

5.3.3. *Specific lectin recognition studies of DOX loaded NSC/Glc-gel beads*

DOX loaded NSC/Glc-gel beads were treated with each of 0.05 mg/mL Con A, PNA and BSA solutions. The supernatant solution was removed at regular time intervals, centrifuged and measured the absorbance at 278 nm.

5.4. Results and discussion

5.4.1. *Synthesis and characterization of NSC/Glc-gel beads*

In this work, we synthesized two NSCs by succinylation of CS with SA at 65 ^{o}C. The reaction proceeded to 75% and 88% of succinylation at 6 h and 9 h, as indicated by elemental analysis and ^{1}H-NMR (Figure 5.2 and Table 5.1) of the products, and was designated as NSC75 and NSC88, respectively. These were converted to the Ca^{2+} cross-linked NSC beads that were unsuitable for drug delivery applications as they had poor mechanical strength and disintegrated fast on DOX loading. Therefore, these beads were reacted with Glc-acryl and Glc-bis under γ-irradiation to obtain the stabilized NSC/Glc-gel beads (Scheme 5.1).

During equilibration with the NSC beads, the Glc-acryl and Glc-bis solutions penetrate into the matrix, and a cross-linked IPN of glycopolymer is formed through the pores of the bead, on γ-irradiation. After glycopolymer loading, the weights of resultant NSC75/Glc-gel and NSC88/Glc-gel beads were enhanced by 88-90 w/w%. The γ-irradiation grafting protocol is suited better for medicinal applications as it was clean and avoided use of any additional chemicals/reagents.

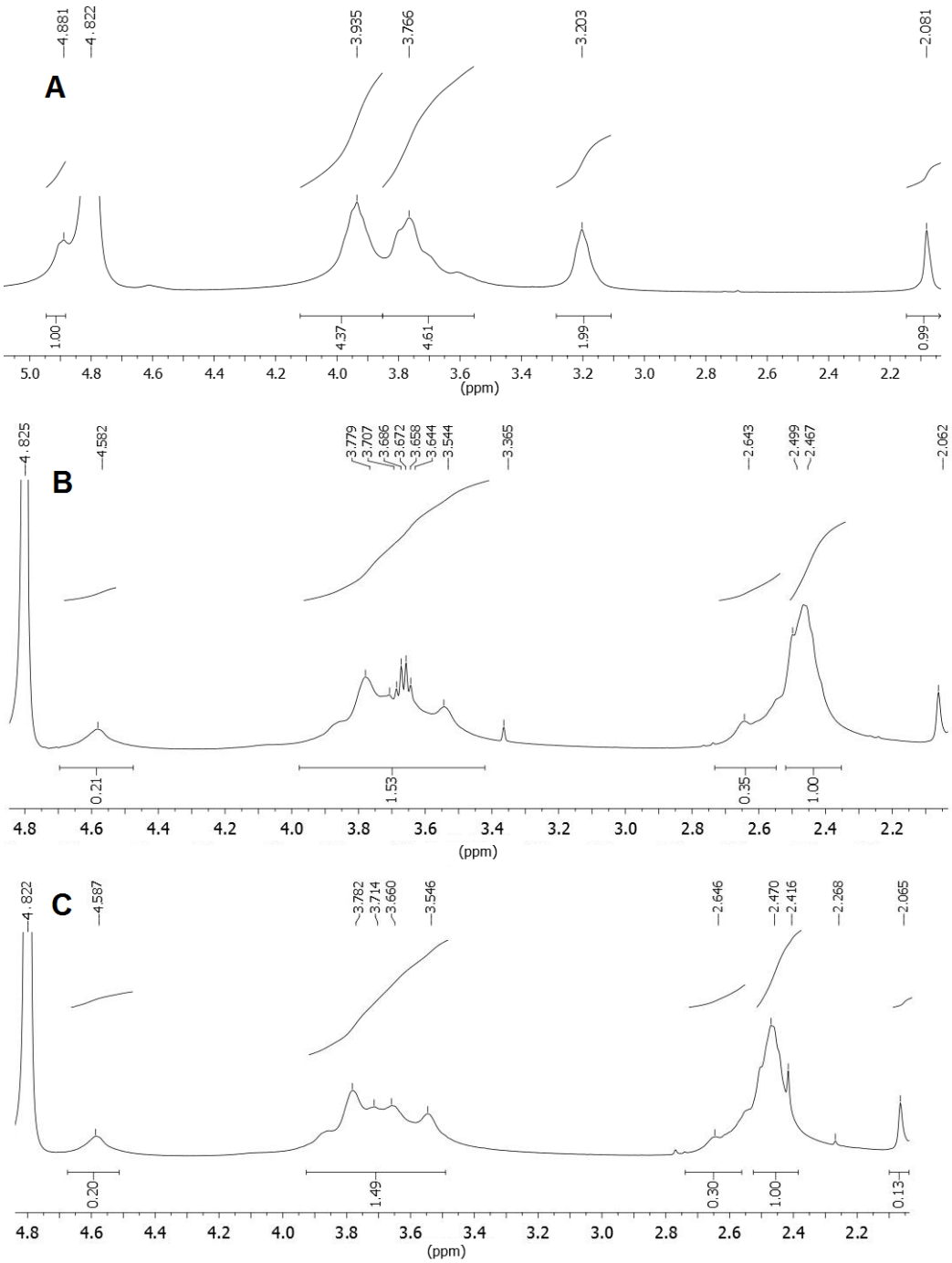

Figure 5.2: ^{1}H NMR spectrum of (A) Chitosan (85% deacetylation (D_2O-0.1% DCl, 25 ^{o}C)), (B) NSC (after 6h of succinylation (D_2O, 25 ^{o}C)), (C) NSC (after 9h of succinylation (D_2O, 25 ^{o}C))

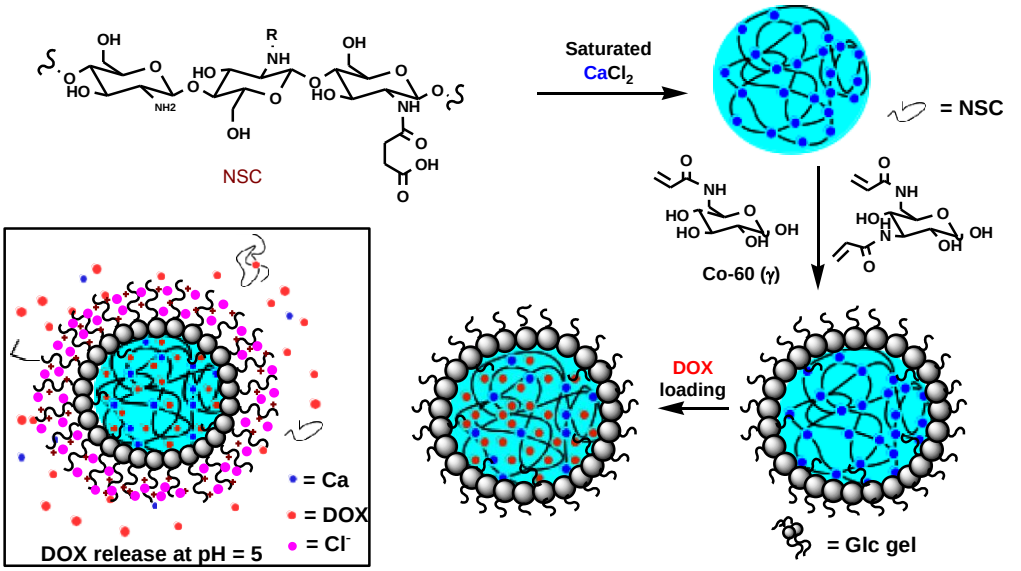

Scheme 5.1: Synthesis of *N*-succinyl chitosan glycopolymeric gel bead (NSC/Glc-gel) and the schematic of DOX release mechanism.

Compounds	Carbon (C)	Hydrogen (C)	Nitrogen (N)	C/N	% DS[184]
Chitosan	42.2	8.8	6.3	6.7	
NSC-6h	39.6	8.1	4.1	9.7	75
NSC-9h	36.7	7.9	3.6	10.2	88

Table 5.1: Elemental analysis data of chitosan and NSC synthesized after 6 h (NSC-6h) and 9h (NSC-9h) of succinylation.

Also, the cell cytotoxicity studies using L929 and INT407 cell lines by MTT assay of Glc-acryl, Glc-bis as well as the Glc-gel did not showed any significant difference between the untreated and treated samples. These results clearly indicated that Glc-acryl and Glc-bis as well as Glc-gel were not toxic to the cells.[180]

For characterization, the FT-IR spectra of CS, and powdered NSC and NSC/Glc-gel beads were recorded and are shown in figure 5.3. The spectrum of CS showed main absorption bands at (i) 1646 cm^{-1} and 1593 cm^{-1}, corresponding to amide I and amide II; and (ii) 1149 cm^{-1} (asymmetric stretching of C-O-C bridge) and (iii) 1068 and 1027 cm^{-1} (skeletal vibration involving the C-O stretching), characteristics of the saccharine moiety. In the case of NSC, appearance of new peak at 1421 cm^{-1} was assigned to the symmetric COO^{-} stretching, while that at 3085 cm^{-1} accounted for the *N*-succinyl $–CH_2$ stretching.

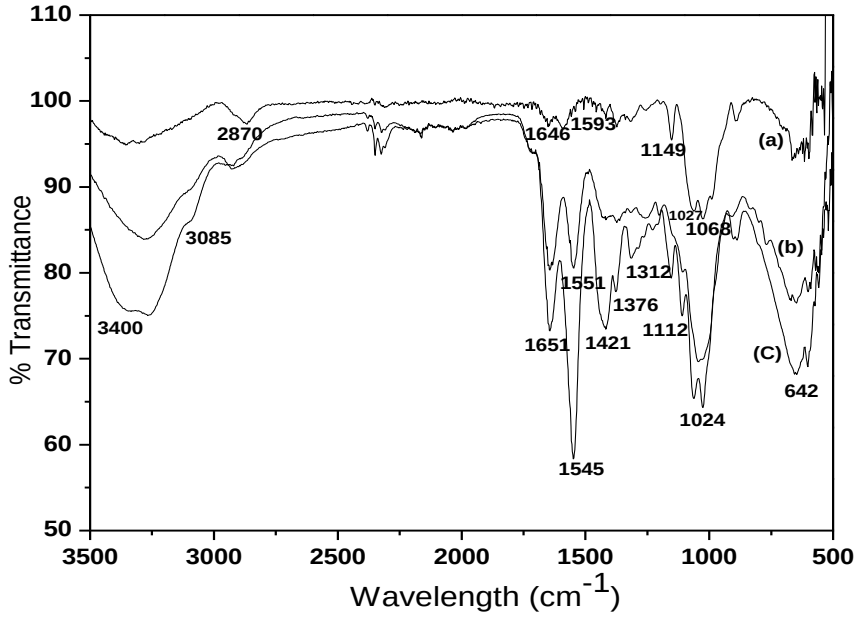

Figure 5.3: FT-IR spectra (a) CS, (b) NSC/Glc-gel and (c) NSC powders.

A new peak at 1545 cm^{-1} (secondary amine) also appeared with simultaneous depletion of the 1593 cm^{-1} ($–NH_2$ bending) peak. This confirmed formation of NSC *via N*-succinylation of CS to produce –NH–CO– bond.[179,188-193] The spectra (b) in figure 5.3 indicates the peaks corresponding to NSC/Glc-gel. The peaks at

1651 and 1551 cm^{-1} which are of equal intensity, involves amide I and amide II peaks of Glc-gel also.

5.4.2. Swelling *studies of NSC/Glc-gel beads*

Initially we tested the acid sensitivity of the Glc-gel as we assumed that this could play a significant part in the controlled release of drug. The studies conducted at different pHs (3, 5 and 7.4) revealed that the Glc-gel was stable and retained its shape at the studied pHs. However, its equilibrium degree of swelling was reduced progressively with lowering the pH of the medium. As shown in figure 5.4A, its maximum swelling capacities were 587% at pH 7.4, 500% at pH 5 and 389% at pH 3. At low pH, on the surface of the bead, the screening effect of amidonium ions by Cl^- counter ions decreases the swelling drastically, due to reduced hydrogen bonding with water molecules. But at pH 7.4, the amide groups remain unprotonated and are freely available for hydrogen bonding with water, facilitating the diffusivity of water molecules into the hydrogel network. Hence, greater equilibrium swelling was observed .[194,195]

Next, the swelling behaviors of the NSC88 and NSC75 gel beads as such, and after grafting Glc-gel were studied at pHs 5 and 7.4. The NSC88 and NSC75 gel beads, i.e. without glycopolymer, swelled rapidly, and disintegrated within a few minutes. On the other hand, the swelling kinetics of the vacuum dried NSC88/Glc-gel and NSC75/Glc-gel beads were found to be pH dependent (Figure 5.4B) with more swelling for NSC88/Glc-gel beads compared to NSC75/Glc-gel

beads at both the pHs, at a fixed ionic strength (154 mM). Higher and faster swelling was observed for both NSC88/Glc-gel and NSC75/Glc-gel beads at pH 7.4 than at pH 5.

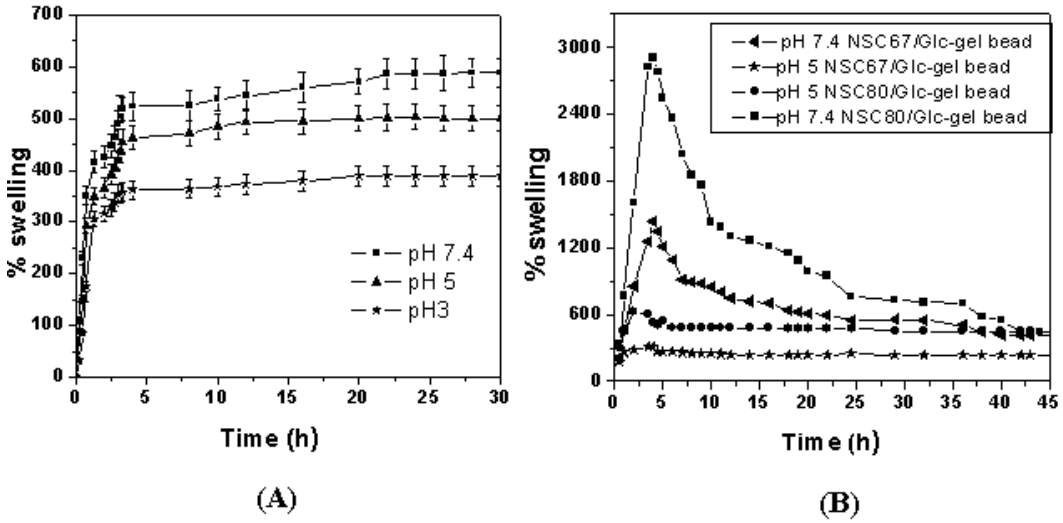

Figure 5.4: Swelling behaviors of (A) Glc-gel at pHs 3, 5 and 7.4 (B) NSC/Glc-gel beads at pHs 5 and 7.4.

The maximum swelling capacities of NSC88/Glc-gel and NSC75/Glc-gel beads were 2906% and 1436%, respectively at pH 7.4. These were reduced to 543% and 313% respectively at pH 5. The higher swelling at the basic pH may be due to the increased repulsive interaction between the $–COO^-$ units of the NSCs. This force the polymeric units to be more stretched out and facilitates higher water uptake compared to the beads containing the uncharged –COOH groups at pH 5.[196,197] The Glc-gel loaded beads were stable during swelling studies at both the pHs (7.4 and 5) for 5-6 h. Later these beads showed weight loss due to leaching out of NSC. Nevertheless the shape of the beads remained intact. However, despite the

initial higher swelling of both the beads at pH 7.4, the swelling percentage attained the same value as that of pH 5 after 45 h. This suggested higher rate of leaching out of NSC from the beads at pH 7.4.[196,198,199]

5.4.3. *DOX encapsulation by the NSC/Glc-gel beads*

Incubation of the DOX solution with the NSC75/Glc-gel and NSC88/Glc-gel beads led to its decolorization, confirming loading of the drug in the beads. Best DOX encapsulation was observed at 12 h of incubation (Figure 5.5(A)). The DOX encapsulation efficiency (EE) of the beads was dependent on the degrees of succinylation in the NSCs. Quantification of the data revealed that the EEs of the NSC88/Glc-gel and NSC75/Glc-gel beads were 92.7% and 75% respectively. This suggested that the mechanism of loading is governed mainly by the electrostatic interaction between the $–COO^-$ groups in the polymer and the NH_2 group of DOX.[181] The DOX loading was also evident from the significant color differences in the appearances of the loaded and unloaded NSC75/Glc-gel beads (Figure 5.5(B)). The NSC88/Glc-gel beads also showed similar changes in their appearances on DOX loading (images not shown).

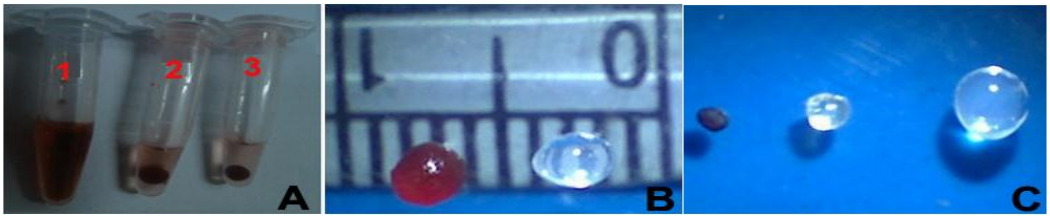

Figure 5.5: (A) Photographic image of DOX solution as such (500 µg/mL) (1), in presence of NSC67/Glc-gel (2) and NSC80/Glc-gel (3) beads (B) Optical

microscope image of DOX loaded (red) and unloaded (transparent) swollen NSC67/Glc-gel beads (C) vacuum dried DOX loaded NSC67/Glc-gel bead (left), NSC67/Glc-gel bead (middle) and swollen NSC67/Glc-gel bead (right).

5.4.4. *Thermal Analysis of the beads*

All the samples showed a small weight loss at about 100 ^{o}C due to the loss of the absorbed and bonded water. The NSC beads showed 20% weight loss at 250-350 ^{o}C, while a similar weight loss was observed at 150-250 ^{o}C in case of Glc-gel (Figure 5.6). The TGA data confirmed enhanced thermal stability of the NSC/Glc-gel beads compared to the blank NSC beads.[196] Notably, higher the degree of succinylation greater the thermal stability, because the NSC88/Glc-gel and NSC75/Glc-gel beads showed 70% and 80 % weight loss respectively at 700 ^{o}C. DOX loaded NSC/Glc-gel bead also showed similar TGA profiles as that of the corresponding unloaded bead.

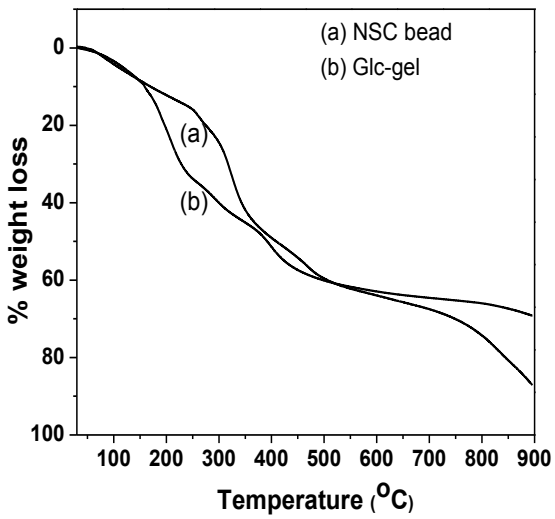

(A)

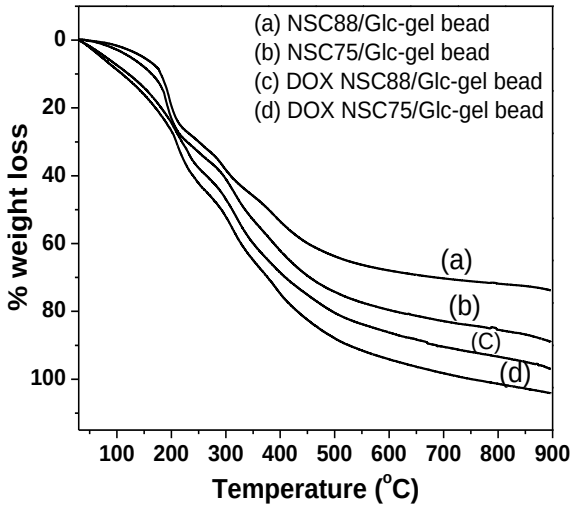

(B)

Figure 5.6: TGA thermograms of NSC beads and Glc-gel (A), unloaded and DOX-loaded NSC/Glc-gel beads (B).

However, the weight loss in the region 150-250 ^{o}C was gradual. A 20% weight loss for DOX loaded beads in the region 250-350 ^{o}C corresponding to NSC decomposition as shown in figure 5.6.

5.4.5 *Swelling and pH responsiveness of the DOX-loaded NSC/Glc-gel beads*

The swelling profile of the DOX-loaded beads was much different from that of the unloaded beads especially at pH 7.4 (Figure 5.7). The DOX loaded NSC75/Glc-gel beads showed lesser degree of weight loss compared to the unloaded beads at pH 7.4, implying their increased stability on DOX loading.

In NSC88/Glc-gel beads, more DOX loading made the beads to swell rapidly compared to NSC75/Glc-gel at pH 7.4 resulting in higher weight loss in DOX loaded NSC88/Glc-gel beads than the unloaded beads. The swelling behaviors of

the loaded and unloaded NSC88/Glc-gel and NSC75/Glc-gel beads were comparable at pH 5.

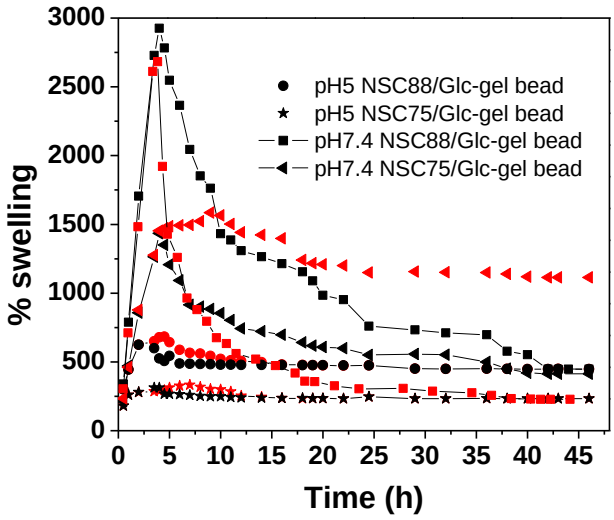

Figure 5.7: Swelling and pH responsiveness of DOX loaded NSC/Glc-gel beads at pH 7.4 and 5. (Red symbols indicate data for DOX loaded beads and black symbols indicate those for unloaded NSC/Glc-gel beads.)

5.4.6. *Drug release studies in vitro*

Figure 5.8 shows the DOX release profiles of the NSC/Glc-gel beads at pHs 7.4 and 5 at 37 ^{o}C. In case of NSC75/Glc-gel beads both at pH 7.4 and 5 the initial burst release was only ~25% over a period of 24 h whereas, the NSC88/Glc-gel beads showed 30% initial burst release of DOX within 6 h at pHs 7.4 and 5. This is in agreement with our results of swelling studies of the corresponding DOX loaded beads. The initially released DOX molecules are those physisorbed in the hydrogel matrix. But at the later stage, a slow and sustained DOX delivery profile was shown by both types of beads, with greater release rate at pH 5.

The increased release at pH 5 may be due to (i) weakened electrostatic interactions between the protonated carboxylic group of NSC and DOX amino group[196], and (ii) precipitation of NSC from the beads at acidic pH as evident visually as well as from the SEM image (Figure 5.11E). The precipitation of a small fraction of NSC would leave behind the uncomplexed DOX, trapped in the glycopolymeric network. This can subsequently diffuse out at a faster rate. A purely electrostatic interaction between the DOX and the matrix would have resulted in a 100% release of DOX at acidic pH. Since this was not observed, we assume that some non-ionic interactions may also be playing significant role. The percentages of maximum cumulative release from the NSC75/Glc-gel beads at pHs 5 and 7.4 were 76% and 36% respectively. The respective values with the NSC88/Glc-gel beads were 88% and 79%. Hence NSC75/Glc-gel beads can be considered as ideal matrices for localized drug delivery to the cancer cells with minimal side effects.

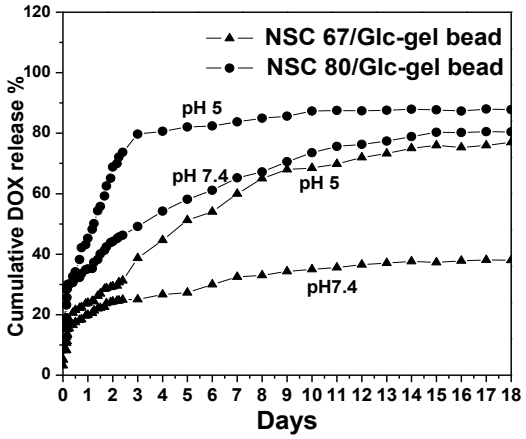

Figure 5.8: DOX release profiles from the loaded NSC/Glc-gel beads at pHs 7.4 and 5.

5.4.7. *Specific interaction between NSC and DOX*

The specific interaction between DOX and NSC was investigated from the UV-Vis spectra of aqueous DOX solution as such and equilibrating for 5 minutes after addition of NSC67. DOX showed an absorption maxima at λ_{max} 480 nm that upon addition of NSC got shifted to 495 nm and the peak intensity was also significantly reduced (Figure 5.9). These spectral changes indicated that a complex is formed between DOX and NSC.[196]

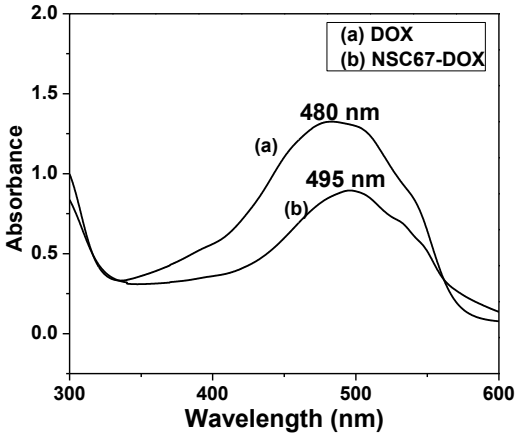

Figure 5.9: UV-Vis spectra of DOX and NSC75-DOX complex in aqueous solution.

5.4.8. *Mechanism of drug release*

In order to understand the different modes of drug release from the gel beads the release profiles were fitted by the exponential Korsemeyer-Peppas equation (5.7).[200]

$$Fr = k\, t^{n} \qquad (5.7)$$

where, 'Fr' is the fraction of drug released at time 't', 'k' is the kinetic constant and 'n' is the diffusion exponent indicative of the drug release mechanism.

The drug release follows fickian-diffusion when n is ≤ 0.43, but takes swelling/erosion controlled (non-fickian diffusion) mode between 0.43<n<0.85 but, when n = 1.0, it corresponds to a zero-order release for non-swellable controlled release systems. The model was applied for release upto Fr = 0.6 (Figure 5.10). From the fitting plots of both beads, at pH 7.4 and 5, the NSC75/Glc-gel beads followed zero-order release kinetics at both the pHs. This is because of low swelling kinetics of NSC75/Glc-gel beads which results in constant rate of release of the drug independent of its concentration.

The fitted data in case of NSC88/Glc-gel bead at pH 5 gave n = 1.52 at the beginning, which is due to rapid release of the physisorbed DOX molecules from the surface of the hydrogel network. At later stage, the value of n dropped to 0.37, indicating fickian-type diffusion of DOX. But at pH 7.4, the values of 'n' were 0.094 and 0.315, at the initial and later stages respectively of DOX release from the NSC88/Glc-gel beads. This implied a fickian-diffusion controlled drug release throughout the kinetic studies at pH 7.4. This may be because of greater swelling of the NSC88/Glc-gel bead and also greater solubility of NSC88 at pH 7.4 and 5. Therefore the major mechanism of release in case of NSC88/Glc-gel bead is by ion exchange mechanism and/or diffusion of the drug through the matrix.

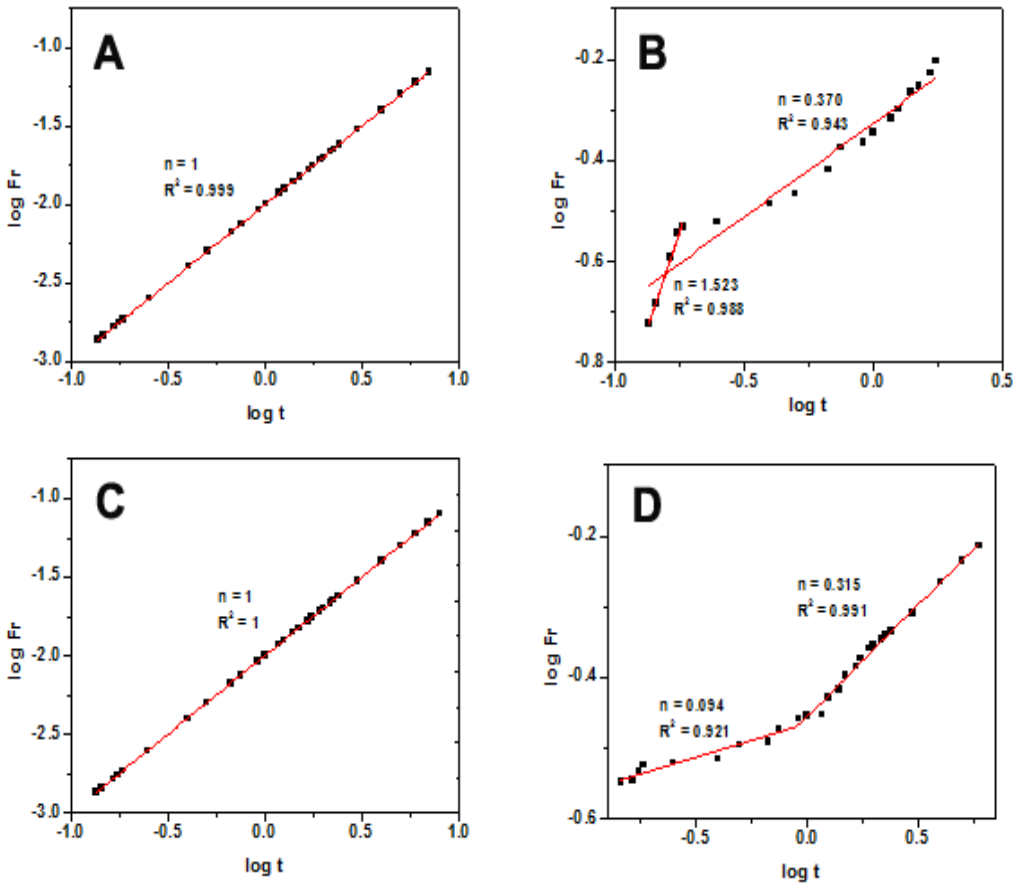

Figure 5.10: Linear fitted curves of drug release applying Korsmeyer-Peppas equation for (A) NSC75/Glc-gel bead at pH5 (B) NSC88/Glc-gel bead at pH 5 (C) NSC75/Glc-gel bead at pH 7.4 (D) NSC88/Glc-gel bead at pH 7.4.

5.4.9. *Surface morphology of the beads*

The drug release studies, showed a slow and sustained delivery from the NSC75/Glc-gel beads, *vide supra*. Hence the freeze dried DOX loaded NSC75/Glc-gel beads were chosen for surface morphology analysis. The SEM images of the freeze dried NSC75/Glc-gel beads showed porous surface with number of interconnecting pores, which control the drug release profile. The

images of the DOX loaded beads after few hours of swelling at pH 5 (Figure 5.11A) and pH 7.4 (Figure 5.11B) buffers were recorded in order to get an insight into the network structure during DOX release. Figure 5.11C-F are the magnified images of the beads showing the glycopolymeric network on the surface swollen at pH 5 and 7.4. In figure 5.11E the precipitated NSC at pH 5 is visually clear and is responsible for the faster release of DOX whereas, in figure 5.11F a uniform, intact network of NSC is observed at pH 7.4 which prevents uncontrolled drug release in to the extracellular body fluids.

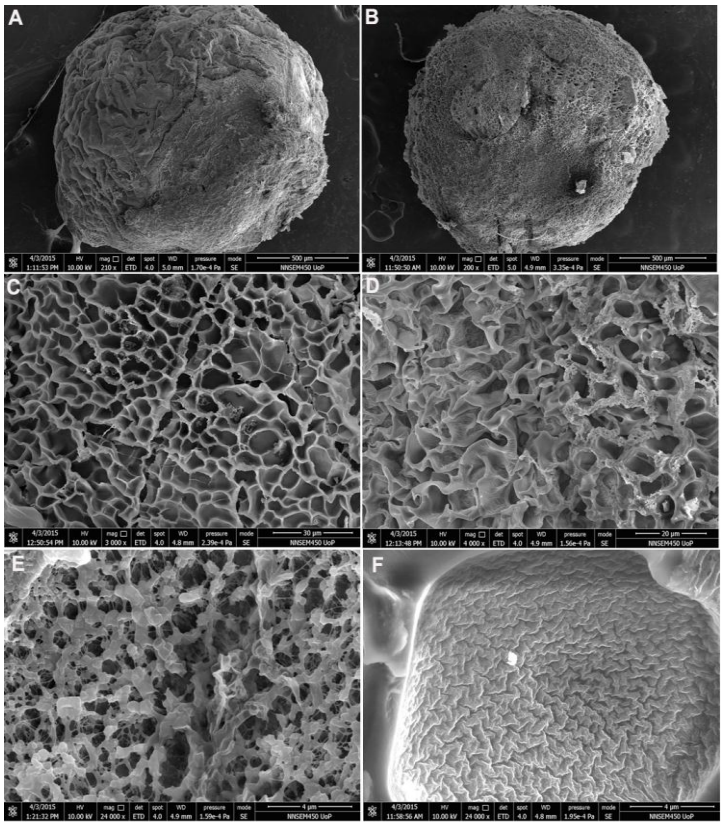

Figure 5.11: SEM images of DOX loaded NSC67/Glc-gel beads after swelling and freeze dried at (A) pH 5 (B) pH 7.4. Magnified images showing Glc-gel

network on the surface at (C) pH 5 (D) pH 7.4. Images of same beads at even higher magnification showing the NSC networks (E) bead with precipitated NSC at pH 5 (F) uniform and intact bead at pH 7.4.

5.4.10. ***Specific interaction between DOX loaded NSC/Glc-gel beads and Con A***

Con A binds specifically to glycopolymers containing glucosyl or mannosyl residues in the presence of Ca^{2+} and Mn^{2+}. Since Con A can activate cellular signaling on the cell surface the glycopolymer attached to Con A can regulate various activities like cell proliferation, adhesion and survival. To understand the interaction between the DOX loaded beads and Con A the UV-vis-absorbance of the buffer in which the bead is equilibrated was measured after centrifugation every minute (Figure 5.12).

The absorbance of the media increased in the beginning but after 4 minutes the solution became turbid and the absorbance dropped down as well. This is because of the aggregation of the glycopolymer components in the solution which, subsequently got adhered to the surface of the glycopolymer gel stabilized beads. Interaction studies of the DOX loaded beads with BSA and PNA under similar conditions showed no significant change in absorbance. It remained constant without much fluctuations and the solution remained relatively transparent indicating no specific interaction between glycopolymer and BSA or PNA.

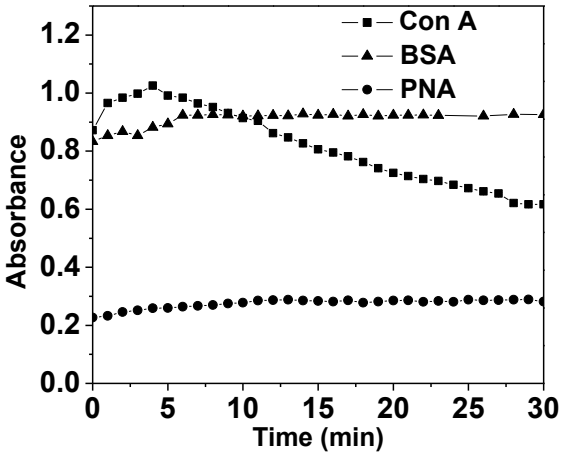

Figure 5.12: Interaction of the DOX loaded NSC/Glc-gel beads with Con A, PNA and BSA.

5.5. Conclusion

In short, we have furnished a carbohydrate based bio-compatible drug delivery system which has pH sensitive matrix in the form of interpenetrating network of NSC and glycopolymeric gel. NSC was synthesized with two different degrees of substitution NSC88 and NSC75 which were then stabilized by the Glc-gel network. A maximum swelling of 2906% and 1436% were reached at pH 7.4 whereas it was 543% and 313% at pH 5 for both the beads respectively. The DOX encapsulation efficiency (EE) of the synthesized beads was found to be dependent on the degree of succinylation. The EE for DOX was found to be 92.7% for NSC88/Glc-gel bead and 75% for NSC75/Glc-gel bead. The spectral characteristics of NSC-DOX complex indicated specific interaction between NSC and DOX. The DOX loaded NSC/Glc-gel beads gave slow and sustained drug delivery at pH 5 but much lesser rate of release at pH 7.4, a situation suitable for

cancer chemotherapy. Upto 76% cumulative drug release was obtained in case of NSC75/Glc-gel bead at pH 5 whereas, for NSC88/Glc-gel bead it was 88% after 18 days. In case of NSC75/Glc-gel bead the release was slower and it sustained better, also it followed a zero order release profile, which is ideal for implant purpose or post surgical treatment of localized cancer; whereas NSC88/Glc-gel beads showed a two stage release profile. The synthesized beads showed specificity to lectin Con A rather than PNA or BSA. Finally, this polysaccharide based glycopolymeric gel coated bead could be a suitable base for pharmaceutical applications.

CHAPTER 6

SELF ASSEMBLED FLUORESCENT GLYCOACRYLAMIDES

6.1. Introduction

The design and synthesis of fluorescent self assembled nanostructures are of great interest due to their applicability in drug delivery, molecular actuators, functional biomaterials, and analytical biosensors. Multiple weak non covalent/secondary interactions play a major role in the formation of such structures with a particular arrangement, which imparts some amazing properties that make them stimuli responsive. This non covalent interaction in self assembled biocompatible systems make them fluorescent which allows it to use in bio-sensing, cell imaging, etc. However, most of the commercially available fluorescent materials often have various disadvantages, which limit their application in bio-medical field. For example, fluorescent proteins are usually expensive, possess low molar absorptivity, and low photobleaching thresholds. The high toxicity of semiconductor quantum dots precludes its use in biomedical applications. In materials like organic dyes there exists a problem of aggregation caused quenching (ACQ) which leads to fluorescence quenching and photobleaching.[201] A good alternative to materials that causes ACQ is to search for materials that can exhibit the phenomenon of aggregation induced emission (AIE). After the first report by Tang *et al*. in 2001 on AIE dyes, many AIE fluorogens have been synthesized.[202] Unlike ACQ, AIE possess various advantages like facile synthesis, ease of modification, stability, good solubility, high emission efficiency in the aggregated states etc.[203,204]

Synthesis of amphiphilic molecules containing carbohydrate moieties, that can self assemble to form well defined nanostructures, can be promising scaffolds for various applications as it can interact with biological receptors. It is well known that carbohydrates play a significant role in many biological events like cell–cell recognition, inflammation, immune response, so on and so forth.[205-212] Self assembled monosaccharide analogues with amide units can mimic natural glycopeptides and hence can be important candidates for cell uptake and related studies. Very few amphiphilic glyco-amides/glyco-monomers have been reported that exhibit self assembly behavior to form well defined structures.[213] These structures can amplify the highly significant protein-saccharide interactions through multivalent effect of clustered saccharides called "cluster glycoside effect".

Molecules having aliphatic chains such as proteins, carbohydrates, lipids which play important roles in biological systems are mostly non-fluorescent or weakly fluorescent in their concentrated as well as dilute solutions due to ultrafast rotation around the single bond.[214] Hence such molecules are not reported to show AIE effect. Thus to study the structure and functions of these macrosystems we ought to have a system that can either mimic them or bind to them. In this regard there are a number of reports on AIE fluorogens such as siloles, tetraphenylethene, tri-phenylethene, cyano-substituted diarylethene, and distyryl-anthracene derivatives which are extensively investigated for chemosensing and bioimaging applications.[211-213]

We had previously synthesized two different monomer units (see chapter 4) with mono and bis-acrylamide units (hydrophobic) in to the C-6 position or C-3 and C-6 positions of glucose units, respectively (Figure 6.1).

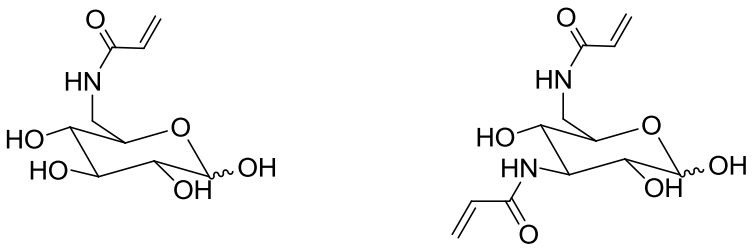

Figure 6.1: sugar acrylamides

This substitution can introduce a hydropohobic-hydrophilic balance in aqueous solution leading to the formation of self assembled structures of glyco-acrylamides and glyco-bis acrylamides. The extensive hydrogen bonding between the neighboring glucose units as well as inter- and intra- molecular H-bonding with the amide units, restricts the motion of hydrophobic acrylamide units and consequently results in the formation of self assembled structures. The restricted rotation in these structures can lead to fluorescence emission as a result of AIE phenomenon.

In this chapter discussion is about the self assembly of Glc-acryl and Glc-bis, the pH dependency on its self assembly and its applicability in aggregation induced fluorescence sensing method for concanavalin A (Con A). Eventhough glycoclusters or glycopolymers exhibiting fluorescence quenching after binding to lectins have been widely studied, fluoresence enhancement upon binding to

specific lectins is less explored and is more efficient in bioimaging of live cells. Fluorescence enhancement upon binding to lectin can be due to deaggregation induced emission, aggregation- induced emission, fluorescence resonance energy transfer (FRET) and/or hydrophobic interaction.[215-219] In the building blocks the presence of hydrophobic acrylamide units could act as the fluorescent probe by virtue of its weak π-π stacking and the hydrophilic glucose units would serve as the lectin binding moiety. The biocompatibility and cell uptake behaviours of Glc-acryl and Glc-bis were studied using human intestinal cell lines (INT407) which contain receptors which can be specifically identified by D-glucose moieties.

6.2. Experimental

The Glc-bis and Glc-acryl which will be commonly called as glyco-acrylamides were synthesized from D-glucose, the details of which along with characterization are given in chapter 4.

6.2.1. S*elf- assembly studies of Glc-acryl and Glc-bis*

2.5 mM stock solutions of Glc-acryl and Glc-bis were prepared in aqueous media. To determine the critical aggregation concentration (CAC), aqueous solutions of Glc-acryl and Glc-bis ranging from 1 µM – 20 µM were added to PBS buffer. After each addition, the sample was stirred and then subjected to fluorescence measurements (λ_{ex} = 330 nm). The pH dependent self assemblies of acrylamides were studied by adjusting the pH using 1 M NaOH/1 M HCl.

6.2.2. *Sample preparation for lectin sensing studies*

A 2.5 mM stock solution of Glc-acryl in a buffer solution (10 mM PBS; pH 7.2, 0.1 mM $MnCl_2$, 0.1 mM $CaCl_2$) was prepared. The stock solution was diluted to 6.25 µM into which aliquots of Con A ranging from 0 nM - 120 nM were added. After each addition, the solution was stirred for 10 minutes and then subjected to fluorescence measurements (λ_{ex} = 330 nm). The same procedure was repeated with 2.5 mM stock solution of Glc-bis.

6.2.3. *Determination of association constant (Ka)*

A typical procedure was followed: Aliquots (2 µl) of Glc-acryl as well as Glc-bis solution (2.5 mM) in buffer solution (10 mM PBS; pH 7.2, 0.1 mM $MnCl_2$, 0.1 mM $CaCl_2$) were added to a solution of FITC-Con A (1 µM, 2 ml) in the same buffer solution. The fluorescence spectra were measured at an excitation wavelength of 492 nm. The same procedure was repeated with FITC-PNA.

The binding constant (Ka) was estimated from the Scatchard plot using the following equation 6.1.[220]

$$\frac{[\text{Sugar}]\,F_0}{\Delta F} = \frac{[\text{Sugar}]\,F_0}{\Delta F_{max}} + \frac{F_0}{K_a\,\Delta F_{max}} \qquad (6.1)$$

where, [sugar] = concentration of the monomer

F_o = initial fluorescence intensity of FITC- Con A/PNA

ΔF = relative change in fluorescence intensity i.e $(F- F_o)/F_o$

6.2.4. *Confocal microscopic imaging of cells using Glc-acryl and Glc-bis*

INT407 cells were grown in DMEM medium with 10% FCS under 5% CO_2 atmosphere at 37 ºC. In a six well plate, sterile cover-slips were placed carefully and 1×10^5 cells/well in 2 ml volume of medium was added to each well. The cells were allowed to attach overnight. Glc-acryl and Glc-bis-acryl at 20 mM each (final concentration) were added to different wells and incubated for 1 h. At the end of the incubation period the individual cover-slip with the cells were picked up with sterile forceps and mildly rinsed in PBS. The cover-slips were then placed on a glass side in such a way that the cells remain between the two surfaces. The slides were immediately observed under a florescent microscope (LSM 780 Carlzeiss fluorescent microscope) with UV filter (excitation 355 nm and emission 395 nm).

6.3. Results and discussion

6.3.1. *Fluorescence spectral properties of Glc-acryl and Glc-bis*

The emission intensity was obtained at varying excitation wavelength ranging from 300 nm-400 nm. For both Glc-acryl and Glc-bis maximum emission intensity was obtained at λ_{ex} = 330 nm. For Glc-acryl there was not much shift in the λ_{max} emission at varying excitation wavelength. But for Glc-bis a red shift was observed in the λ_{max} emission with increasing λ_{ex} (Figure 6.2).

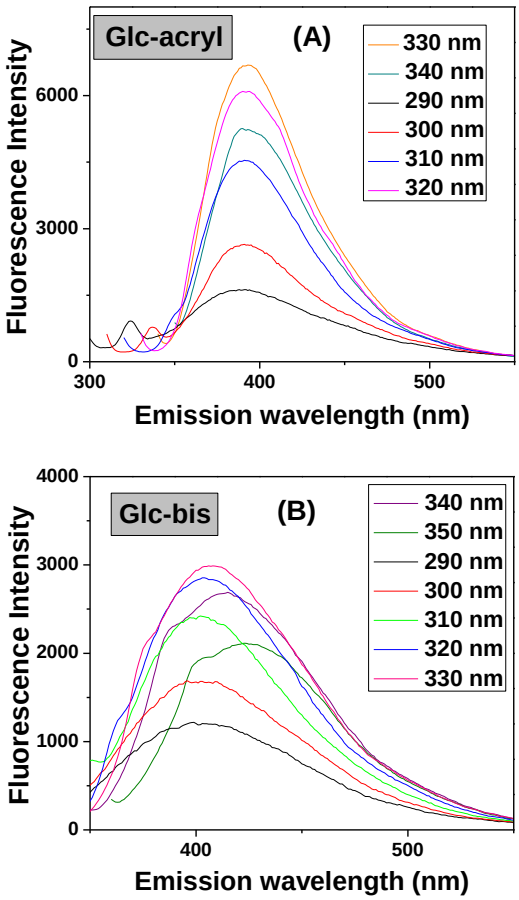

Figure 6.2: Emission spectra of Glc-acryl (A) and Glc-bis (B) at varying excitation wavelengths.

The emissions at different wavelengths were observed by fluorescent and bright field images of the glyco mono-acrylamides/bis-acrylamides. The red, yellow and blue emissions as shown in figure 6.3 could be possibly arising from the hydrophobic channels of a concentrated glycoacrylamide solution coated on a glass slide.

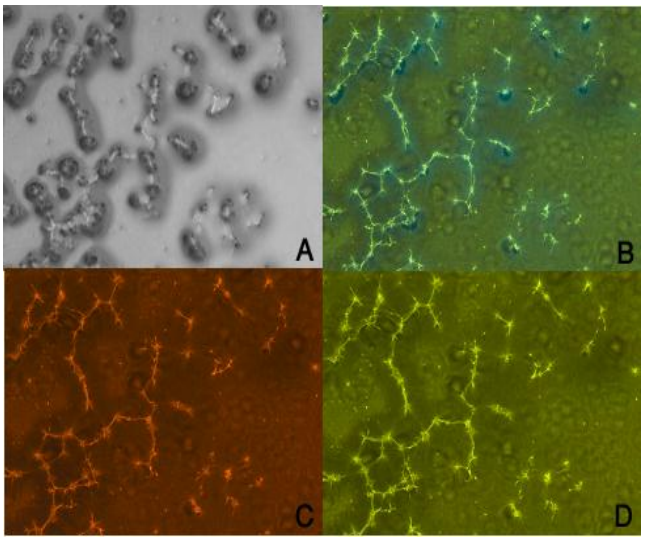

Figure 6.3: Bright field image (A) and fluorescent images (B, C, D) showing blue, red and yellow emissions of glycoacrylamide.

6.3.2. *Critical aggregation concentration (CAC)*

Effect of concentration of Glc-bis from (1 µM to 20 µM) on fluorescence intensity was explored and it showed an increase with increase in concentration.

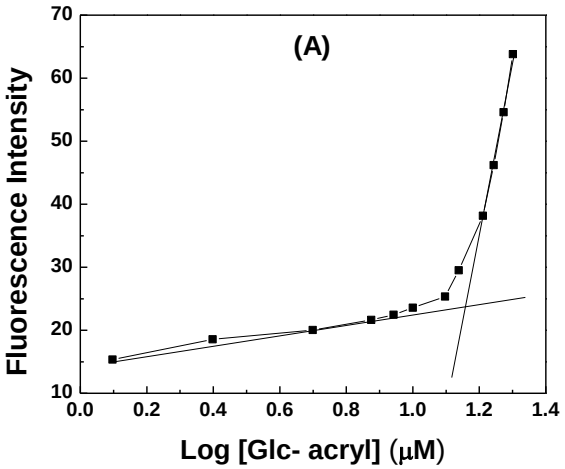

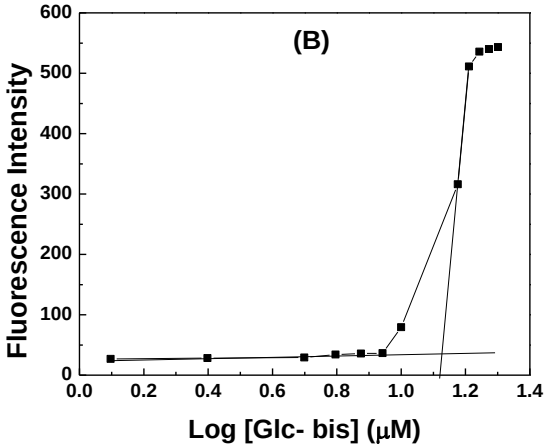

Figure 6.4: Log of concentration *vs* fluorescence intensity plot for Glc- acryl (A) and Glc- bis (B).

From the plot of log of concentration *vs* fluorescence intensity, the critical aggregation concentration (CAC) for Glc-bis was calculated to be 13.18 μM (Figure 6.4). Similarly, for Glc-acryl CAC was found to be 14.45 μM.

6.3.3. *pH dependent self assembly and fluorescence emission*

Glc-acryl as well as Glc-bis showed a pH dependent variation in fluorescence emission (Figure 6.5).

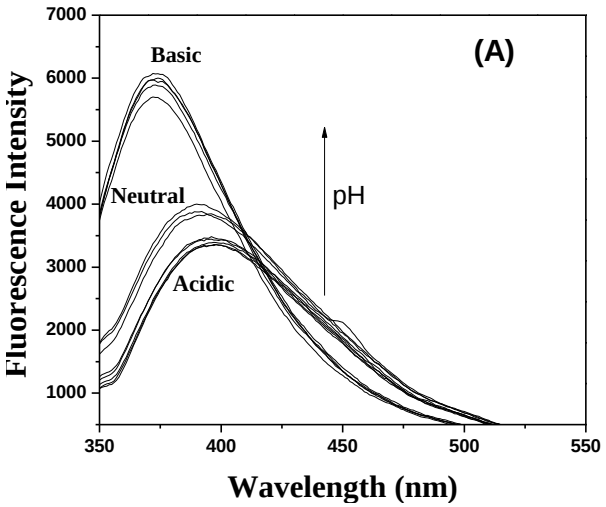

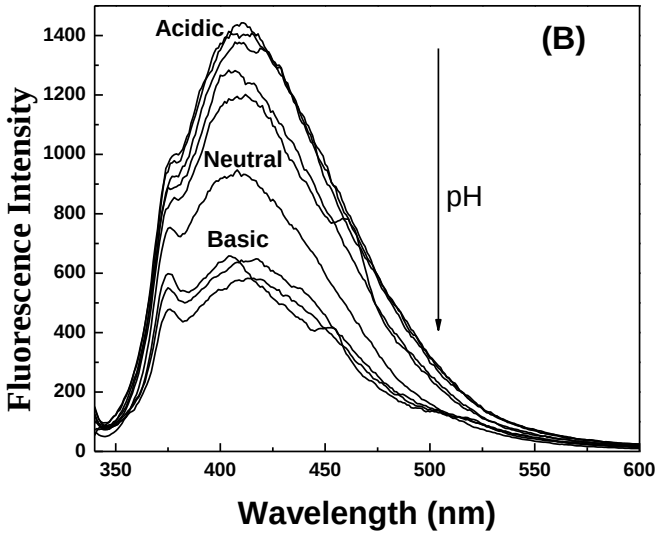

Figure 6.5: pH dependent fluorescent emission of (A) Glc-acryl and (B) Glc-bis.

At basic pH Glc-acryl showed higher emission whereas at acidic pH the emission intensity decreased with a red shift in emission maxima λ_{em}. Conversely, Glc-bis showed higher emission at acidic pH but emission intensity lowered at basic pH without any significant shift in emission maxima λ_{em}. This was further confirmed by TEM images (Figure 6.6).

TEM images revealed that at basic pH the self assembled Glc-acryl undergoes aggregation to form elongated hair like structures, but under neutral conditions the self assembled molecules are in the form of small granular structures. As the pH drops to acidic range these Glc-acryl particles self assemble to form small well separated rod like structures, which makes them less emissive. Whereas in the case of Glc-bis the TEM images reveal that at neutral pH the assembly is almost

similar to that of Glc-acryl but at acidic pH, smaller aggregates come closer to become more emissive.

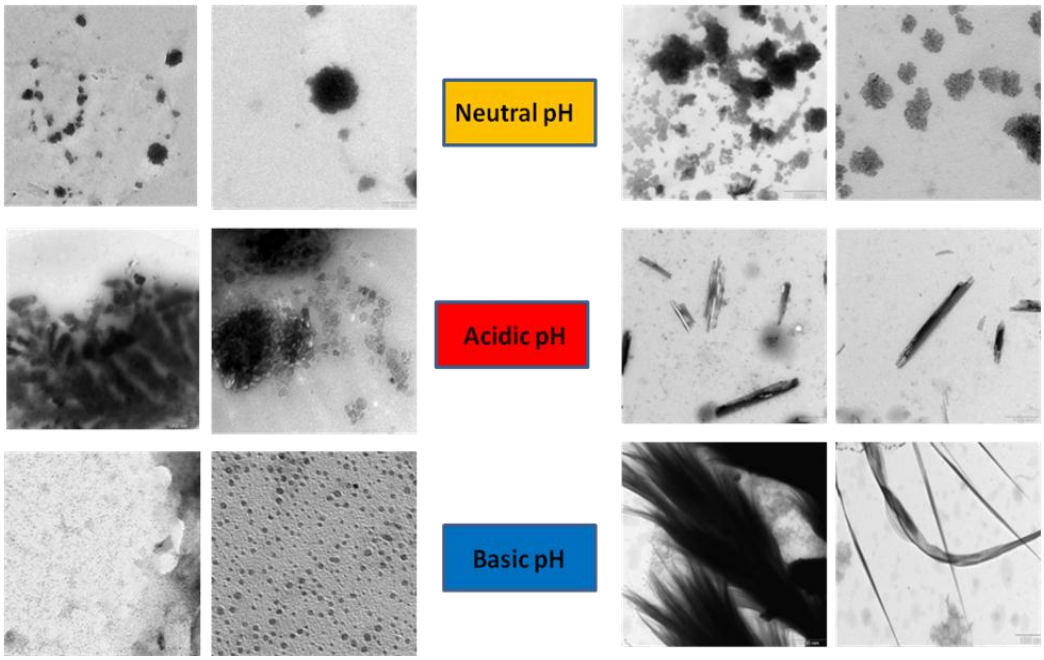

Figure 6.6: TEM images of Glc-bis and Glc-acryl at different pH.

While under basic pH, the Glc-bis form very fine particles with an average size of 5-10 nm. This highly dispersed nature of Glc-bis nanoparticles make them weakly emissive at basic pH.

6.3.4. *Fluorescence "turn on" sensing of Con A*

The effect of binding of Con A to glucose based acrylamide and bis-acrylamide was studied using fluorescence spectroscopy. Concanavalin A (Con A), which is a well-studied lectin from Canavalia ensiformis (Jack bean), was used as a model protein in the present study to understand protein–carbohydrate interactions. Con

A exists as a tetramer above neutral pH and it can selectively recognize α-mannopyranoside and its C-2 epimer α-glucopyranoside residues.[221-223]

As shown in figure 6.7, a progressive increase in the fluorescence emission intensity of Glc-acryl and Glc-bis was observed with increasing Con A concentration, but with no obvious shift in the emission maxima. The binding of the self assembled Glc-acryl and Glc-bis to Con A results in the formation of aggregates through secondary interactions. This aggregation results in enhancement in fluorescence due to AIE and thus the solution of glycoacrylamides which were usually very weakly emissive, starts to emit better in presence of Con A. The extent of fluorescence enhancement was found to be more in the case of Glc-acryl than in Glc-bis. Therefore Glc-acryl is a better fluorescence "turn on" sensor for Con A compared to Glc-bis.

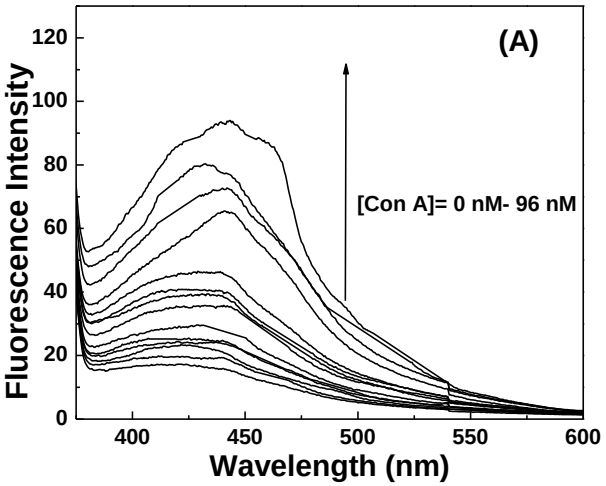

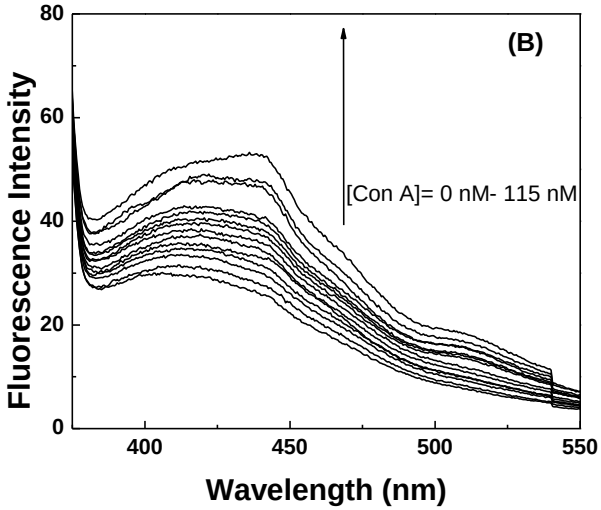

Figure 6.7: Fluorescence enhancement of Glc-acryl (A) and Glc-bis (B) upon addition of Con A.

6.3.5. *Binding affinities and limit of detection (LOD) of Glc-acryl and Glc-bis towards lectins*

In order to elucidate the binding affinities of glycoacrylamides towards Con A, the fluorescence quenching titration of fluoroscein isothiocyanate labeled Con A (FITC-ConA) as well PNA (FITC-PNA) was carried out. FITC groups have an intrinsic emission peak at 517 nm, which quenches upon binding with saccharides, making it possible to quantify the extent of binding. Figure 6.8 indicate the relative change in fluorescence intensity (F/F_0) with concentration of Glc-acryl and Glc-bis.

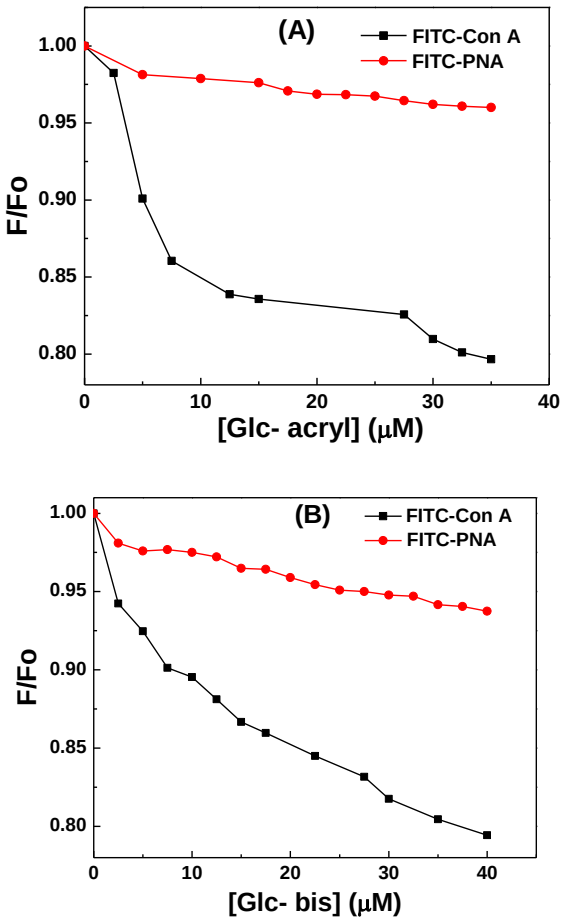

Figure 6.8: Fluorescence quenching of FITC-Con A and FITC-PNA by Glc-acryl (A) and Glc-bis (B).

A non linear decrease in fluorescence intensity with concentration was observed. The association constant (K_a) was calculated from the scatchard plot. The scatchard plot of Glc-acryl and Glc-bis binding to FITC-Con A and FITC-PNA are shown in figure 6.9. The K_a value of Glc-acryl to FITC-Con A was 144.00 X 10^3 M^{-1} which was twice as compared to Glc-bis (76.31 X 10^3 M^{-1}). The K_a value of Glc- acryl to FITC- PNA is 57.90 X 10^3 M^{-1} whereas of Glc- bis to FITC- PNA is 46.54 X 10^3 M^{-1}. This observation agrees with the observed enhancement in

fluorescence on addition of Con A to glycoacrylamide monomer solutions. The enhanced affinity of glycoacrylamide to Con A when compared to monosaccharides like methyl *β*-D-glucopyranoside (K_a = 70 M^{-1}) could be due to the "glyco cluster effect" arising from the self assembly of Glc-acryl and Glc-bis which is absent/less in latter.

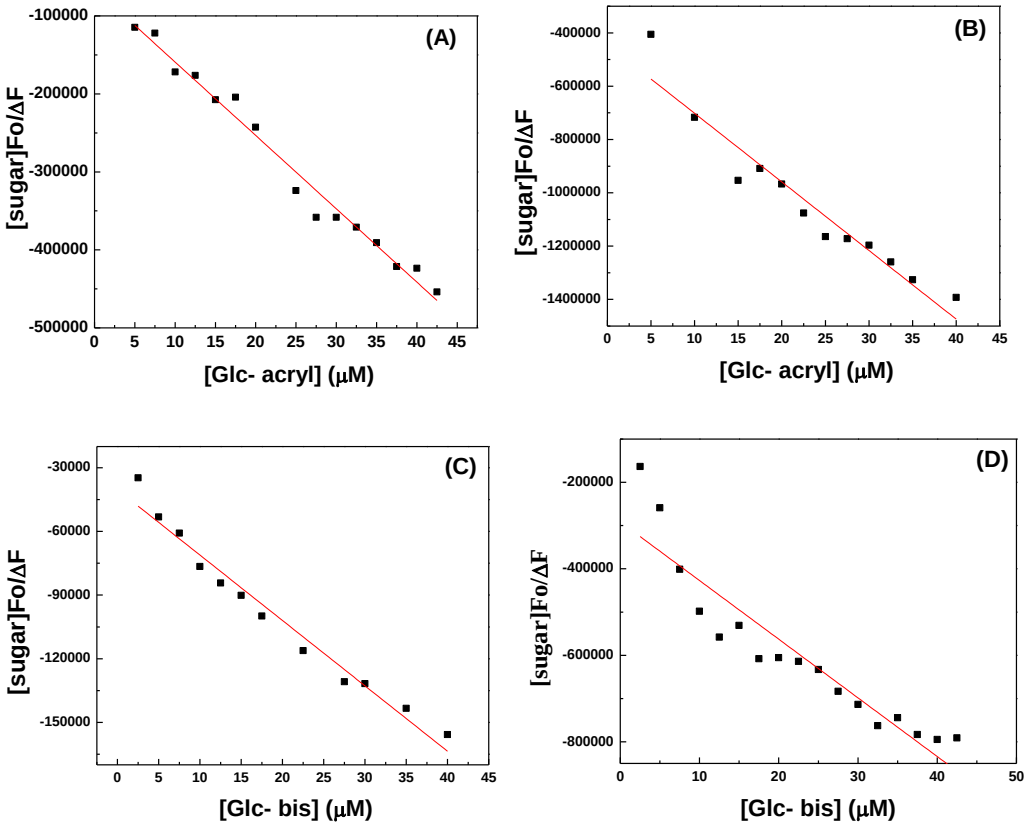

Figure 6.9: Scatchard plot for Glc-acryl upon addition of (A) FITC- Con A (B) FITC- PNA; for Glc-bis upon addition of (C) FITC- Con A (D) FITC- PNA.

Limit of detection was calculated from the enhancement in fluorescence intensity on addition of Con A to 6.25 μM Glc-acryl as well as Glc-bis. The typical limit of detection (LOD) as evaluated from the ratio of signal to noise (S/N) higher than 3,

was estimated to be 7.85 pM for Glc-acryl and 3.49 nM for Glc-bis. Thus, unlike Glc-bis, Glc-acryl showed high sensitivity to Con A which is more than any Con A sensors reported so far.

Compound	Ka (M^{-1})		LOD (nM) (for Con A)
	Con A	PNA	
Glc-acryl	144.00 X 10^3 M^{-1}	57.90 X 10^3 M^{-1}	7.85 pM
Glc-bis	76.31 X 10^3 M^{-1}	46.54 X 10^3 M^{-1}	3.49 nM

Table 6.1: Association constants (Ka) and Limit of Detection (LOD) of Glc-acryl and Glc-bis towards Con A and PNA.

6.3.6. *Cell imaging application of Glc-acryl and Glc-bis*

Taking advantage of the fluorescent properties, biocompatibility and hydrophilicity of the synthesized glyco-acrylamides, the cell uptake behavior was explored using confocal microscopy as demonstrated in figure 6.10. INT407 cell lines showed strong blue fluorescence after equilibrating with 20 mM of glyco-acrylamides for 1 hr. Most of the fluorescent nanoparticles were found to be dispersed in the cytoplasm. Interestingly, the cells stained with Glc-bis were more fluorescent than Glc-acryl. These finding are against the results from Con A interaction studies, in terms of selectivity of Con A to Glc-acryl and Glc-bis. This automatically suggest that apart from Con A there could be other carbohydrate binding proteins/molecules present in the cytoplasm that can aggregate to show fluorescence enhancement. These results also suggest that the glycoacrylamides

can be good candidates for cell imaging applications with good water dispersibility and intense fluorescence even under dilute body fluid conditions.[224]

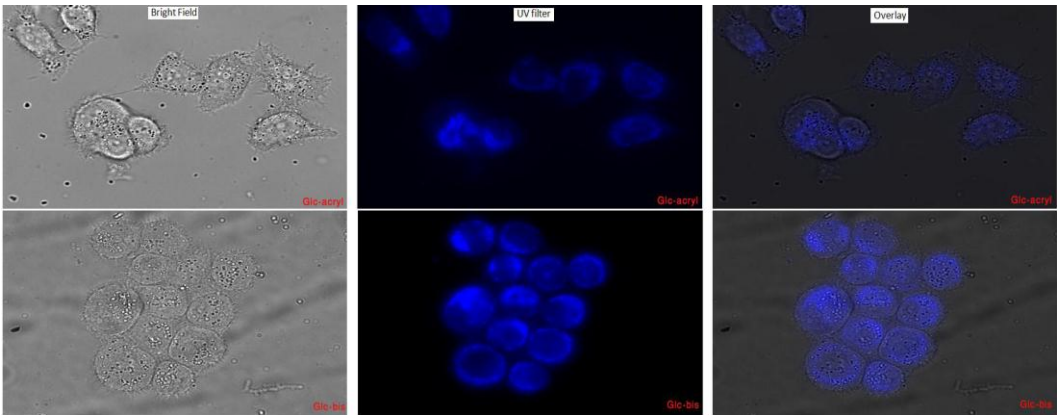

Figure 6.10: Confocal microscopy images of INT407 cell lines incubated with Glc-acryl (Top row) and Glc-bis (Bottom row): (A) & (B) bright field, (C) & (D) fluorescent images after excitation at 355 nm, (E) & (F) merged image.

6.4. Conclusions

In summary, glyco-acrylamides synthesized from D-glucose, were found to self assemble in aqueous solution to form fluorescent nanoparticles. These particles showed variable emission at different excitation wavelengths. The self assembly of Glc-acryl as well as Glc-bis was found to be pH dependent and both of them showed opposite behaviours with varying pH. Also, the self assembly enhances the glyco cluster effect, thereby leading to specific recognition of lectin Con A even in pico molar range which is much better than the Con A sensors reported so far. The lectin sensing takes place by a fluorescence "turn on" mechanism. The fluorescence enhancement upon interaction with Con A is more in case of Glc-

acryl than with Glc-bis as association constant (K_a) measurements with Con A for Glc-acryl was twice that of Glc-bis. The synthesized glycoacrylamides could also be promising candidates for cell imaging applications.

CHAPTER 7

CONCLUSIONS AND FUTURE PERSPECTIVES

7.1. Outcome of present work

The work incorporated in the thesis emphasize on the utility of natural polysaccharides along with synthetic polymers/monomers for various biomedical applications. Composites of natural polysaccharides with synthetic polymers were utilized for the production of hydrogels for applications like wound dressings and drug delivery. In this regard special care has been given for biocompatibility of the synthesized material applying green methods for synthesis. Hence all the crosslinking and synthesis of hydrogels work has been carried out by radiation induced method without addition of any external chemical agents.

Silver nanoparticle loaded PVA-GA hydrogels were synthesized for antibacterial wound dressing applications and were found to be effective against gram negative E. *Coli* bacteria. We were able to determine the gel point of the synthesized hydrogels rheologically which is the most accurate method among the existing ones. The key information which we got from this work was that the size of the silver nanoparticles determines its antibacterial activity.

The rest of the thesis is based on two D-glucose based acrylamide molecules synthesized in our laboratory which are named Glc-acryl and Glc-bis and together mentioned as glyco-acrylamides. These glucose based mono-acrylamide and bis-acrylamide were made from economically cheap D-glucose as the starting material, in a high yielding reaction sequence, consisting of few steps.

A synthetic glycopolymeric hydrogel was made from these molecules using gamma radiation induced crosslinking. This hydrogel matrix was synthesized with an aim to develop a new targeted drug delivery vehicle. Since glycopolymers can selectively recognize the lectins, which are carbohydrate interacting proteins, present on the cell surface and are responsible for a number of biological events, we expected that the synthesized glycopolymeric hydrogel (Glc-gel) would be of great importance in biomedical field. The Glc-gel showed specificity to lectin concanavalin A, which is a glucose/mannose binding lectin.

To test the applicability of the glycopolymeric gel in targeted drug delivery, a hydrogel bead of *N*-succinyl chitosan was made, which was mechanically stabilized by Glc-gel network. This network not only renders stability but also helps to guide the gel bead to the target site. *N*-succinyl chitosan was chosen because of its well known biocompatibility, long systemic circulation time and appropriate water solubility. Chitosan was succinylated to different degrees of 75% and 88%. The calcium ion crosslinked beads thus synthesized were utilized for DOX loading and it was observed that we can tune the extent of loading by varying the degree of succinylation. The DOX delivery was studied in simulated body fluids under varying pH conditions. This matrix showed a slow and sustained delivery of the drug over a period of 18 days and also displayed specificity to lectin Con A. The drug release was faster in acidic pH rather than normal body fluid conditions making it a localized drug delivery vehicle. Another important feature of this bead was that it started degradation after 3-4 hours of

delivery due to leaching out of NSC, but still maintaining its spherical shape. Hence it is a self degrading system which can be a suitable candidate to satisfy the localized and targeted drug delivery needs of the biomedical industry.

Fluorescent nanoparticles are always in demand both in industry as well in biomedical field. The glyco-acrylamides can also form such fluorescent nanoparticles due to their hydrogen bond induced self assembly leading to AIE. The major outcome of this work was that we were able to synthesize a material which can self assemble in water with good solubility, emit at varying wavelengths depending on the excitation and most importantly the emissions were pH dependent. The self assembled glyco-acrylamides can act as a biosensor for lectins like Con A. Sensing is generally done by observing variation in some property of the material which can be measured. Fluorescence "turn on" is one of the best way of sensing since it eliminates unnecessary noise and background. Glc-acryl showed better fluorescence enhancement compared to Glc-bis, which was also clear from its binding studies with Con A. The LOD for Con A in the case of Glc-acryl is in the picomolar range. Also these glyco-acrylamides were found to perform as good cell imaging agents. They can penetrate in to the cell cytoplasm and exhibit good emission and dispersability even in the body fluid conditions. The double bond/hemiacetal groups which are freely available could also help us to integrate other functional components like drugs, imaging agents, targeting agents, etc. which can widen the scope of the synthesized glyco-acrylamides. Therefore multifunctional theranostic platforms can be manufactured

using these glyco-acrylamides, which can find wide range of biomedical applications.

7.2. Future Scope

Currently lot of work has been carried out in developing new polymers as well as modifying the naturally existing ones to generate a system which cater the demands of the biomedical industry. This thesis is also a dedicated effort to introduce systems which are biocompatible, non cytotoxic, biodegradable and economical. Also we have attempted to utilize radiation technology which in future could be extended to make more advanced systems. Gum acacia and *N*-succinyl chitosan are derived from natural products which can be utilized in biomedical field without any worries of toxicity, biodegradability etc. We have also emphasized on the extensive applications of carbohydrate chemistry through the glyco-acrylamides as well as the glycopolymers synthesized from them. The future scope of the carbohydrate chemistry lies in the fact that precise biorecognition properties can be achieved by an absolute control over the microstructure of the glycopolymers. The carbohydrate units critically control the specific biological functions of the cells and play a major role in cell-cell recognition. The advances in synthetic chemistry allow us to prepare well defined and multifunctional glycopolymers in a facile manner.

Targeted drug delivery vehicles are in increasing demand, especially those can exhibit slow and sustained delivery properties. In the global drug delivery market the largest segment is for targeted systems, which reached $80.2 billion in 2014.

Incorporating an existing medicine in to a new drug delivery system can enhance its performance in terms of its efficacy, safety and patient compliance. The increasing need for delivery of drug with minimal side effects has prompted pharmaceutical industries to develop new drug delivery systems. Also localized delivery systems like microspheres or beads could find application in delivering drugs to sites less accessible to systemic circulation or those which degrade in the systemic circulation. In future, drugs are going to be more challenging in terms of delivery system development, which makes it a more exiting task ahead.

References

1. N. Kashyap, N. Kumar and M. N. V. Ravi Kumar, *Critical Review in Therapeutic Drug Carrier Systems*, 2005, **22**,107.
2. B. D. Ratner and A. S. Hoffman, *ACS Symposium Series*, 1976, **31**, 1.
3. M. R. Huglin, CRC Press, Boca Raton, FL, **1-3**, 1987.
4. K. Park, W. S. W. Shalaby and H. E. Park, Technomic, Lancaster, PA, 1993.
5. L. Varshney, *Nuclear Instruments and Methods in Physics Research B*, 2007, **255**, 343.
6. Z. Ajji, I. Othman and J. M. Rosiak, *Nuclear Instruments and Methods in Physics Research B*, 2005, **229**, 375.
7. Y. N. Rao, D. Banerjee, A. Datta, S. K. Das, R. Guin and A. Saha, *Radiation Physics and Chemistry*, 2010, **79**, 1240.
8. S. H. Allan, *Advanced Drug Delivery Reviews*, 2002, **54**, 3.
9. G. Iwona and H. Janik, *Chemistry and Chemical Technology*, 2010, **4**, 297.
10. (a) Y. Liu, H. Meng, S. Konst, R. Sarmiento, R. Rajachar and B. P. Lee, *ACS Applied Material Interfaces*, 2014, **6**, 16982; (b) S. Skelton, M. Bostwick, K. O'Connor, S. Konst, S. Casey and B. P. Lee, *Soft Matter*, 2013, **9**, 3825.
11. G. Marcelo, M. López-González, F. Mendicuti, M. P. Tarazona, M. Valiente, *Macromolecules*, 2014, **47**, 6028.
12. P. Thoniyot, M. J. Tan, A. A. Karim, D. J. Young and X. J. Loh, *Advanced Science*, 2015, **2**, 1400010.

13. K. Vimala, K. S. Sivudu, Y. M. Mohan, B. Sreedhar and K. M. Raju, *Carbohydrate Polymers*, 2009, **75**, 463.

14. G. R. Bardajee, Z. Hooshyar and H. Rezanezhad, *Journal of Inorganic Biochemistry*. 2012, **117**, 367.

15. Y. M. Mohan, K. Lee, T. Premkumar and K. E. Geckeler, *Polymer*, 2007, **48**, 158.

16. Q.-B. Wei, F. Fu, Y.-Q. Zhang and L. Tang, *Journal of Polymer Research*, 2014, **21**, 1.

17. K. A. Juby, C. Dwivedi, M. Kumar, S. Kota, H. S. Misra and P. N. Bajaj, *Carbohydrate Polymers*, 2012, **89**, 906.

18. R.-C. Luo, Z. H. Lim, W. Li, P. Shi and C.-H. Chen, *Chemical Communications*, 2014, **50**, 7052.

19. Y.-Q. Ma, J.-Z. Yi and L.-M. Zhang, *Journal of Macromolecular Science, Part A: Pure and Applied Chemistry*, 2009, **46**, 643.

20. H. L. Abd El-Mohdy, *Journal of Polymer Research*, 2013, **20**, 1.

21. C. Wang, N. T. Flynn and R. Langer, *Advanced Materials*, 2004, **16**, 1074.

22. M. Liu, Y. Ishida, Y. Ebina, T. Sasaki and T. Aida, *Nature Communications*, 2013, **4**, 2029.

23. L. S. Nair and C. T. Laurencin, *Journal of Biomedical Nanotechnology*, 2007, **3**, 301.

24. H. Oka, T. Tomioka, K. Tomita, A. Nishino and S. Ueda, *Metal-Based Drugs*, 1994, **1**, 511.

25. A. Oloffs, C. Crosse-Siestrup, S. Bisson, M. Rinck, R. Rudolvh and U. Gross, *Biomaterials*, 1994, **15**, 753.

26. T. Tokumaru, Y. Shimizu and C. L. Fox, *Research communications in chemical pathology and pharmacology*. 1984, **8**,151.

27. G. V. James, *Water treatment*, 1971, 4th ed., p. 38. CRC Press, Cleveland, OH.

28. M. Herrera, P. Carrion, P. Baca, J. Liebana and A. Castillo, *Microbios*, 2001, **104**, 141.

29. Y. Matsumura, K. Yoshikata, S. Kunisaki and T. Tsuchido, *Appied. Environmental Microbiology,* 2003, **69**, 4278.

30. M. Bosetti, A. Masse, E. Tobin and M. Cannas, *Biomaterials*, 2002, **23**, 887.

31. P. Li, J. Li, C. Wu, Q. Wu and J. Li, *Nanotechnology*, 2005,**16**,1912.

32. I. Sondi and B. Salopek-Sondi, *Journal of Colloid and Interface Science*, 2004, **275**,177.

33. J. L. Elechiguerra, J. L. Burt, J. R. Morones, A. Camacho-Bragado, X. Gao, H. H. Lara and M. J. Yacaman, *Journal of Nanobiotechnology*, 2005, **3**, 6.

34. J. R. Morones, J. L. Elechiguerra, A. Camacho, K. Holt, J. B. Kouri, J. T. Ramirez and M. J. Yacaman, *Nanotechnology*, 2005, **16**, 2346.

35. D. E. Owens, J. K. Eby, Y, Jian and N. A. Peppas, *Journal of Biomedical Materials Research Part A*, 2007, **83**, 692.

36. A. K. Gaharwar, N. A. Peppas and A. Khademhosseini, *Biotechnology and Bioengineering*, 2014, **111**, 441.

37. K.Y. Lee and D. J. Mooney, *Chemical Reviews*, 2001, **101**, 1869.

38. H. J. v-d Linden, S. Herber, W. Olthuis and P. Bergveld, *Analyst*, 2003, **128**, 325.

39. A. C. Jen, M. C. Wake and A. G. Mikos, *Biotechnology and Bioengineering*, 1996, **50**, 357.

40. K. Wang, J. Burban and E. Cussler, *Responsive gels*: *volume transitions II* , 1993, 67.

41. S. L. Bennett, D. A. Melanson, D. F. Torchiana, D. M. Wiseman and A. S. Sawhney, *Journal of Cardiac Surgery*, 2003,**18**, 494.

42. T. R. Hoare and D. S. Kohane, *Polymer*, 2008, **49**, 1993.

43. C. S. Satish, K. P. Satish and H. G. Shivakumar, *Indian Journal of Pharmaceutical Sciences*, 2006, **68**, 133.

44. O. Wichterle and D. Lim, *Nature*, 1960, **185**, 117.

45. N. A. Peppas and A.G. Mikos, N.A. Peppas, Eds,. *In Preparation Methods and Structure of Hydrogels*, *Hydrogels in Medicine and Pharmacy*, Vol I, CRC Press, Boca Raton, FL, 986, 1.

46. N.A, Peppas and E.W, Merrill, *Journal of Applied Polymer Science*, 1977, **21**, 1763.

47. P. Kofinas, V. Athanasssiou and E. W. Merrill, *Biomaterials*, 1996, **17**, 1547.

48. E. W. Merrill, K. A. Dennison and C. Sung, *Biomaterials*, 1993, **14**, 1117.

49. J. L. Stringer and N.A. Peppas, *Journal of Controlled Release*, 1996, **42**, 195.

50. E. Jabbari and S. Nozari, *European Polymer Journal*, 2000, **36**, 2685.

51. N. A. Peppas, *Hydrogels in Medicine and Pharmacy*, 1986, vol. 1–3, CRC Press, Boca Raton, FL, 180.

52. B. Amsden, *Macromolecules*, 1998, **31**, 8382.

53. L. Masaro and X. X. Zhu, *Progress in Polymer Science*, 1999, **24**, 731.

54. N. A. Peppas, Y. Huang, M. Torres-Lugo, J. H. Ward and J. Zhang, *Annual Review of Biomedical Engineering*. 2000, **2**, 9.

55. M. Chasin and R. Langer. (eds), *Biodegradable Polymers as Drug Delivery Systems*, New York, Marcel Dekker, 1990

56. Y. W. Chien, *Novel Drug Delivery Systems*, New York, Marcel Dekker, 1982.

57. N. A. Peppas, P. Bures, W. Leobandung and H. Ichikawa, *European Journal of Pharmaceutics and Biopharmaceutics*. 2000, **50**, 27.

58. J. Siepmann and N. A. Peppas, *Advanced Drug Delivery Reviews*, 2001, **48**, 139.

59. M. A. Rice, J. Sanchez-Adams and K. S. Anseth, *Biomacromolecules*, 2006, **7**, 1968.

60. R. A. Dwek, *Chemical Reviews*, 1996, **96**, 683.

61. H. Lis and N. Sharon, *Chemical Reviews*, 1998, **98**, 637.

62. J. J. Lundquist and E. J. Toone, *Chemical Reviews*, 2002,**102**, 555.

63. M. Mammen, S.-K. Chio and G. M. Whitesides, *Angewandte Chemie International Edition*, 1998, **37**, 2754.

64. Y. Miura, *Journal of Polymer Science Part A: Polymer Chemistry*, 2007, **45**, 5031.

65. V. Horoejsí, O. Chaloupecká and J. Kocourek, *Biochimica et Biophysica Acta (BBA) - General Subjects*, 1978, **539**, 287.

66. C. J. Hawker and K. L. Wooley, *The convergence of synthetic organic and polymer chemistries Science*, 2005, **309**, 1200.

67. L. L. Kiessling, L. E. Strong and J. E. Gestwicki, *Principles for multivalent ligand design, Annual Reports in Medicinal Chemistry*, Academic Press Inc., San Diego, 2000, 321.

68. B. Voit and D. Appelhans, *Macromolecular Chemistry and Physics*, 2010, **211**, 727.

69. R. Roy, F. D. Tropper and A. Romanowska, *Bioconjugate Chemistry*, 1992, **3**, 256.

70. M. Okada, *Progress in Polymer Science*, 1992, **26**, 67.

71. D. M. Haddleton, R. Edmonds, A. M. Heming, E. J. Kelly and D. Kukulj, *New Journal of Chemistry*, 1999, **23**, 477.

72. K. Ohno, Y. Tsujii and T. Fukuda, *Journal of Polymer Science Part A: Polymer Chemistry*, 1998, **36**, 2473.

73. S. R. S. Ting, A. M. Granville, D. Quémener, T. P. Davis, M. H. Stenzel and C. Barner-Kowollik, *Australian Journal of Chemistry*, 2007, **60**, 405.

74. R. Roy, F. D. Tropper and A. Romanowska, *Bioconjugate Chemistry*, 1992, **3**, 256.

75. V. Ladmiral, E. Melia and D. M. Haddleton, *European Polymer Journal*, 2004, **40**, 431.

76. R. Roy, *Trends in Glycoscience and Glycotechnology*, 1996, **8**, 79.

77. S. Slavin, J. Burns, D. M. Haddleton and C. R. Becer, *European Polymer Journal*, 2011, **47**, 435.

78. M. C. García-Oteiza, M. Sánchez-Chaves and F. Arranz, *Macromolecular Chemistry and Physics*, 1997, **198**, 2237.

79. R. A. Dwek , *Chemical Reviews*, 1996, **96**, 683.

80. N. Sharon and H. Lis, *Scientific American*, 1993, **268**, 82.

81. N. Sharon and H. Lis, *Science*, 1989, **246**, 227.

82. E. E. Simanek, G. J. McGarvey, J. A. Jablonowski and C.-H. Wong, *Chemical Reviews*. 1998, **98**, 833.

83. Y.C. Lee and R.T. Lee, *Accounts of Chemical Research*, 1995, **28**, 321.

84. H. Lis and N. Sharon, *Chemical Reviews*, 1998, **98**, 637.

85. M. Ambrosi, N. R. Cameron and B. G. Davis, *Organic and Biomolecular Chemistry*, 2005, **3**, 1593.

86. R. Loris, T. Hamelryck, J. Bouckaert and L. Wyns, *Biochimica et Biophysica Acta (BBA) - Protein Structure and Molecular Enzymology*, 1998, **1383**, 9.

87. N. Sharon, *Trends in Biochemical Sciences*, 1993, **18**, 221.

88. R. J. Pieters, *Organic and Biomolecular Chemistry*, 2009, **7**, 2013.

89. C. S. Wright, *Journal of Molecular Biology*, 1987, **194**, 501.

90. D. C. Kilpatrick, *Biochimica et Biophysica Acta (BBA) - General Subjects*, 2002, **1572**, 187.

91. L. A. J. M. Sliedregt, P. C. N. Rensen, E. T. Rump, P. J. Van Santbrink, M. K. Bijsterbosch, A. R. P. M. Valentijn, G. A. Vander Marel, J. H. Van Boom, T. J. C. Van Berkel and E. A. L. Biessen, *Journal of Medicinal Chemistry*, 1999, **42**, 609.

92. A. David, P. Kopeckova, A. Rubinstein and J. Kopecek, *Bioconjugate Chemistry*, 2001, **12**, 890.

93. P. R. Taylor, L. Martinez-Pomares, M. Stacey, H. H. Lin, G. D. Brown and S. Gordon, *Annual Review of Immunology*, 2005, **23**, 901.

94. H. Leffler, S. Carlsson, M. Hedlund, Y. N. Qian and F. Poirier, *Glycoconjugate Journal*, 2002, **19**, 433.

95. B. Ernst, G. W. Hart and P. Sinaý, *Carbohydrates in Chemistry and Biology*, Wiley-VCH Verlag GmbH, 2000,1045.

96. K. Landsteiner, *The Specificity of Serological Reactions*, Dover, New York, 1962.

97. L. R. Olsen, A. Dessen, D. Gupta, S. Sabesan, J. C. Sacchettini and C. F. Brewer, *Biochemistry*, 1997, **36**, 15073.

98. E. Freire, O. L. Mayorga and M. Straume, *Analytical Chemistry*, 1990, **62**, 950A.

99. C. W. Cairo, J. E. Gestwicki, M. Kanai and L. L. Kiessling, *Journal of American Chemical Society*, 2002, **124**, 1615.

100. Z. Deng, S. Li, X. Jiang and R. Narain, *Macromolecules*, 2009, **42**, 6393.

101. Q. Yang, M.-X. Hu, Z.-W. Dai, J. Tian and Z.-K. Xu, *Langmuir*, 2006, **22**, 9345.

102. T. Furuike, N. Nishi, S. Tokura and S.-I. Nishimura, *Macromolecules*, 1995, **28**, 7241.

103. Y. Hong, J. W. Y. Lam and B. Z. Tang, *Chemical Society Reviews*, 2011, **40**, 5361.

104. Q. Peng, Y. Yi, Z. Shuai and J. Shao, *Journal of American Chemical Society*, 2007, **129**, 9333.

105. A. Iida and S. Yamaguchi, *Chemical Communications*, 2009, **21**, 3002.

106. Z. Jovanovic´, A. Krkljeˇs, J. Stojkovska, S.Tomic´, B. Obradovic´, V. Miˇskovic´-Stankovic´ and Z. Kacˇarevic´-Popovic´, *Radiation Physics and Chemistry*, 2011, **80**, 1208.

107. L. Varshney, *Nuclear Instruments and Methods in Physics Research B*, 2007, **255**, 343.

108. V. K. Sharma, R. A. Yongard and Y. Lin, *Advances in Colloid and Interface Science*, 2009, **145**, 83.

109. H. Kong and J. Jang, *Langmuir*, 2008, **24**, 2051.

110. V. Thomas, M. Namdeo, Y. M. Mohan, S. K. Bajpai and M. Bajpai, *Journal of Macromolecular Science Part A: Pure Applied Chemistry*, 2008, **45**, 107.

111. V. Thomas, Y. M. Mohan, B. Sreedhar and S. K. Bajpai, *Journal of Biomaterial Science, Part A: Polymer Edition*, 2009, **20**, 2129.

112. S. K. Bajpai, Y. M. Mohan, M. Bajpai, R. Tankhiwale and V. Thomas, *Journal of Nanoscience and Nanotechnology*, 2007, **7**, 2994.

113. Y. Dror, Y. Cohen and R. Yerushalmi-Rozen, *Journal of Polymer Science: Part B: Polymer Physics*, 2006, **44**, 3265.

114. Y. N. J. Rao, D. Banerjee, A. Datta, S. K. Das, R. Guin and A. Saha, *Radiation Physics and Chemistry*, 2010, **79**, 1240.

115. S. Lu, W. Gao and H. Y. Gu, *Burns*, 2008, **34**, 623.

116. K. Vimala, Y. M. Mohan, K. Varaprasad, N. N. Reddy, S. Ravindra, N. S. Naidu and K. M. Raju, *Journal of Biomaterials and Nanobiotechnology*, 2011, **2**, 55.

117. J. Malý, H. Lampová, A. Semerádtová, M. Štofik and L. Kováčik, *Nanotechnology*, 2009, **20**, 385101.

118. K. Varaprasad, Y. M. Mohan, K. Vimala and K .M. Raju, *Journal of Applied Polymer Science*, 2011, **121**, 784.

119. S. Francis, L. Varshney and K. Tirumalesh, *Radiation Physics and Chemistry*, 2006, **75**, 747.

120. D. Mahl, J. Diendorf, W. Meyer-Zaika and M. Epple, *Colloids and Surfaces A: Physicochemical and Engineering Aspects*, 2011, **377**, 386.

121. T. Fuchs, W. Richtering, W. Burchard, K. Kajiwara and S. Kitamura, *Polymer Gels and Networks*, 1997, **5**, 541.

122. F. Chambon, Z. S. Petrovic, W. J. MacKnight and H. H. Winter, *Macromolecules*, 1986, **19**, 2146.

123. A. B. Rodd, J. J. Cooper-white, D. E. Dunstan and D. V. Boger, *Polymer*, 2001, **42**, 3923.

124. A. B. Rodd, J. J. Cooper-white, D. E. Dunstan and D.V. Boger, *Polymer*, 2001, **42**, 185.

125. S. Francis, L. Varshney and M. Kumar, *Radiation Physics and Chemistry*, 2004, **69**, 481.

126. A. Montembault, C. Viton and A. Domard, *Biomaterials*, 2005, **26**, 1633.

127. C. Sandolo, P. Matricardi, F. Alhaique and T. Coviello, *Food hydrocolloids*, 2009, **23**, 210.

128. (a) N. Peppas, *Hydrogels in Medicine and Pharmacy* (CRC) Boca Raton, Florida, 1987. (b) N. Vyavahare and J. Kohn, *Journal of Polymer Science*, 1994, **32**, 1271. (c) R.

Bahulekar, T. Tokiwa, J. Kano, T. Matsumura, I. Kojima and M. Kodama, *Carbohydrate Polymers,* 1998, **37**, 71. (d) G. Wulff, J. Schmid and T. Venhoff, *Macromolecular Chemistry and Physics*, 1996, **197**, 259. (e) M. J. Carneiro, A. Fernandes, C. M. Figueiredo, A. G. Fortes and A. M. Freitas, *Carbohydrate Polymers*, 2001, **45**, 135.

129. J-Y. Sun, X. Zhao, W. R. K. Illeperuma, O. Chaudhuri, K. H. Oh, D. J. Mooney, J. J. Vlassak and Z. Suo, *Nature*, 2012, **489**, 133.

130. (a) N. A. Peppas, P. Bures, W. Leobandung and H. Ichikawa, *European Journal of Pharmaceutics and Biopharmaceutics*, 2000, **50**, 27. (b) N. Bhattarai, J. Gunn and M. Zhang, *Advanced Drug Delivery Reviews*, 2010, **62**, 83. (c) O. Wichterle and D. Lim, *Nature*, 1960, **185**, 117. (d) R. Yoshida, K. Uchida, Y. Kaneko, K. Sakai, A. Kikuchi, Y. Sakurai and T. Okano, *Nature*, 1995, **374**, 240. (e) Q. Wang, J. S. Dordick and R. Linhardt, *Chemistry of Materials*, 2002, **14**, 3232. (f) A. S .Hoffman, *Advanced Drug Delivery Reviews*, 2002, **54**, 3.

131. (a) E. A. Appel, X. J. Loh, S. T. Jones, F. Biedermann, C. A. Dreiss and O.A. Scherman, *Journal of American Chemical Society*, 2012, **134** , 11767. (b) M. Kurecic, M. Sfiligoj-Smole and K. Stana-Kleinschek, *Materials and Technology*, 2012, **46**, 87.

132. (a) V. Ladmiral, E. Melia and D. M. Haddleton, *European Polymer Journal*, 2004, **40**, 431. (b) S. Slavin, J. Burns, D. M. Haddleton and C. R. Becer, *European Polymer Journal*, 2011, **47**, 435.

133. (a) J. F. Lutz, O. Akdemir and A. Hoth, *Journal of American Chemical Society*, 2006, **128**, 13046. (b) J. F. Lutz and A. Hoth, *Macromolecules*, 2006, **39**, 893. (c) J. Tavakoli, E. Jabbari, M. E. Khosroshahi and M. Boroujerdi, *Iranian Polymer Journal*, 2006, **15**,

891. (d) M. A. Casadei, G. Pitarresi, R. Calabrese, P. Paolicelli and G. Giammona, *Biomacromolecules*, 2008, **9**, 43.(e) H. Shin, J. W. Nichol and A. Khademhosseini, *Acta Biomaterialia*, 2011, **7**, 106. (f) X. Chen, B. D. Martin, T. K. Neubauer, R. J. Linhardt, J. S. Dordick and D. G. Rethwisch, *Carbohydrate Polymers*, 1995, **28**, 15.

134. (a) J. S. Dordick, R. J. Linhardt and D. G. Rethwisch, *ChemTech*, 1994, **24**, 33. (b) X. M. Chen, J. S. Dordick and D. G. Rethwisch, *Macromolecules*, 1995, **28**, 6014. (c) R. Bahulekar, T. Tokiwa, J. Kano, T. Matsumura, I. Kojima and M. Kodama, *Carbohydrate Polymers*, 1998, **37**, 71. (d) J. K. F. Suh and H. W. T. Matthew, *Biomaterials*, 2000, **21**, 2589. (e) S. H. Kim, M. Goto, C. S. Cho and T. Akaike, *Biotechnology Letters*, 2000, **22**, 1049.

135. (a) N. Sharon and H. Lis, *Scientific American*, 1993, **268**, 82. (b) R. A. Dwek, *Chemical Reviews*, 1996, **96**, 683. (c) Y. C. Lee and R. T. Lee, *Accounts of Chemical Research*, 1995, **28**, 321. (d) E. E. Simanek, G. J. McGarvey, J. A. Jablonowski and C. -H. Wong, *Chemical Reviews*, 1998, **98**, 833. (e) A. Pfaff, L. Barner, A. H. E. Müller and A. M. Granville, *European Polymer Journal*, 2011, **47**, 805.

136. J. Kopecek, P. Kopeckova, H. Brondsted, R. Rathi, B. Rihova, P. Y. Yeh and K. Ikesue, *Journal of Controlled Release*, 1992, **19**, 121.

137. (a) S. Nandi, H. -J. Altenbach, B. Jakob, K. Lange, R. Jhizane, M. P. Schneider, Ü. Gün and A. Mayer, *Organic Letters*, 2012, **14**, 3826. (b) A. R. Hirst, I. A. Coates, T. R. Boucheteau, J. F. Miravet, B. Escuder, V. Castelletto, I. W. Hamley and D. K. Smith, *Journal of American Chemical Society*, 2008, **130**, 9113. (c) K. A. Houton, K. L. Morris, L. Chen, M. Schmidtmann, J. T. A. Jones, L. C. Serpell, G. O. Lloyd and D. J. Adams,

Langmuir 2012, **28**, 9797. (d) J. Raeburn, A. Z. Cardoso and D. J. Adams, *Chemical Society Reviews*, 2013, **42**, 5143.

138. (a) N. S. Khelfallah, G. Decher and P. J. Mésini, *Macromolecular Rapid Communications*, 2006, **27**, 1004. (b) Y. S. Casadio, D. H. Brown, T. V. Chirila, H. -B. Kraatz and M. V. Baker, *Biomacromolecules*, 2010, **11**, 2949. (c) S. M. Paterson, J. Clark, K. A. Syubbs, T. V. Chirila and M. V. Baker, *Journal of Polymer Science Part A: Polymer Chemistry*, 2011, **49**, 4312. (d) B. D. Martin, S. A. Ampofo, R. J. Linhardt and J. S. Dordick, *Macromolecules*, 1992, **25**, 7081.

139. S. H. Kim, M. Goto and T. Akaike, *The Journal of Biological Chemistry*, 2001, **276,** 35312.

140. B. Cursaru, O. `P. Stănescu and M. Teodorescu, *UPB Scientific Bulletin, Series B: Chemistry and Materials Science*, 2010, **72**, 99.

141. (a) K. P. R. Kartha, *Tetrahedron Letters*, 1986, **27**, 3415. (b) J. M. J. Tronchet, B. Getile, J. Ojha-Poncet, G. Moret, D. Schwarzanbach and F. Barblat-Ray, *Carbohydrate Research*, 1977, **59**, 87.

142. (a) Y. Miura, *Polymer Journal*, 2012, **44**, 679 and the references cited therein. (b) V. S. Shinde and V. U. Pawar, *Journal of Applied Polymer Science*, 2009, **111**, 2607.

143. (a) W. S. Hlavacek, R. G. Posner and A. S. Perelson, *Biophysical Journal*, 1999, **76**, 3031. (b) T. Furuike, N. Nishi, S. Tokura and S. - I. Nishimura, *Macromolecules*, 1995, **28**, 7241. (c) Y. Miura, D. Koketsu and K. Kobayashi, *Polymers for Advanced Technologies*, 2007, **18**, 647.

144. (a) R. U. Lemieux, *Pure and Applied Chemistry*, 1971, **25**, 527 and references therein. (b) S. Wolfe, M. H. Whangbo and D. Mitchell, *Journal of Carbohydrate Research*, 1979, **69**, 1. (c) V. G. S. Box, *Heterocycles*, 1990, **31**, 1157. (d) I. Tvaroska and T. Bleha, *Advances in Carbohydrate Chemistry and Biochemistry*, 1989, **47**, 45.

145. L. -M. Stefan, A. -M. Pana, G. Bandur, P. Martin, M. Popa and L. -M. Rusnac, *Journal of Thermal Analysis and Calorimetry*, 2013, **111**, 789.

146. (a) J. D. Ferry, *Viscoelastic Properties of Polymers*,Wiley, New York, 1961.(b) J. You, J. Zhou, Q. Li and L. Zhang, *Langmuir*, 2012, **28**, 4965. (c) O. Okay and W. Oppermann, *Macromolecules*, 2007, **40**, 3378.

147. M. J. Moura, M. M. Figueiredo and M. H. Gil, *Biomacromolecules*, 2007, **8**, 3823.

148. X. Li, X. Kong, Z. Zhang, K. Nan, L. Li, X. Wang and H. Chen, *International Journal of Biological Macromolecules*, 2012, **50**, 1299.

149. M. Jaiswal, V. Koul, *Journal of Biomaterials Applications*, 2013, **27**, 848.

150. L. Jiawei, Z. Weidong, R. Sarah-Jane, G. I. Matthew and C. Gaojian, *Polymer Chemistry*, 2014, **5**, 2326.

151. M. Chen, W. Feng, S. Lin, C. He, Y. Gao, and H. Wang, *RSC Advances*, 2014, **4**, 53344.

152. Q. Wang, and A. Q. Wang, *Journal of Functional Polymer*, 2004, **17**, 51 (in Chinese).

153. S. Feng, and S. Chien, *Chemical Engineering Science*, 2003, **58**, 4087.

154. M. Singh, S. Kundu, A. M. Reddy, V. Sreekanth, R. K. Motiani, S. Sengupta, A. Srivastava and A. Bajaj, *Nanoscale*, 2014, **6**, 12849.

155. X. Zhao, L. Yang, X. Le, X. Jia, L. Liu, J. Zeng, J. Guo and P. Liu, *Bioconjugate Chemistry*, 2015, **26**,128.

156. H. Freichels, R. Jerome and C. Jerome, *Carbohydrate Polymers*, 2011, **86**, 1093.

157. M. L. Huan, S. Y. Zhou, Z. H. Teng, B. L. Zhang, X. Y. Liu, . P. J. Wang and Q. B. Mei, *Bioorganic and Medicinal Chemistry Letters*, 2009, **19**, 2579.

158. B. S. Chhikara, N. Jean, D. Mandal, A. Kumar and K. Parang, *European Journal of Medicinal Chemistry*, 2011, **46**, 2037.

159. M. Talelli, K. Morita, C. J. Rijcken, R. W. Aben, T. Lammers, H. W. Scheeren, C. F. van Nostrum, G. Storm and W. E. Hennink, *Bioconjugate Chemistry*, 2011, **22**, 2519.

160. J. J. Lundquist and E. J. Toone, *Chemical Reviews*, 2002, **102**, 555.

161. H. T. Ta, C. R. Dass, I. Larson, P. F. M. Choong and D. E. Dunstan, *Biomaterials*, 2009, **30**, 3605.

162. J. H. Maeng, D. H. Lee, K. H. Jung, Y. H. Bae, I. S. Park, S. Jeong, Y. S. Jeon, C. K. Shim, W. Kim, J. Kim, J. Lee, Y. M. Lee, J. H. Kim, W. H. Kim and S. S. Hong, *Biomaterials*, 2010, **31**, 4995.

163. C. Zhang, W. Wang, T. Liu, Y. Wu, H. Guo, P. Wang, Q. Tian, Y. Wang and Z. Yuan, *Biomaterials*, 2012, **33**, 2187.

164. K. C. Weng, C. O. Noble, B. P-Sternberg, F. F. Chen, D. C. Drummond, D. B. Kirpotin, D. H. Wang, Y. K. Hom, B. Hann and J. W. Park, *Nano Letters*, 2008, **8**, 2851.

165. D. D. Von Hoff, M. Rozencweig and M. Piccart, *Seminars in Oncology*, 1982, **9**, 23.

166. P. Singal, N. Iliskovic, T. Li and D. Kumar, *FASEB Journal*, 1997, **11**, 931.

167. L. J. Goldstein, H. Galski, A. Fojo, M. Willingham, S-L. Lai, A, Gazdar, R. Pirker, A. Green, W. Crist, G. M. Brodeur, M. Lieber, J. Cossman, M. M. Gottesman and I. Pastan, *Journal of the National Cancer Institute*, 1989, **81**, 116.

168. Y. Bae, S. Fukushima, A. Harada and K. Kataoka, *Angewandte Chemie International Edition,* 2003, **42**, 4640.

169. J. Shi, W. Guobao, H. Chen, W. Zhong, X. Z. Qiu and M. M. Q. Xing, *Polymer Chemistry*, 2014, **5**, 6180.

170. M. Dadsetana, Z. Liu, M. Pumberger, C. V. Giraldo, T. Ruesink, L. Lu and M. J. Yaszemski, *Biomaterials,* 2010, **31**, 8051.

171. C. Duan, J. Gao, D. Zhang, L. Jia, Y. Liu, D. Zheng, G. Liu, X. Tian, F. Wang and Q. Zhang, *Biomacromolecules,* 2011, **12**, 4335.

172. Y. Kato, H. Onishi and Y. Machida, *Biomaterials*, 2004, **25**, 907.

173. S. M. Moghimi, A. C. Hunter and J. C. Murray, *Pharmacological Reviews*, 2001, **53**, 283.

174. Y. Kato, H. Onishi and Y. Machida, *Biomaterials*, 2000, **21**, 1579.

175. Y. Matsumura and H. Maeda, *Cancer Research*, 1986, **46**, 6387.

176. H. Maeda, *Advances in Enzyme Regulation*, 2001, **41**, 189.

177. H. Maeda, J. Wu, T. Sawa, Y. Matsumura and K. Hori, *Journal of Controlled Release*, 2000, **65**, 271.

178. H. Maeda and Y. Matsumura, *Critical Reviews in Therapeutic Drug Carrier Systems*, 1989, **6**, 193.

179. Y. N. Dai, P. Li, J. P. Zhang, A.Q. Wang and Q. Wei, *Biopharmaceutics and Drug Desposition,* 2008, **29**, 173.

180. J. K. Ajish, K. S. A. Kumar, M. Subramanian and M. Kumar, *RSC Advances*, 2014, **4**, 59370.

181. D. Das, P. Ghosh, S. Dhara, A. B. Panda and S. Pal, *ACS Applied Materials & Interfaces*, 2015, **7**, 4791.

182. C. Ding, L. Zhao, F. Liu, J. Cheng, J. Gu, S. Dan, C. Liu, X. Qu and Z. Yang, *Biomacromolecules*, 2010, **11**, 1043.

183. Z. Aiping, C. Tian, Y. Langue, W. Hao and L. Ping, *Carbohydrate Polymers*, 2006, **66**, 274.

184. C. Yan, D. Chen, J. Gu, H. Hu, X. Zhao and M. Qiao, *Pharmaceutical Society of Japan*, 2006, **126**, 789.

185. M. Gonçalves, P. Figueira, D. Maciel, J. Rodrigues, X. Shi, H. Tomás and Y. Li, *Macromolecular Bioscience*, 2014, **14**, 110.

186. P. Yousefpour, F. Atyabi, E. V. Farahani, R. Sakhtianchi and R. Dinarvand, *Int. J. Nanomedicine*, 2011, **6**, 1487.

187. N. N. Mobarak and Md. P. Abdullah, *The Malaysian Journal of Analytical Sciences*, 2010, **14**, 82.

188. X. Y. Hu, L. D. Feng, A. M. Xie, W. Wei, S. M. Wang, J. F. Zhang and W. Dong, *Journal of Material Chemistry B*, 2014, **2**, 3646.

189. X. Y. Hu, L. D. Feng, W. Wei, A. M. Xie, S. M. Wang, J. F. Zhang and W. Dong, *Carbohydrate Polymers*, 2014, **105**, 135.

190. A. H. Xiu, Y. Kong, M. Y. Zhou, B. Zhu, S. M. Wang and J. F. Zhang, *Carbohydrate Polymers*, 2010, **82**, 623.

191. E. Jabbari, N. Wisniewski and N. A. Peppas, *Journal of Controlled Release*, 1993, **26**, 99.

192. M. V. Dinu, M. M. Perju and E. S. Dragan, *Macromolecular Physics and Chemistry*, 2011, **212**, 240.

193. M. K. Rao, B. Mallikarjuna, K. K. S. V. Rao, K. Sudhakar, C. K. Rao and M. C. S. Subha, *International Journal of Polymeric Materials and Polymeric Biomaterials*, 2013, **62**, 565.

194. H. Zhang, Y. Dong, L. Wang, G. Wang, J. Wu, Y. Zheng, H. Yang and S. Zhuc, *Journal of Material Chemistry*, 2011, **21**, 13530.

195. Y. Liu, V. S. Bryantsev and M. S. Diallo, *Journal of American Chemical Society*, 2009, **131**, 2798.

196. B. Manocha and A. Margaritis, *Journal of Nanomaterials*, 2010, Article ID 780171, doi:10.1155/2010/780171.

197. R. Jin, L. S. M. Teixeira, P. J. Dijkstra, M. Karperien, C. A. van Blitterswijk, Z. Y. Zhong and J. Feijen, *Biomaterials*, 2009, **30**, 2544.

198. W. G. Duan, C. H. Chen, L. B. Jiang and G. H. Li, *Carbohydrate Polymers*, 2008, **73**, 582.

199. M. C. I. M. Amin, N. Ahmad, N. Halib and I. Ahmad, *Carbohydrate Polymers*, 2012, **88**, 465.

200. R. W. Korsemeyer, R. Gurny, E. Doelker, P. Buri and N. A. Peppas, *International Journal of Pharmaceutics*, 1983, **15**, 25.

201. J. Mei, N. L. C. Leung, R. T. K. Kwok, J. W. Y. Lam and B. Z. Tang, *Chemical Reviews*, 2015, **115**, 11718.

202. J. Luo, Z. Xie, J. W. Y. Lam, L. Cheng, H. Chen, C. Qiu, H. S. Kwok, X. Zhan, Y. Liu, D. Zhuc and B. Z. Tang, *Chemical Communications*, 2001, **18**, 1740.

203. Y. Hong, J. W. Y. Lam and B. Z. Tang, *Chemical Communications*, 2009, **29**, 4332.

204. J. Mei, Y. Hong, J. W. Lam, A. Qin, Y. Tang and B. Z. Tang. *Advanced materials*, 2014, **26**, 5429.

205. M. S. Mathew, K. Sreenivasan and K. Joseph, *RSC Advances*, 2015, **5**, 100176.

206. Y. Hong, J. W. Y. Lam and B. Z. Tang, *Chemical Society Reviews*, 2011, **40**, 5361.

207. R. Hu, N. L. C. Leung and B. Z. Tang, *Chemical Society Reviews*, 2014, **43**, 4494.

208. J. Chen, C. C. W. Law, J. W. Y. Lam, Y. Dong, S. M. F. Lo, I. D. Williams, D. Zhu and B. Z. Tang, *Chemistry of Materials*, 2003,**15**, 1535.

209. K-R. Wang, Y-Q. Wang, H-W. An, J-C. Zhang and X-L. Li, *Chemistry A European Journal*, 2013, **19**, 2903.

210. O. Rusin, V. Kr_l, J. O. Escobedo and R. M. Strongin, *Organic Letters*, 2004, **6**, 1373.

211. A. Makky, J. P. Michel, A. Kasselouri, E. Briand, Ph. Maillard and V. Rosilio, *Langmuir*, 2010, **26**, 12761.

212. T. Sanji, K. Shiraishi, M. Nakamura and M. Tanaka, *Chemistry-An Asian Journal*, 2010, **5**, 817.

213. Q. Guo, T. Zhang, J. An, Z. Wu,Y. Zhao, X. Dai, X. Zhang and C. Li, *Biomacromolecules* 2015, **16**, 3345.

214. Q. Chen, N. Bian, C. Cao, X. L. Qiu, A. D. Qi and B. H. Han, *Chemical Communications*, 2010, **46**, 4067.

215. J. X. Wang, Q. Chen, N. Bian, F. Yang, J. Sun, A. D. Qi, C. G. Yan and B. H. Han, *Organic and Biomolecular Chemistry,* 2011, **9,** 2219.

216. X. M. Hu, Q. Chen, J. X. Wang, Q. Y. Cheng, C. G. Yan, J. Cao, Y. J. He and B. H. Han, *Chemistry- An Asian Journal,* 2011, **6**, 2376.

217. K. Shiraishi, T. Sanji and M. Tanaka, *Tetrahedron Letters,* 2010, **51**, 6331.

218. J. Shi, L. Cai, K. Y. Pu and B. Liu, *Chemistry-An Asian Journal*, 2010, **5**, 301.

219. K. Y. Pu, J. Shi, L. Wang, L. Cai, G. Wang and B. Liu, *Macromolecules*, 2010, **43**, 9690.

220. H. Shi, L. Liu, X. Wang and J. Li, *Polymer Chemistry*, 2012, **3**, 1182.

221. I. Otsuka, T. Otsuka, H. Nakade, A. Narumi, R. Sakai, T. Satoh, H. Kaga and T. Kakuchi, *Macromolecules*, 2007, **40**, 8930.

222. T. Sanji, K. Shiraishi, M. Nakamura and M. Tanaka, *Chemistry- An Asian Journal,* 2010, **5**, 817.

223. H. Bittiger and H. P. Schnebli, *Concanavalin A as a Tool*, Wiley, London, 1976.

224. K. Wang, X. Zhang, X. Zhang, B. Yang, Z. Li, Q. Zhang, Z. Huanga and Y. Wei, *Polymer Chemistry*, 2015, **6**, 1360.